Cost effectiveness of the first stage recovery of a small satellite launcher

Merle Snijders

Master Thesis

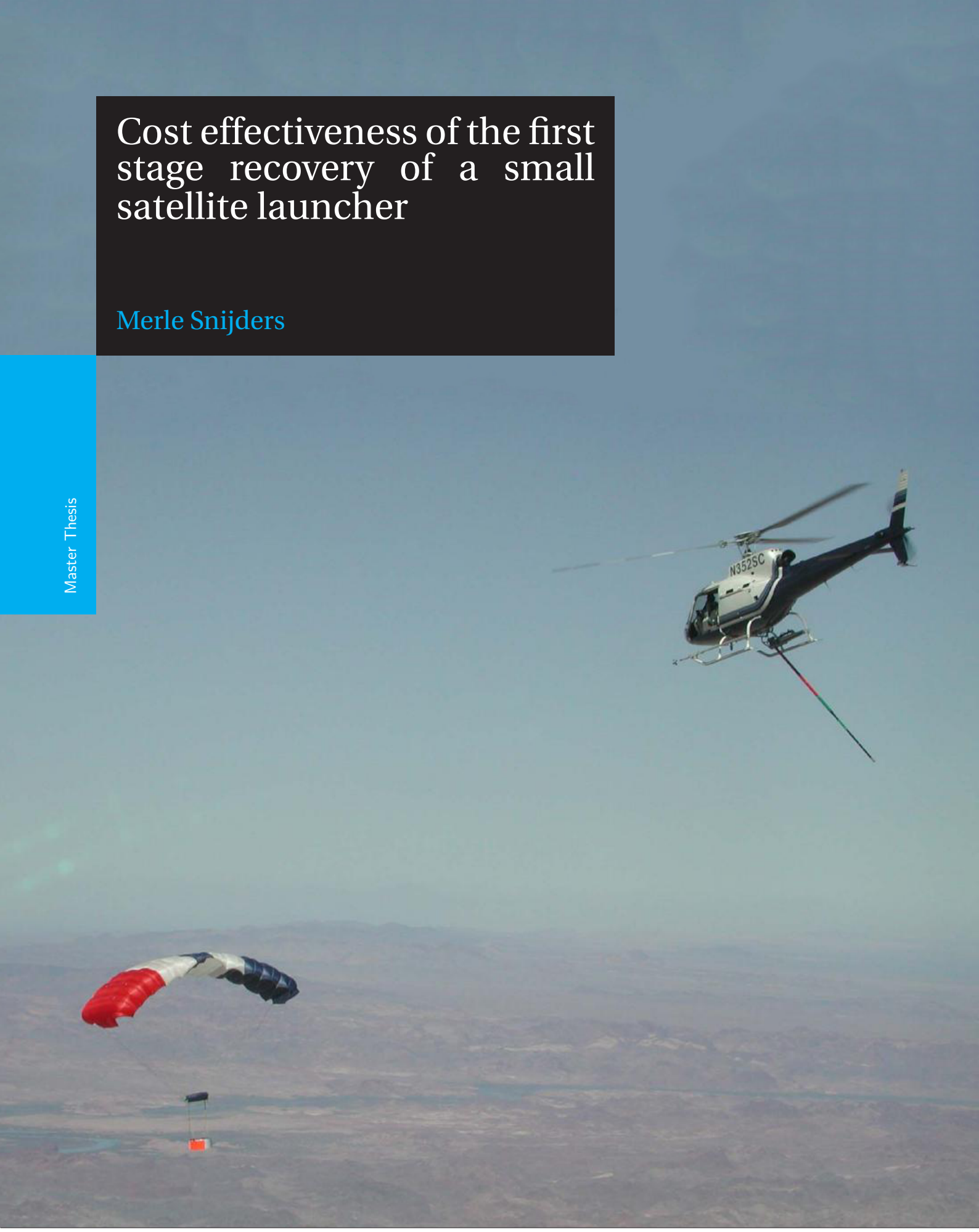

TU Delft Delft University of Technology

Challenge the future

COST EFFECTIVENESS OF THE FIRST STAGE RECOVERY OF A SMALL SATELLITE LAUNCHER

by

Merle Snijders

in partial fulfillment of the requirements for the degree of

Master of Science
in Aerospace Engineering

Student number: 4143647
Supervisor: Ir. M. C. Naeije, Delft University of Technology
Ir. B. A. Oving, Netherlands Aerospace Center
Cover image credits: NASA [1]

TU Delft Delft University of Technology

ABSTRACT

An increase in the amount of launched satellites can be seen in the last decade. And it is expected that even more satellites will be launched in the upcoming years. Most of these small satellites are launched as piggy back together with a large spacecraft. The location and time of launch and orbit will therefore be determined by another mission. A dedicated launcher for small satellites will contribute to the success of small satellites by bringing the satellite at the right time in the right orbit.

Fourteen European companies and institutes are working together in a European Union (EU) Horizon 2020 project called "SMall Innovative Launcher for Europe" (SMILE). The project aims at designing a launcher for satellites up to 70 kg and a European-based launch facility at Andøya. To make this project a success the launch cost must be below the € 50 000 per kg and a total launch cost of 3.5 €M. One of the ways to cut the costs of the launcher is by the re-use of the first stage.

This research will answer the question if recovering of the first stage will be cost-beneficial, answering the following research question; *What is the performance gain in terms of cost when reusing the first stage of the launcher within the SMILE project?* To answer this question, three different steps are taken.
The first step is to investigate the boundaries of the recovery of the first stage. The impact region, velocity and maximum altitude and loads are investigated to understand the recovery mechanisms needed. It is found that the impact region of the first stage is between the coast of Norway and Jan Mayen. This means that the first stage needs to land on water. Using the information found, seven different recovery options are designed. During the second phase the different designs are optimised to the minimum take-off weight. This optimisation is done by first making use of Monte Carlo simulations to find the region were the minimal is found. The results of the Monte Carlo simulation are used in a genetic algorithm the find the minimum system weight. After this evaluation two different options remained; retro-propulsion option and a parachute system option. The last step is to evaluate these two options in more detail with a six degrees of freedom simulation. After the evaluation of the two options, the options are designed in more detail. Three different landing techniques are discussed; resulting in three different options. The first option found is the retro-propulsion with an airbag landing. The second option considered is the parachute system with an air bed landing. The last option found is the parachute system with a mid air capture performed by a helicopter.
The different options are re-designed and the extra weight and volume needed is computed. The cost of the different options is calculated and compared. It is shown that if the first stage is used four times of more per year, recovering is cost-beneficial for all options.

Merle Snijders
Marknesse, August 2017

PREFACE

This document concludes the work of a Master Thesis about recovery of the first stage of a small launcher. The study is conducted as a part of my Master of Science at the Delft University of Technology. This master thesis work has been done in corporation with the Netherlands Aerospace Center.

Hereby, I would take this opportunity to thank the people who supported me during the execution of the thesis work. I could never have have done it without their support, and I will always be thankful.

First of all I would like to thank my supervisors. My daily supervisors at the NLR, Bertil Oving, and Arnaud van Kleef who advised my during my thesis with their expertise. And Marc Naeije, who supported me on a technical and personal level with his endless Skype meetings.

I would also like to thank my colleagues and other interns for the great work environment, coffee breaks and advise. And a special mention of my friends, for providing a sympathetic ear, and for visiting me in the far North East; Zwolle.

Finally, I would like to express my gratitude towards my wonderful parents, and brother who have always supported me throughout my studies. Also my boyfriend, Ernst, for his unending patience and optimism exactly at the times when I needed it.

Merle Snijders
Marknesse, August 2017

List of Figures

List of Tables

List of Abbreviations

AGU	Airborne Guidance Unit
CBS	Cost Breakdown Structure
CEM	Cost Estimation Method
CER	Cost Estimation Relationships
CFD	Computational Fluid Dynamics
DOF	Degrees of Freedom
ECEF	Earth-centred Earth-fixed
ECI	Earth-Centred Inertial
EGSE	Electrical Ground Support Equipment
EOM	Equations of Motion
FBD	Free Body Diagram
GA	Genetic Algorithm
GNC	Guidance Navigation and Control
GNSS	Global Navigation Satellite System
IAD	Inflatable Aerodynamic Decelerator
IMU	Inertial Measurement Unit
IRVE	Inflatable Re-entry Vehicle Experiment
ITAR	International Traffic in Arms Regulations
MAR	Mid Air Recovery
OBC	On Board Computer
RK4	Runge Kutta-4
SMILE	SMall Innovative Launcher for Europe
SSO	Sun Synchronous Orbit
STK	Systems Tool Kit
TPS	Thermal Protection System
TVC	Thrust Vector Control
WBS	Work Breakdown Structure

List of Symbols

Sign	Description	Unit
C_D	Drag coefficient	-
C_L	Lift coefficient	-
S	Surface area	m^2
V	Velocity	m/s
ρ	Density	kg/m^3
A_e	Exhaust area	m^2
C_Y	Side slip coefficient	-
C_l	Roll moment coefficient	-
C_m	Pitch moment coefficient	-
C_n	Yaw moment coefficient	-
D	Drag	N
F_{RT}	Strength radial tapes	[N
F_{SL}	Strength suspension lines	N
F_{g_0}	Gravitational acceleration	m/s^2
G	Gravitational constant	m^3/kgs^2
I_{cg}	Mass moment of inertia around the centre of gravity	$kg{\cdot}m^2$
I_{sp}	Specific Impulse	s
L_S	Length suspension lines	m
L	Lift	N
M	Mass	kg
M	Mach number	-
N_G	Number of gores	-
N_{SL}	Number of suspension lines	-
P_e	Pressure at exhaust	N/m^2
Pr	Prandtl number	Pr
P	Pressure	N/m^2
R_e	Radius Earth	m
R_n	Nose radius	m
$R_{specific}$	Specific gas constant	J/(kg K)
R	Radius	m
S_0	Surface of the finished canopy	m^2
St	Stanton number	-
T_{wad}	Adiabatic wall temperature	K
T_{wall}	Actual wall temperature	K
T	Temperature	K
T	Thrust	N
T	Thrust force	N
Y	Side slip	N
Ω_t	Rotational speed of the Earth	rad/s
α	Angle of attack	rad
α	Angle of attack	rad
β	Launch azimuth	°
β	Angle of side slip	rad
δ	Latitude	rad
$\dot{m}$	Mass flow rate	kg/s
ϵ	Emissivity	kg
ϵ	Emissivity	-

Sign	Description	Unit
γ	Adiabatic index	-
γ	Flight path angle	rad
λ	Efficiency	-
λ	Latitude	$^\circ$
ϕ	Latitude	$^\circ$
ϕ	Roll angle	rad
ψ	Yaw angle	rad
σ	Stefan-Boltzmann constant	$W/(m^2K^4)$
τ	Longitude	rad
θ	Pitch angle	rad
θ	Pitch angle	rad
a	Speed of Sound	m/s
a	Acceleration	m/s^2
c_p	Pressure coefficient	-
c	Chord length	m
g_0	Gravitational acceleration at the Earth's surface	m/s^2
g	Gravitational acceleration	m/s^2
h_c	Convective heat transfer coefficient	$W/(m^2K)$
h	Heat	J
h	Step size	s
k	Thermal conductivity	W/mK
m_i	Mass of particle	kg
m_{prop}	Mass propellant	kg
n	Number of particles	-
r_i	Coordinate of particle	m
r	Distance	m
r	Recovery factor	-
s	Distance	m
t_0	Stellar time of the point 0	s
t	Time	s
v	Velocity	m/s
w_c	Specific weight canopy	kg/m^2
w_{SL}	Specific weight suspension lines	kg/m
w_{rt}	Specific weight radial tapes	kg/m

Contents

1

INTRODUCTION

Due to the rise in demand of cubesats and micro satellites in the last years, there is much interest in a dedicated small satellite launcher. A big part of the mission costs of a satellite mission are the launch cost. For small satellites the cost for a dedicated launcher are too high. Small satellites are therefore often launched as a piggy pack. A major disadvantage is that the primary client determines the launch date and destination. This leads often to limitation of the mission of the small satellite. An affordable dedicated launch mission is needed to launch small satellites.

Fourteen European companies and institutes are joining forces in a Horizon2020 programme called "SMall Innovative Launcher for Europe" (SMILE). The project aims at designing a small launcher for satellites up to 70 kg, demonstrating critical technologies on propulsion, avionics, and production for cost-effective solutions, and designing a European-based launch facility at Andøya. An overview of the SMILE consortium is shown in Table 1.1.

The technology in the SMILE context involves:

- reusable liquid rocket engines
- low cost hybrid rocket engines
- low cost automated manufacturing of composites and advanced materials
- low cost avionics equipment
- efficient, easy-to-use payload deployment system
- low cost ground segment

One of the major costs of a launcher are the costs of the first stage of the launcher. To reduce the cost, reusability of the first stage might be an option. Different companies are working on the re-usability of the launcher and/or first stage. However less research has been done to the (partially) re-use of small launchers. In this master thesis it is investigated if the re-use of the first stage will be beneficial within the SMILE project in terms of cost. A three stage launcher with a liquid first stage aerospike engine will be assumed.

This research answers the question if recovering of the first stage will be cost-beneficial. The research question is formulated as;

What is the performance gain in terms of cost when reusing the first stage of the launcher within the SMILE project?

Table 1.1: Partners in SMILE consortium

Partner	Origin	Responsible
Netherlands Aerospace Centre (NLR)	NL	launcher, structures, avionics, EGSE(Electrical Ground Support Equipment) , cost analysis, project coordinator
INCAS	RO	launcher, aerodynamics, trajectory
Nammo Raufoss AS	N	launcher, hybrid engines, cost analysis
German Aerospace Centre (DLR)	D	launcher, liquid engines, cost analysis
WEPA-Technologies	D	turbopumps: LOX/kerosene, H2O2
PLD Space	SP	liquid engine testing
ISIS - Innovative Solutions In Space	NL	business development, market analysis, payload deployment system
Airborne Composites Automation	NL	production methods, structures
Heron Engineering	GR	structural analysis
3D Systems	BE	3D printing of metal parts
Tecnalia	SP	advanced low-weight materials
Andøya Space Centre (ASC)	N	ground segment, market analysis
BoesAdvies	NL	business development, market analysis
Terma	DE	avionics, EGSE

To answer this question three different steps are taken to answer the sub-questions below.

- *What are the boundaries of recovering the first stage of a small launcher launched from Andøya?*
- *What is the performance gain in terms of gross take-off weight of the different options within the SMILE project?*
- *Which of the different options within the SMILE project is the best option in terms of gross take-off weight, cost, sustainability and operational flexibility for recovering the first stage?*

The first step is to investigate the boundaries of the recovery of the first stage using a simple 2 degrees of freedom simulation. Using results of the 2 degrees of freedom simulation different recovery option are formed. During the second phase the different options are optimised to the minimum take-off weight. This optimisation is done using Monte Carlo simulations to find the region where the minimal is found. The results of the Monte Carlo simulation are used in a genetic algorithm to find the minimum system weight. The optimisation is performed by making use of three degrees of freedom. The last step is to evaluate the remaining options in more detail with a six degrees of freedom simulation. After the evaluation of the options, the options are designed in more detail. A cost analysis is performed. The cost analysis is used to answer the research question. And the results are used to conclude on the best option within the SMILE project. An overview of the process is shown in Figure 4.3.

The first step described above is treated in the next chapter, Chapter 2. The following chapter treats the different designs followed by the results found in Chapter 3. In Chapter 4 the software and method, used in step two and three, is discussed. The different modules used in the software are treated in the Chapters 5-8. Information on the cost estimations can be found in Chapter 9. The code written is verified and validated, the results can be found in Chapter 10. The results found for step 2, the three degrees of freedom optimisation, is shown in Chapter 11 and 12. The six degrees of freedom simulation results are shown in Chapter B. The detailed design of the best options is shown in Chapter 14. In Chapter 15 some extra analysis is shown. This chapter includes a temperature analysis, a fin analysis, and a sensitivity analysis. All results found in the former chapters are used to formulate the conclusion shown in Chapter 16. To conclude, some recommendations for further research can be found in the same chapter.

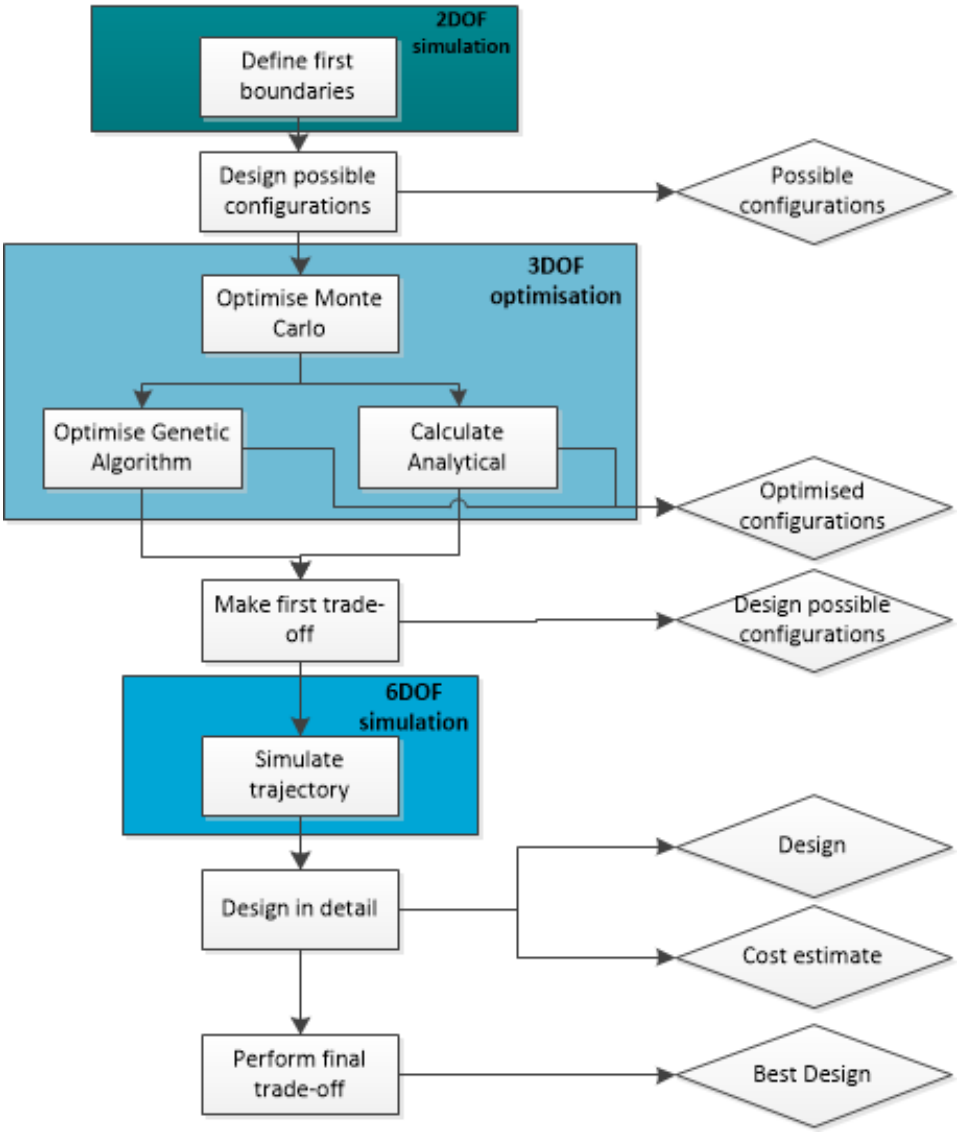

Figure 1.1: Schematic overview of the process

2

BOUNDARIES

To investigate if recovery of the first stage is cost-beneficial the best recovery design is needed. Before designing the best design the boundaries are needed to be investigated. This will be done by simulating the trajectory of the first stage. Next to the distance covered, also the velocity, Mach number and temperature achieved will be investigated. By searching for the distance covered and the temperature reached the first boundaries can be set on the system.

Most small satellites are launched in a Sun Synchronous Orbit (SSO). A satellite in a sun synchronous orbit will passes any given point of the Earth at the same local solar time. This results in a nearly constant illumination of the surface of the Earth every time the satellite passes it. These lighting conditions can be very useful for satellites observing the Earth o the visible or the infrared wavelength. A Sun synchronous orbit is a near polar orbit, with an inclination of over the 90°. SMILE will launch the satellite from Andøya, an island in the Nothern region of Norway. The satellite will rotate retrograde around the Earth. The high latitude of Andøya, makes it suitable launch position. At a higher latitude the the rotation of the Earth will have less influence the energy needed for orbit insertion. A SSO launched from Andøya will be considered in this report.

2.1. EQUATIONS

A Matlab script has been written to simulate the trajectory of the first stage. The numbers found in this analysis do not need to be very precise. The following aspects can therefore be assumed in this stage of the project:

- Flat, non-rotating Earth
- Spherical gravity
- No wind
- Ideal gas

The following Free Body Diagram (FBD) in Figure 2.1 has been used. In this diagram it can be seen that the forces dealt with are the thrust (T), gravity (g) and the drag (D). Using this formulation of the forces the following force equations are constructed.

$$F_y = Tsin\theta - Dsin\gamma - mg \tag{2.1}$$

$$F_x = Tcos\theta - Dcos\gamma \tag{2.2}$$

For the angles, angle of attack (α), the pitch angle (θ), and the flight path angle (γ) holds the following relation:

$$\gamma = \theta - \alpha \tag{2.3}$$

To propagate this force equation, the Euler method is used. In the following formulae the propagation of the velocity (v), distance (s) using the acceleration (a) are shown.

$$a = \frac{F}{m} \tag{2.4}$$

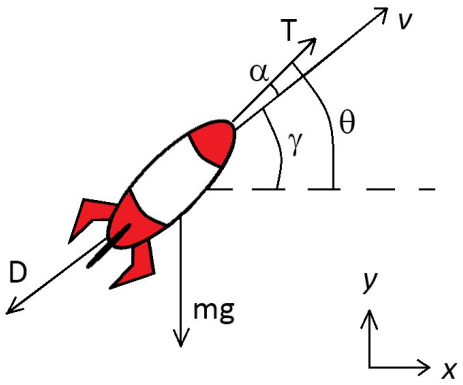

Figure 2.1: Free Body Diagram propulsion rocket

$$v = a \cdot dt + v \tag{2.5}$$

$$s = \frac{1}{2} a \cdot dt^2 + v \cdot dt + s \tag{2.6}$$

During the first phase of the flight the first stage will be propelled. The burn time has been calculated with Formula 2.7 and 2.8. The thrust (T), specific impulse (I_{sp}), the acceleration due to gravity at the Earth's surface (g_0) are used to calculate the mass flow($\dot{m}$). The mass flow and the total propellant mass (m_{prop}) of the first stage are used to calculate the burn time.

$$\dot{m} = \frac{T}{I_{sp} \cdot g_0} \tag{2.7}$$

$$t_b = \frac{m_{prop}}{\dot{m}} \tag{2.8}$$

If the velocity and the altitude are known, the Mach number (M) can be calculated with the following simple relation, Equation 2.9. In this equation the velocity (v) and the speed of sound (a) are needed. The speed of sound can be calculated with Equation 2.10, using the adiabatic index (γ), the molar gas constant (R) and the temperature of the air (T).

$$M = \frac{v}{a} \tag{2.9}$$

$$a = \sqrt{\gamma \cdot R \cdot T} \tag{2.10}$$

NOSE TEMPERATURE

The next step is estimating the temperature reached by the system. This will be done by calculating the equilibrium temperature at the wall of the nose of the system. It will be assumed that no heat conduction will occur. In reality the first stage will start to heat up and will take energy from the wall. This assumption will result in higher temperatures found then in reality will occur.

To calculate the radiation heat Equation 2.11 is used [9]. In this equation the emissivity (ϵ), a ratio of the radiant flux emitted by the surface and the radiant flux emitted by a black body is needed. Further more the Stefan-Boltzman constant (σ) and the temperatures of the wall and the air are used.

$$q_{rad} = \epsilon \cdot \sigma \cdot (T_w^4 - T_{air}^4) \tag{2.11}$$

The heat convection in hypersonic flow can be estimated by using Equation 2.12 [9], using the the adiabatic wall temperature (T_{wad}), and the wall temperature (T_{wall}). The convective heat coefficient (h_c) can be calculated with Equation 2.13. In this equation the Stanton number (St), the density of the flow (ρ), the velocity and the pressure coefficient (c_p) are used. The Stanton number can be calculated with Equation 2.14. In the formulation for the Stanton number, Equation 2.15, the Prandtl number (Pr) and a recovery coefficient (r)

are used. The constant α equals $\frac{1}{2}$ for laminar flow and $\frac{1}{3}$ for turbulent flow. As in this case the temperature is estimated at the nose of the system laminar flow can be assumed.

$$q_{conv} = h_c \cdot (T_{wad} - T_w) \tag{2.12}$$

$$h_c = St \cdot \rho \cdot v \cdot cp \tag{2.13}$$

$$St = \frac{1}{2} \frac{c_f}{Pr^{2/3}} \tag{2.14}$$

$$r = Pr^{\alpha} \tag{2.15}$$

Equation 2.12 will now be rewritten to make it easier to use. First the adiabatic wall temperature can be written as in Equation 2.16 using the adiabatic index, the recovery factor, and the Mach number. Combining this formulation and Equation 2.12, will result in the formulation in Equation 2.17.

$$T_{wad} = T_{air}(1 + r\frac{\gamma - 1}{2}M^2) \tag{2.16}$$

$$St \cdot \rho \cdot v \cdot cp \cdot (T_{wad} - T_w) = St \cdot \rho \cdot v \cdot cp \cdot T_{air} \cdot r\frac{\gamma - 1}{2}M^2(\frac{T_{wad} - T_w}{T_{wad} - T_{air}}) = St \cdot r \cdot \frac{1}{2} \cdot \gamma \cdot T_{air} \cdot \rho \cdot R \cdot M^2 \cdot v(\frac{T_{wad} - T_w}{T_{wad} - T_{air}}) \tag{2.17}$$

Combining Equation 2.17 and 2.15 will result in Equation 2.18. Equation 2.18 and 2.11 are used in Matlab to balance these equation and find the wall temperature.

$$q_{conv} = St \cdot Pr^{\alpha} \cdot \frac{1}{2} \cdot \gamma \cdot P \cdot M^2 \cdot v(\frac{T_{wad} - T_w}{T_{wad} - T_{air}}) \tag{2.18}$$

IMPACT POINT

Once the distance travelled is calculated the results are used to calculate the impact point. This has been done by transforming the distance (s), the launch longitude (λ) and latitude (ϕ) and the launch azimuth (β) in the longitude and latitude of the impact point. Equation 2.19 is used to calculate the latitude of the impact point and Equation 2.20 for the longitude of the impact point [10]. In this equation the radius of the Earth (R_e) has been used to calculate the impact point. As the first stage travels into the rotation of the Earth the rotation of the Earth is added to the distance travelled.

$$\phi_2 = asin(sin(\phi_1) \cdot cos(\frac{s}{R_e}) + cos(\phi_1) \cdot sin(\frac{s}{R_e}) \cdot cos(\beta)) \tag{2.19}$$

$$\lambda_2 = \lambda_1 + atan2(cos(\frac{s}{R_e}) - sin(\phi_1) \cdot sin(\phi_2), sin(\beta) \cdot sin(\frac{s}{R_e}) \cdot cos(\phi_1)) \tag{2.20}$$

2.2. VERIFICATION AND VALIDATION

This section contains the verification and validation results found while checking the validity of the model constructed. First some numbers found by the model will be compared with analytic formulae. Next the model will be compared with other tools.

2.2.1. VERIFICATION

First the velocity at separation will be verified this will be done by making use of the Tjolkovsky equation, shown in Equation 2.21[9]. This equation gives the end velocity as function of the specific impulse, gravitational constant at the Earth surface and the begin (M_0) and end mass (M_e) of the system.

$$\Delta V = I_{sp} \cdot g_0 ln(\frac{M_0}{M_e}) \tag{2.21}$$

Using Equation 2.21 and the numbers shown in Table 2.1 a difference in velocity of 3.9 km/s has been found. The velocity difference found by the Matlab tool if drag is not taken into account is 2.9 km/s. This number includes a gravity loss, as the burn time is 105 seconds, this gravity loss sums up to be 1 km/s. Adding this number to the 2.9 km/s found, will also give a velocity difference of 3.9 km/s as expected to be found using the Tjolkovsky equation.

Table 2.1: Verification velocity at separation 2DOF simulation

		Tjolkovsky	Matlab model
Input	I_{sp} [s]	271.9	271.9
	Lift-off Mass (M_0) [kg]	15300	15300
	Propellant Mass [kg]	11800	11800
	Burntime [s]	-	105
Output	Bruto Δ V [km/s]	3.93	2.93
	Δ V gravitation loss [km/s]	-	1.0
	Δ V [km/s]	**3.93**	**3.93**

2.2.2. TRAJECTORY VALIDATION

The trajectory of the systems has been validated with STK (Systems Tool Kit). This has been done by defining the separation speed, altitude and angle, being 2.93 km/s, 67 km and 54° respectively. Using these numbers the Figures 2.2 and 2.3 are produced. In these figures it can be seen that the altitude found by STK is slightly higher. For the last part of the trajectory the tool in Matlab finds a shallow part while the system in STK decreases very steep. These differences can be explained by the fact that the Matlab tool takes into account drag, whereas STK does not. Next the same can be seen for the validation figures of the velocity. The velocity will increase till impact for the STK model, while the Matlab model will decrease in velocity due to drag.

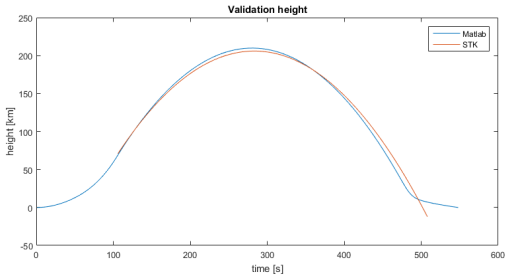

Figure 2.2: Validation boundaries script, the altitude profile

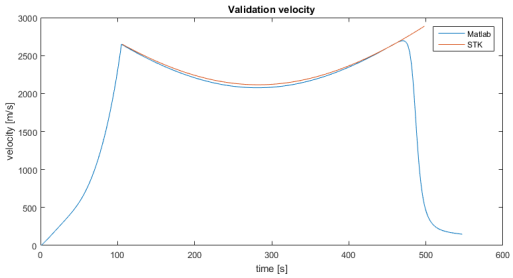

Figure 2.3: Validation boundaries script, the velocity profile

2.3. RESULTS

This section will discuss the results obtained. First the parameters, concerning the flight path, the engine and the geometry used in this first order prediction, are shown in Table 2.2.

Table 2.2: Values of the parameters used for the first estimation on the return of the first stage

Flight path		
γ_0	90	°
γ_{tb}	25	°
Engine		
I_{sp}	275	s
T	400	kN
m_{prop}	11700	kg
Geometry		
m_{tot}	16000	kg
m_s	1700	kg
S	2.01	m^2
C_d	0.7	-

Using these values and the formulae given in Section 2.1 the following figures are made. In Figure 2.4 the velocity versus the time is shown. The second figure, Figure 2.5, shows the altitude of the first stage versus vertical distance travelled. In Figure 2.6 the Mach number and velocity reached are shown versus the altitude of the first stage. The last figure, Figure 2.7, in this series gives the temperature obtained and the altitude

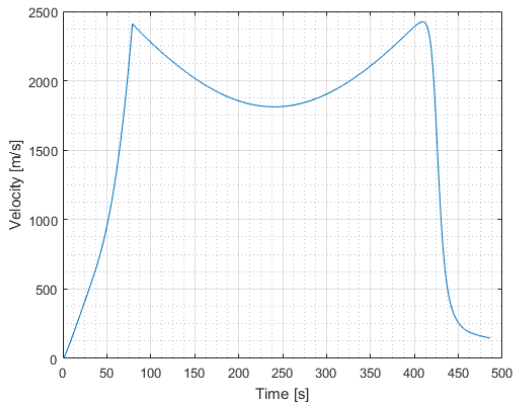

Figure 2.4: Results boundary script, Velocity vs Time diagram

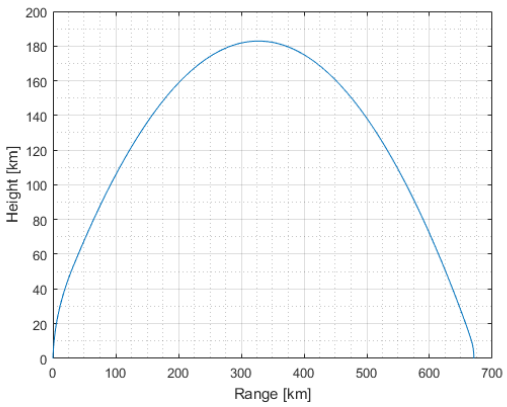

Figure 2.5: Results boundary script, altitude vs Range diagram

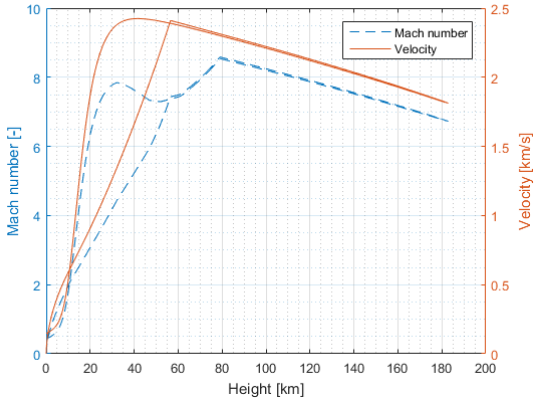

Figure 2.6: Results boundary script, Mach number and Velocity vs Height

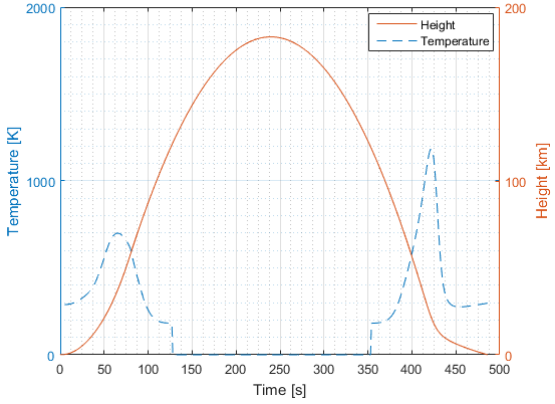

Figure 2.7: Results boundary script, Temperature and Height vs Time

reached versus the time since launch.

In these figures it can be seen that the first stage will accelerate to 2.331 km/s and bring the rocket to an altitude of around 50 km. At this point the first stage will separate from the rest of the rocket. The first stage will have after separation a vertical and horizontal velocity. The vertical velocity will bring the stage to an altitude of 183 km. At this point, the culmination point, the system still has a vertical velocity of 1.8 km/s. The first stage will decrease its altitude again and increase the velocity. With increasing the velocity the temperature of the wall will increase again. Due to the increasing density and so increasing drag the first stage will now be decelerated. A bit below the 20 km the density of the atmosphere will increase such that the vertical velocity will reduce even more. After 486 second and 670 km further the first stage will crash with 148 m/s onto the ground or water.

The impact point has been calculated with a range of numbers. The parameters used can be found in Table 2.3. The first parameter varied is the launch azimuth, this angle will influence the spread in the North-East South-West line. The second parameter, the flight path angle at launch will influence the range covered by the first stage. The last parameter, the specific impulse will also influence the range covered. The results can be found in Figure 2.8.

The results in Figure 2.8 show that if the first stage is not equipped with any deceleration mechanisms it will crash onto the sea between Norway and Jan Mayen. Jan Mayen is a volcanic island in the Arctic Ocean and is part of Norway. Between Jan Mayen en Norway partly the waters belong to Norway and are partly international ground.

Table 2.3: Parameters for calculating the impact point using 2DOF simulation

Parameters for calculating impact point

parameter	begin & end value	step size	unit
Ω	35-50	5	deg
γ_0	81-90	1.8	deg
I_{sp}	260-280	5	s

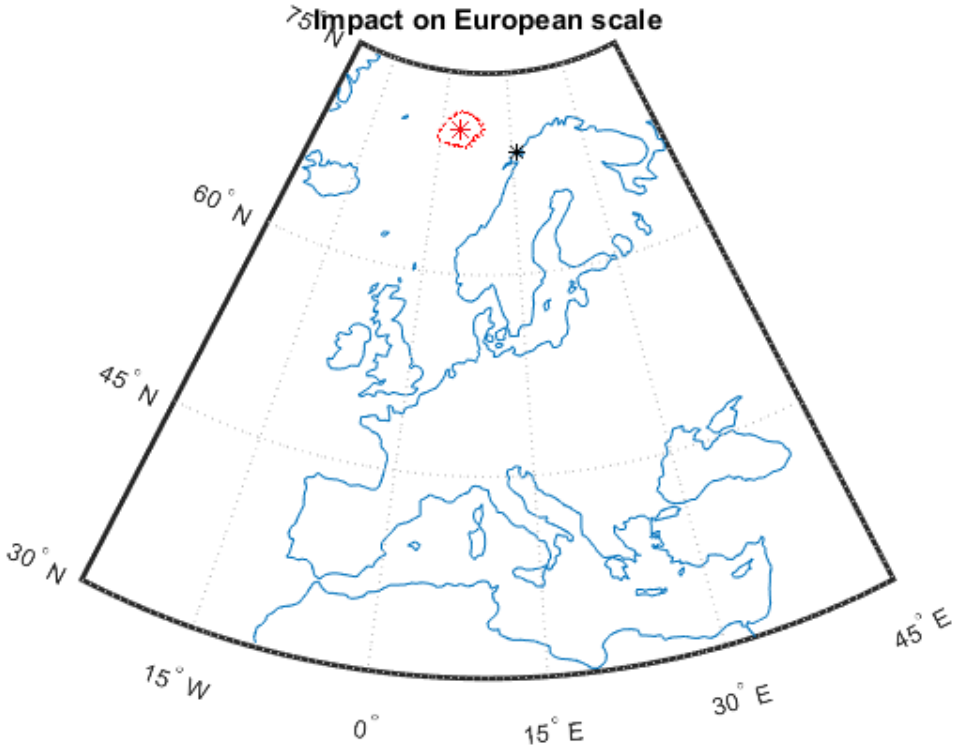

Figure 2.8: Impact point first stage

2.4. CONCLUSION

Using the results found it can be concluded that a recovery mechanism is needed as 148 m/s is too fast for a first stage to survive. The temperatures achieved during the descent are very high and the velocity should be controlled. Furthermore without decelerating the system will have an impact zone between Norway and Jan Mayen, which is Norwegian and international territory. This means that Norwegian and international agreements should be followed up for the recovery. Due to the distance to the coast a water landing is advised.

3

Recovery Designs

In the former chapter it was investigated that a recovery mechanism is needed to land the first stage safely. The first stage can be recovered in multiple ways. In the literature review a trade-off had been made of the different systems. Two of the candidates were equipped with wings. After a discussion with the NLR it was decided to not take these options into account. It was predicted that the wings of the first stage would first of all generate too much drag, and would increase the weight of the first stage much. The second factor was the needed certification of a winged vehicle. In this thesis work the three remaining mechanisms will be considered, being; a parachute system, retro-propulsion and an inflatable aerodynamic decelerator. These mechanisms are discussed in Section 3.1. Using these mechanisms, seven different configuration are designed and explained in the Section 3.2.

In this section, the recovery will be considered as the flight phase from separation to 100 meters above the ground or sea level. First the best recovery mechanisms will be found before the landing mechanisms will be taken into account. The landing mechanisms are dependent on the recovery mechanism. The landing itself will be considered in Chapter 14.1.2.

3.1. Recovery mechanisms

Three different deceleration mechanisms are used in the different configurations. The different configuration are introduced in this section.

Parachute system

The first concepts of a parachute were already shown by Leonardo da Vinci, who designed an earliest type of a parachute in 1495 [11]. Since then a lot has changed, the materials used and the applications for which a parachute would has been used, however the main idea has remained the same, using the aerodynamic drag to decelerate. The parachute has been used in multiple space missions, for example for a Soyuz capsule landing.

Two types of parachutes are used in this research, a drogue parachute and a parafoil. A drogue parachute will induce drag at an high altitude and high velocity to decelerate the vehicle [12]. A drogue parachute will also provide stability to the system and will help to deploy the parafoil. The parafoil has an aerodynamic cell structure which will inflated by the wind. In the Genesis sample return mission the parafoil was planned to be used to decelerate the vehicle such that the helicopter could catch the vehicle [13]. In the last decade research has been done to increasing the size of the parafoil, to be used on the X-38 Crew Return Vehicle, the International Space Station "lifeboat"[14]. The biggest parafoil produced and tested in this program has a total surface area of 696.8 square meters[15]. This surface ares will be used as maximum size in this research.

Retro-propulsion

Retro-propulsion will make use of the engines of the first stage. Where the upwards force produced by a rocket system will first accelerate the rocket to certain height, it will now decelerate the system by producing a force in the opposite direction of the velocity. This system has been used successfully by Blue Origin and SpaceX to land on solid ground or even on a ship [16][17].

INFLATABLE AERODYNAMIC DECELERATOR

An inflatable aerodynamic decelerator (IAD) is a device that inflates a large shield during descent to induce the aerodynamic drag and to protect the system from heat generation. The shield is made from an inflatable, flexible thermal protection system (TPS) structure. The potential value of the inflatable aerodynamic decelerator has been demonstrated in the successful flights of the Inflatable Re-entry Vehicle Experiment (IRVE)-2 and IRVE-3. In the IRVE-3 a HIAD of 6 meter was produced and successfully testes[18]. This size will be used as maximum diameter in this research. The development of this technology is still on going and is funded by NASA's Office of Chief Technologist's Game Changing Program [19].

3.2. RECOVERY CONFIGURATIONS

The recovery mechanisms introduced in Section 3.1 are used to design seven different configuration, explained in this section. For all configurations a schematic drawing is made and is shown at the end of this section.

3.2.1. CONFIGURATION 1

The first recovery design is making use of retro-propulsion. During the ascent phase the engine will be used to climb and accelerate. After separation the stage will turn around with its engine pointed into the velocity vector direction. The engine will then be used to slow down the system and land the first stage softly. The engine will only be fired once. A schematic drawing of this configuration can be found in Figure 3.1.

3.2.2. CONFIGURATION 2

The second recovery design is similar to configuration 1. After separation the stage will again be turned and the engine will be used to decelerate the first stage. However in this configuration two different engine burns will be used. The first engine burn will be done to decelerate before the atmosphere is reached. This to decrease the loads the first stage will encounter in the atmosphere. The second burn will be used to land the first stage softly. In Figure 3.2 a drawing of this configuration can be found.

3.2.3. CONFIGURATION 3

The third configuration will make use of two different deceleration mechanisms, retro-propulsion and a parachute system. The first part is again similar to configuration 1 and configuration 2. After separation the first stage will turn around with its engine pointed towards the velocity vector. The engine will then be used to decelerate the system before entering the atmosphere. This will be done to make sure the first stage will not encounter too high G-loads and temperature. The first stage will slow down and at an altitude of around 20 km the drogue parachute will deploy. The system will reduce its speed further till an altitude of 3 km. At this altitude the parafoil will be deployed. The parafoil will make sure the system will land safely. An overview of this procedure has been sketch and shown in Figure 3.3.

3.2.4. CONFIGURATION 4

The next configuration will make use of two different deceleration mechanisms, retro-propulsion and an inflatable aerodynamic decelerator. First, retro-propulsion will be used to decelerate the system before entering the atmosphere. The IAD will then inflate and make sure that the heat load can be withstand. The IAD will decrease the velocity of the system further by inducing drag. The IAD will provide a safe landing. A schematic overview of this recovery technique is shown in Figure 3.4.

3.2.5. CONFIGURATION 5

The fifth configuration considered will only make use of the inflatable aerodynamic decelerator. The hypersonic inflatable aerodynamic decelerator has been designed to land a heavy vehicle on Mars and should therefore be able to handle high entry velocities. In this configuration the IAD will inflate after separation. The IAD will induce enough drag to decelerate and make sure the maximum G-load is not reached. The IAD will also make sure the system will not burn up in the atmosphere. The IAD will not be discarded before landing. The IAD will therefore also decelerate the system enough to enable a safe landing. An overview of this configuration can be found in Figure 3.5.

3.2.6. CONFIGURATION 6

Configuration 6 will again make use of the inflatable aerodynamic decelerator, this time in combination with a parachute system. The IAD will inflate after separation to induce drag and slow the system down. The IAD will be discarded at a certain point. Once the system has reached 20 km the drogue parachute will be deployed. The drogue parachute will slow the first stage further down. The system will now decrease its altitude further to an altitude of 3 km. At an altitude of 3 km the parafoil will be deployed. The parafoil system will provide a safe landing of the first stage. Figure 3.6 shows a schematic drawing of this concept.

3.2.7. CONFIGURATION 7

The last recovery design, configuration 7 will make use of two different recovery mechanisms. This design will make use of the inflatable aerodynamic decelerator and retro propulsion. After separation the IAD will be inflated. This system will increase the aerodynamic drag experienced and will decelerate the system. It will make sure that the system will not experience too high G-loads or too high temperatures. Once in the atmosphere, the IAD will be discarded. Just before touch down the retro-propulsion system will fire to reduce the velocity further and to land the system safely. An overview of the last configuration can be found in Figure 3.7.

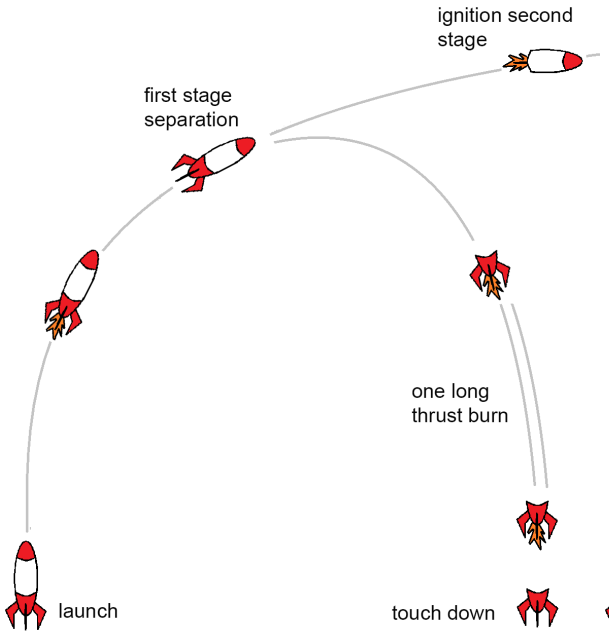

Figure 3.1: Schematic drawing of process configuration 1

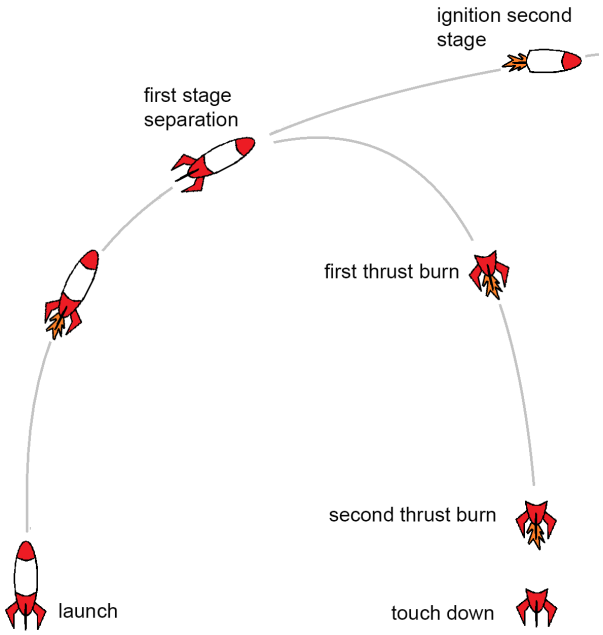

Figure 3.2: Schematic drawing of process configuration 2

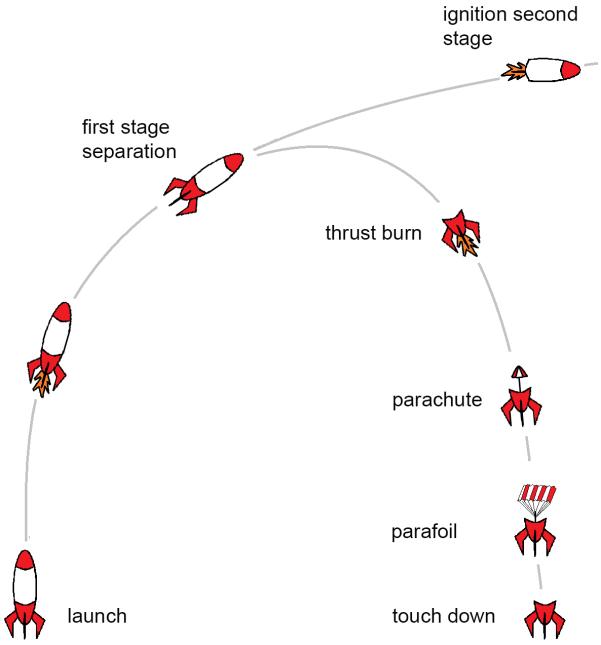

Figure 3.3: Schematic drawing of process configuration 3

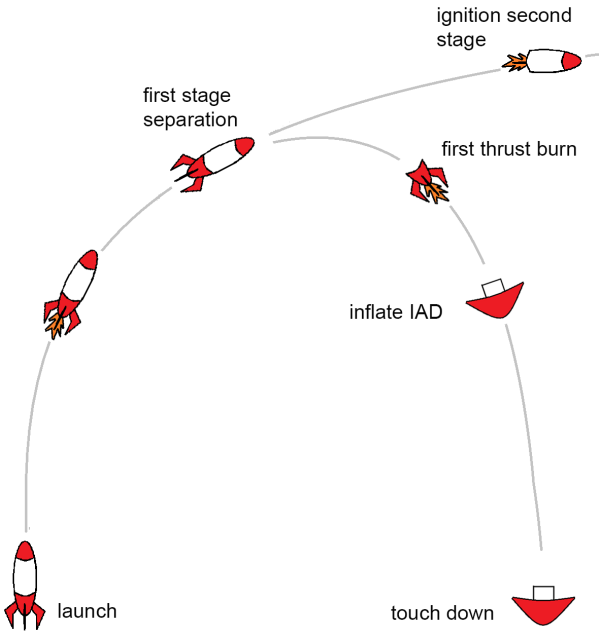

Figure 3.4: Schematic drawing of process configuration 4

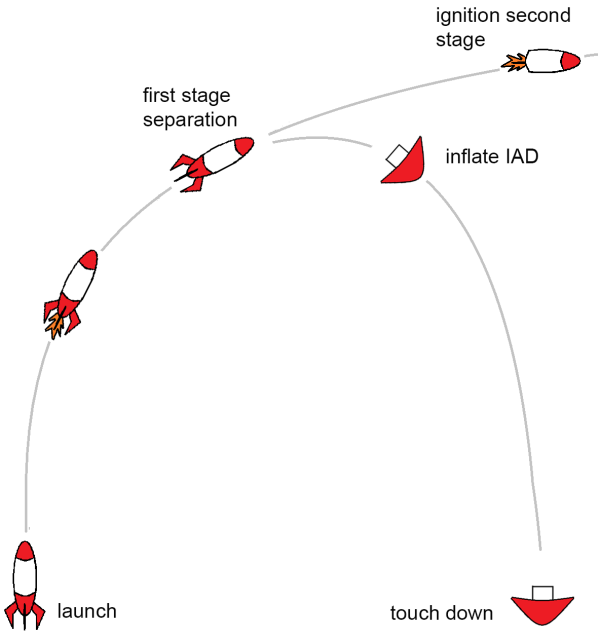

Figure 3.5: Schematic drawing of process configuration 5

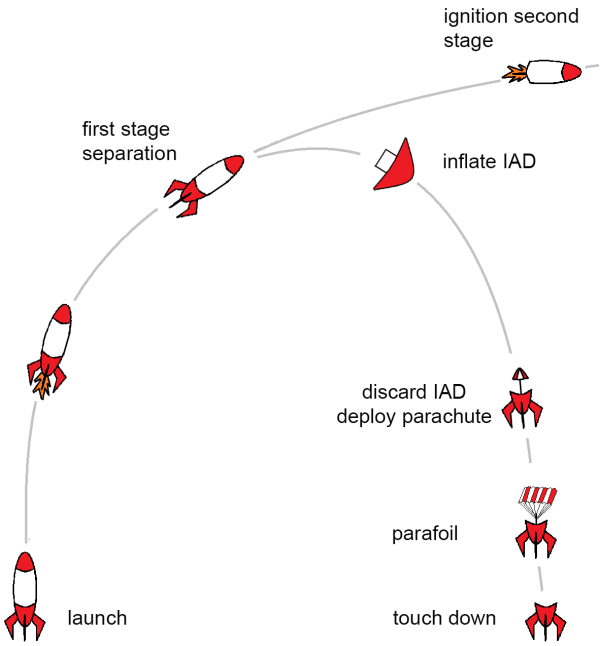

Figure 3.6: Schematic drawing of process configuration 6

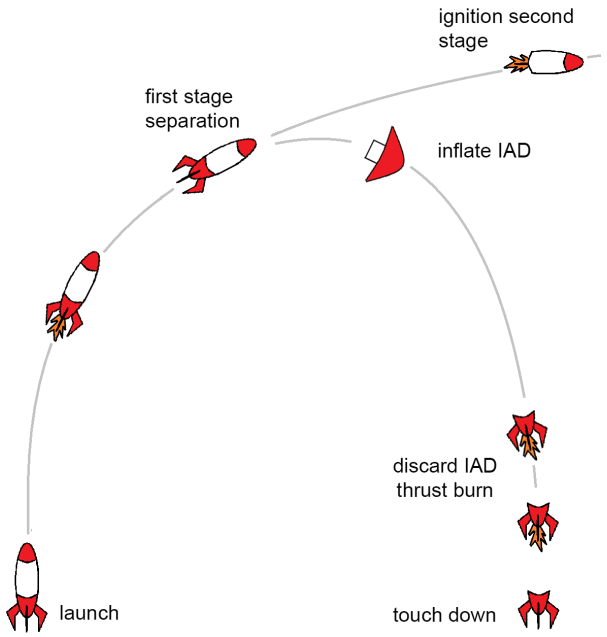

Figure 3.7: Schematic drawing of process configuration 7

4

SOFTWARE AND METHOD

To design the best possible configuration a tool is needed that can optimise the configurations. In this chapter the software constructed to obtain the best configuration will be discussed. First a general overview of the software tools will be given in Section 4.1. The modules used in the software will be described in detail in Section 4.2. The next section, Section 4.3 will describe the optimiser used to optimise the different configurations. Once the different designs are optimised a trade-off is needed. The last section, Section 4.4, will explain that trade-off criteria will be used.

4.1. OVERVIEW

To understand what kind of tool is needed, first the specifications are needed. The tool should be able to give a mass estimation of the different optimised configurations. Once all configurations are optimised, the different configurations will be compared by mass, cost, and operational flexibility. The different configurations will be constructed using a combination of one or two different decelerate mechanisms. The different mechanisms used are propulsion, a hypersonic aerodynamic decelerator and a parachute/parafoil, as discussed in Chapter 3.

To run the tool three different inputs are needed. First of all, the tool needs to know which configuration will be optimised. Every configuration has its own constraints. For example, the maximum velocity for opening a parachute needs to be known. These system constraints are also needed as input for the tool. The third input of the system is the constraints set by the project. This includes the velocity, height, and flight path angle at separation, but also the geometry and masses of the first stage. These inputs will be used by the tool, to compute the three different outputs.

The three different outputs will consist first of all out of the calculated masses of the different systems. The second output is the impact point of the first stage. The third output will give the optimised design variables. Which design variables are used will differ from configuration to configuration. The variables for the different parts of the configuration can be found below.

Propulsion

- Start and end time (t_{start}, t_{end})
- Thrust angle ($\theta(t)$)
- Thrust force ($F(t)$)

Hypersonic inflatable aerodynamic decelerator

- Start and end time (t_{start}, t_{end})
- Surface area (S)

Parachute/Parafoil

- Surface area drogue parachute (S_{dp})
- Surface area parafoil (S_{pf})

In Figure 4.1 an overview can be found of the inputs and outputs of the tool.

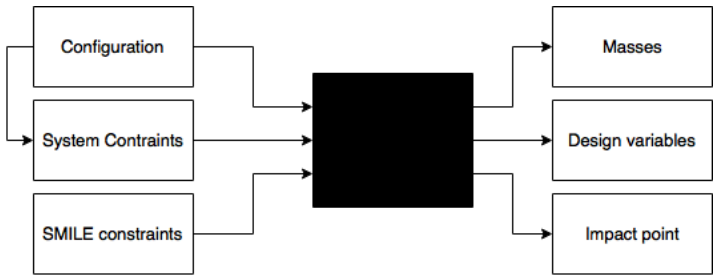

Figure 4.1: Black box overview software

4.2. MODULES

To compute the output discussed in Section 4.1 and fill the black box in Figure 4.1 different modules are needed. To compute a correct estimate of the impact point the movement of the first stage is needed in three dimensions. To take into account the rotation around the different axes, six degrees of freedom are needed. Optimising a 6DOF (Degrees of Freedom) system will need much more computing time than for a 3DOF system. Therefore it has been chosen to make two different tools, one optimiser and one simulator. The optimiser will be used to calculate the most optimal design variables. This optimiser will optimise to a minimum system mass of the chosen configuration. The optimiser will make use of 3DOF. The design variables found will then be used in a simulator which will calculate the masses and the impact point of the system. The simulator will make use of 6DOF.

The optimiser and simulator will consists out of almost the same modules. The modules found in the optimiser can be seen as a simplified version of the simulator. The main differences are that the simulator will use 6DOF and a control system. This will make the 6DOF system a bit more complex, as the geometry, in terms of moment of inertia, centre of gravity and centre of pressure, are needed. Because the simulator is the most extended of the two, a diagram of this system can be found in Figure 4.2.

In Figure 4.2 the different modules can be found, which will be used in the 6DOF simulator. The theory of these modules will be discussed in Chapter 5 to 8. In this section it will be explained how these modules are used in the software. For every module the differences between the 3DOF integrator and the 6DOF simulator will be given.

ENVIRONMENT

The module on environment will obtain the density and temperature of the environment using the location of the system. Using the temperature, the speed of sound will be calculated. Next to the information on the atmospheric properties, the gravitational force will also be calculated in this module. The gravitational force in this module will be calculated in the inertial frame, discussed in Section 5.1. For the six degrees of freedom simulator the zonal and meridional winds will be included in this module. More information on the content of this module can be found in Chapter 6.

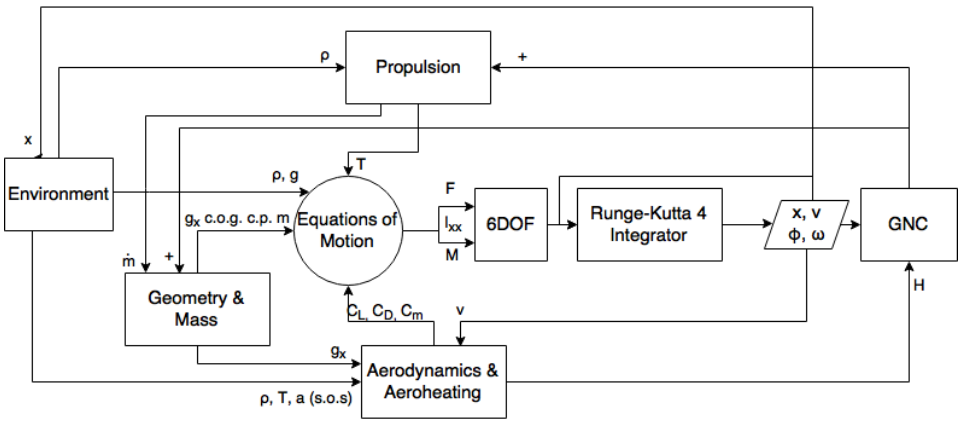

Figure 4.2: Simulator flow diagram

PROPULSION

The module on the propulsion of the system will produce both the thrust forces during the ascent trajectory and the forces produced during the descent phase. For the descent phase this module will only produce a force if a propelled design is tested. This module uses the thrust, specific impulse, pressure of the atmosphere, time, burn time and pitch to calculate the thrust force produced in the body system. This module will also give the mass flow rate needed by the *Geometry & Mass* module to calculate the mass of the system. More information on the propulsion module can be found in Section 7.4.1.

GEOMETRY & MASS

The module on geometry and mass calculates the geometry parameters and mass parameters of the system. For the three degrees of freedom optimisation this includes the size and the masses of the system. For the six degrees of freedom simulation the centre of gravity, mass moments of inertia are also included. More details on the geometry and mass can be found in Chapter 7.

AERODYNAMICS & AERO HEATING

The module on aerodynamics and aero heating calculates the aerodynamic force coefficient obtained by the system. The three degrees of freedom optimiser will only use the lift and drag forces. For the six degrees of freedom simulator the moment coefficient produced by the aerodynamic force will also be calculated. The module is as well responsible for the checking the heating of the system. If the system would heat up too much the first stage might burn up in the atmosphere or become too damaged to recover. More information on the *Aerodynamics & Aero heating* module can be found in Chapter 8.

CONTROL

For the six degrees of freedom a control mechanism will be used. The control mechanism will be used to turn the vehicle and to make sure the angle of attack and side slip will be controlled. The control of the system will be done by making use of cold gas thrusters. By making use of the thruster a moment will be produced. The moment produced will result in a rotation and the vehicle will re-orientate itself. In Chapter B and Subsection 14.1.1 the control system will be designed.

EQUATIONS OF MOTION

The module on the Equations of Motion collects all the different forces (and moments) to sum up and calculates the accelerations. The forces are collected in the body frame and will be transformed to Earth-Centred Inertial (ECI) frame. In the ECI-frame the forces are integrated. For more information on the Equations of motion and reference frames used see Section 5.2.

RUNGE KUTTA-4 INTEGRATOR

The trajectory will be integrated by making use of the Runge Kutta-4 integrator. The integrator will explained in detail in Section 5.3.

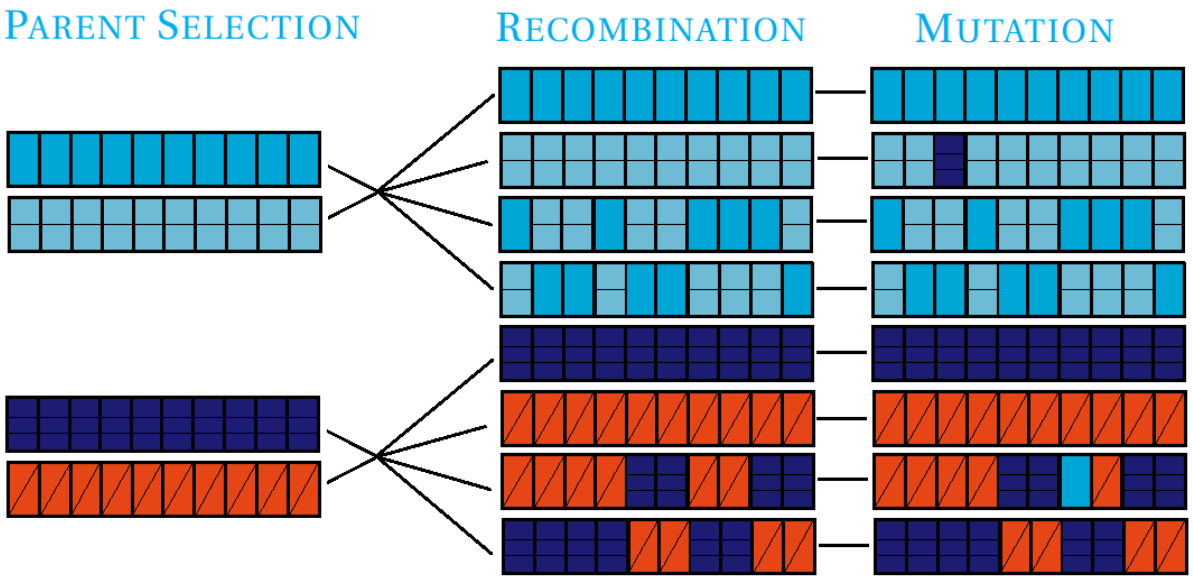

Figure 4.3: Schematic overview of the genetic algorithm

4.3. OPTIMISER

The different designs are optimised to the minimum weight. This optimisation has been done by using a Genetic Algorithm. Genetic Algorithm (GA), is a gradient-free optimiser. A gradient-free algorithm does not need the gradient of the function, and is therefore useful in this research, as the gradient of the function is not known. The genetic algorithm is based on the Theory of Evolution of Charles Darwin, Survival of the Fittest[20]. A population is defined and this population will evolve by propagation and mutation. The way of propagation, random cuts, cross over, but also the parents' selection can be chosen by the user. The following paragraphs will explain the structure of the Genetic Algorithm used. Figure 4.3 shows a schematic overview of the process in a genetic algorithm.

INITIAL POPULATION

Taking into account the boundaries of the variable an initial population will be formed. This will be done by making use of a pseudo-random number generator. The numbers are represented in bit-strings.

PARENT SELECTION

Once the initial population has been found the parents will be selected. The parents with the best fit, the lowest function value, will have the biggest chance to be chosen. If the two parents are equal, one of the parents will be replaced by another parent.

RECOMBINATION

If the parents are known they will create a family. Both parent bit-strings are randomly cut in nine pieces; with those eighteen pieces two offspring are formed. The family now consists out of four numbers, two parents and two children. In Figure 4.3 an example with six pieces for the first two parents, and four pieces for the lower two parent, is shown.

MUTATION

In the next step both the parents and children have a change of mutation of one of their bits. The change of mutation is 0.01%. This has been simulated by using the pseudo-random generator. A mutation will take please if the round off value of the pseudo-random number equals 0.0001. If this is the case a bit will change from 0 to 1 or vice versa.

SELECTION
A family has now been formed including possible mutations. The function values of all family members are calculated and will be compared. The best two in the family are now selected and will be used in the next generation.

FILL POPULATION
This procedure will be repeated until a full new generation is created. To create a full new generation this procedure needs to be executed the number of half of the population.

FILL GENERATION
Once the whole population for the new generation is filled, the procedure will start over again. The loop will be repeated till the minimum found does not change more that 0.01% than the minimum of two generations before. These two steps are chosen to make sure that the model will not stop because two generations will have the same minimum 'by accident'. The script will also stop if more than 100 generations are needed to reach convergence.

4.4. TRADE-OFF
Once the software has been used to optimise the different configuration to minimum mass, the different configuration need to be compared. As been described before cost is one of the major trade-off criteria, however more trade-off criteria are of importance. Four different criteria will be used: the cost, weight, operational flexibility and sustainability. All criteria will be considered below.

COST
The first trade-off criterion considered is the cost of the recovery. The cost of the recovery will in the end determine if recovery will be cost beneficial. The lower the extra cost needed for recovery, the fewer launches are needed to become cost beneficial. The cost calculations will be explained in Chapter 9.

MASS
The second trade-off criterion is the extra weight of the system. The heavier the system the more propellant is needed for lift-off. This will result in a bigger and more expensive launcher or in less payload capacity. In this way the weight of the system will directly influence the cost of the launcher. In other words, the lighter the recovery system, the better. The mass calculations are shown in Chapter 7.

OPERATIONAL FLEXIBILITY
The third trade-off criterion is the operational flexibility. If the launcher is more flexible more launches can be performed a year. In this way the more flexible the system the cheaper the recurring cost will be. The second aspect of the operational flexibility, is the impact on the launcher. The more adaption should be made to make the first stage recoverable, the less attractive this option will be. More adaptions will means more spending more energy and money in making the first stage recoverable.

SUSTAINABILITY
The last criterion is sustainability of the recovery. This aspect is not directly linked to the cost of the launcher. However if in the end two configurations with more or less the same score on cost, weight, and operational flexibility is found, the system with the least amount of impact on the environment will be chosen.

5

TRAJECTORY

To know where the system is at what time, the trajectory of the system should be known. In this chapter it will be explained how the trajectory is calculated in the optimiser and simulation tool. First the reference frames will be explained in Section 5.1. Once the frames are known the equations of motion are explained in Section 5.2. In this section both the equations used for the optimiser, in three degrees-of-freedom, and for the simulator in six degrees-of-freedom are given. Once all forces and moments are known, they need to be integrated. Integration will be done by making use of the Runge Kutta-4 method, explained in Section 5.3

5.1. REFERENCE FRAMES

A reference frame is a coordinate system in which the properties, position, orientation of the object are defined. At least one frame is needed to describe the motion or position of a system. Newton's laws are applied in an inertial reference frame and therefore all forces and movements should be known in this frame. The reason to use multiple reference frames is two-fold. The first reason is that the definition of a vector makes more sense in one particular reference frame than in another frame. The second reason is that additional frames will make the derivation of the equations of motion easier. Certain motions are more easily described in one particular reference frame before a translation is made to the reference frame for which the equations of motion are derived [21].

In the tools different reference frames are used, which will be discussed here. Three different kinds of frames are specified. The first frame is the inertial reference frame. The second frame is fixed to the Earth, the so called Earth-fixed frames. The third kind of frames are attached to the vehicle. Three different vehicle-fixed frames are used in the tools, the local-level frame, the body frame, and the aerodynamic frame.

EARTH-CENTRED INERTIAL (ECI)

The first frame of the Earth-fixed frames is the inertial reference frame, called the Earth-Centred Inertial (ECI) reference frame. This frame is a right-handed orthogonal axis-system. The centre of mass of the Earth is considered as the origin of this frame. The z-axis is directed to the North along the spin axis of the Earth. The x-axis is pointed through the equator at the point of the ecliptic, also known as the vernal equinox.

EARTH-CENTRED EARTH-FIXED (ECEF) REFERENCE FRAME

The second frame of the Earth-fixed frame is the Earth-centred, Earth-fixed reference frame (ECEF). This frame is also a right-handed coordinate axis-system. The z-axis is again pointed to the North along the spin axis of the Earth. The x-axis is pointed to the Greenwich meridian. This means that the frame is rotating around the z-axis in respect to the ECI-frame.

LOCAL-LEVEL REFERENCE FRAME

The location of the origin O of this frame, sometimes also referred to as the vertical frame, is chosen as the vehicle's centre of gravity. This plane is tangent to the Earth surface. The X-axis is directed to the north and the negative z-axis is directed to the centre of the Earth.

BODY-FIXED REFERENCE FRAME

The second vehicle-fixed frame is the body-fixed reference frame. The centre of mass is chosen to be the origin of the frame. The frame is a right-handed orthogonal axis-system with the origin at the vehicle's reference point. The reference frame remains fixed to the body even in perturbed motion. The X-axis is in the symmetry plane of the vehicle and points forward. The Z-axis also lies in the symmetry plane and points up.

AERODYNAMIC REFERENCE FRAME

The aerodynamic reference frame is coupled to the air velocity. The air velocity is the velocity of the centre of the mass relative to the undisturbed air [21]. The X-axis is in the direction of the air velocity. The Z-axis is in the symmetry plane of the aircraft pointed up. The orientation of the frame with respect to the body frame is defined by two angles, the angle of attack and the aerodynamic side slip angle.

5.1.1. TRANSFORMATION MATRICES

As described above different reference frames are used. To express all movements and forces in the inertial frame the different frames need to be transformed. The transformation from one frame to another can be done by making use of Euler angles. Euler angles are often used as the orientation and the angles can easily be visualised. Euler angles do have the disadvantage of suffering from singularities. Therefore all singularities will be discussed for the different transformations. Using the Euler angles and the specific rotation sequences, one can set up so-called transformation matrices, which will be discussed in this subsection.

To use the transformation matrices information is needed regarding the orientation of the different reference frames with respect to each other. The transformation matrices do not contain any information on the translations. The different transformation matrices used in the tools are given below.

TRANSFORMATION FROM ECI TO ECEF

The transformation from the ECI reference frame to the ECEF reference frame can be done by using one single rotation. This rotation is about z-axis over an angle of $\Omega_t t_0$. Where Ω_t is the rotational speed of the Earth and t_0 is the stellar time of the point 0.

$\Omega_t t_0$ is always positive, is fully repetitive, and has a range of:

$$0 \leq \Omega_t t_0 < 2\pi$$

The transformation matrix can be written as

$$\mathbb{T}_{EI} = \begin{bmatrix} cos\Omega_t t_0 & sin\Omega_t t_0 & 0 \\ -sin\Omega_t t_0 & cos\Omega_t t_0 & 0 \\ 0 & 0 & 1 \end{bmatrix} \tag{5.1}$$

TRANSFORMATION FROM ECEF TO LOCAL-LEVEL FRAME

The transformation from the ECEF-frame to the local-level frame will need two rotations. The first rotation is with the angle τ around the z-axis. The second rotation is around the y-axis with an angle of $\frac{\pi}{2} - \delta$. The angles τ and δ are respectively the longitude and latitude of the position of the vehicle.

τ is positive if the vehicle position is east of the Greenwich meridian and negative when west. δ is positive if the system is on the northern hemisphere, and negative on the south hemisphere. The ranges of the angles are shown below. On the poles the transformation will reach a singular point.

$$-\pi \leq \tau < \pi$$
$$-\frac{\pi}{2} \leq \delta < \frac{\pi}{2}$$

The transformation matrix found is shown in Equation 5.2.

$$\mathbb{T}_{LE} = \begin{bmatrix} -sin\delta & 0 & cos\delta \\ 0 & 1 & 0 \\ -cos\delta & 0 & -sin\delta \end{bmatrix} \begin{bmatrix} cos\tau & sin\tau & 0 \\ -sin\tau & cos\tau & 0 \\ 0 & 0 & 1 \end{bmatrix} \tag{5.2}$$

TRANSFORMATION FROM LOCAL-LEVEL TO BODY FRAME

The transformation from the local-level frame to the body frame is done with three different transformations, first a rotation with the yaw angle ψ about the z-axis. Then the pitch angle (θ) is rotated around the y-axis. To conclude a rotation of the roll angle ϕ around the x-axis is performed.

The angles are all defined following the right hand rule. The ranges of the angles are found below.

$$-\pi \leq \psi < \pi$$

$$-\frac{\pi}{2} < \theta < \frac{pi}{2}$$

$$-\pi \leq \phi < \pi$$

Using the yaw, pitch and roll angle, the transformation matrix shown in Equation 5.3 is found.

$$\mathbb{T}_{bL} = \begin{bmatrix} 1 & 0 & 0 \\ 0 & cos\phi & sin\phi \\ 0 & -sin\phi & cos\phi \end{bmatrix} \begin{bmatrix} cos\theta & 0 & -sin\theta \\ 0 & 1 & 0 \\ sin\theta & 0 & cos\theta \end{bmatrix} \begin{bmatrix} cos\psi & sin\psi & 0 \\ -sin\psi & cos\psi & 0 \\ 0 & 0 & 1 \end{bmatrix} \tag{5.3}$$

TRANSFORMATION FROM BODY FRAME TO AERODYNAMIC FRAME

The transformation from the body frame to aerodynamic frame is executed with two rotations. The first rotation is the rotation around the y-axis with the angle α, being the angle of attack. The second rotation is around the z-axis with an angle of β, being the side slip angle.

The angles are defined positive following the right hand rules with the following limits:

$$-\pi < \alpha < \pi$$

$$-\frac{\pi}{2} \leq \beta < \frac{\pi}{2}$$

The angle of attack can be calculated with Equation 5.4 using the air velocity in 'x' and 'z' direction. The angle of side slip can be calculated with Equation 5.5 with the air velocity in 'y'-direction and the norm of the velocity.

$$\alpha = tan^{-1}(\frac{w^b}{u^b}) \tag{5.4}$$

$$\beta = sin^{-1}(\frac{v^b}{V}) \tag{5.5}$$

Using the angle of attack and the angle of side slip the following transformation matrix can be found, shown in Equation 5.6.

$$\mathbb{T}_{ab} = \begin{bmatrix} cos\beta & sin\beta & 0 \\ -sin\beta & cos\beta & 0 \\ 0 & 0 & 1 \end{bmatrix} \begin{bmatrix} cos\alpha & 0 & sin\alpha \\ 0 & 1 & 0 \\ -sin\alpha & 0 & cos\alpha \end{bmatrix} \tag{5.6}$$

5.2. EQUATIONS OF MOTION

The Equations of Motion (EOM) is a set of differential equations which will be used to describe the dynamics of the vehicle. The laws of Newton form the bases for the Equations of Motion and are described below.

- **Newton's 1^{st} law**: A body is in rest or moves at a constant velocity, unless a force acts on the body.
- **Newton's 2^{nd} law**: If a force acts on a body, the force is equal to the time derivative of the momentum.
- **Newton's 3^{rd} law**: If two bodies are at rest, or moving with a constant velocity, exert forces upon one another, the force of the first body is equal to the magnitude but opposite in direction to the force of the second body.

Newton's laws are applied in an inertial reference frame. Transformations to the inertial frame has been described as in Section 5.1. Assuming a rigid body and not considering the effects of rotating masses the following formula for the translation can be used, Equation 5.7.

$$F^I_{ext} = m\frac{d^2 r^I_{cm}}{dt^2} + 2\Omega^I_{bI} \mathrm{x} \int_m \frac{\delta \tilde{r}}{\delta t} dm + \int_m \frac{\delta^2 \tilde{r}}{\delta t^2} dm \tag{5.7}$$

As mentioned before for the optimiser a three degrees of freedom system will be used, and for the simulator a six degree of freedom will be used. This means that for the simulator also the rotational motion needs to be taken into account. Rotational motion with respect to an inertial space is described in Equation 5.8. In this equation the first term is the apparent moment due to the angular acceleration of the vehicle with respect to the inertial frame. The second term is the apparent moment due to the angular velocity of the vehicle with respect to the inertial frame. The Coriolis moment is found in the third term and the relative moment in the fourth term.

$$M^b_{cm} = \int_m \tilde{r} \mathrm{x} (\frac{d\Omega^b_{bI}}{dt} \mathrm{x}\, \tilde{r}) dm + \int_m \tilde{r} \mathrm{x} [\Omega^b_{bI} \mathrm{x} (\Omega_b I^b \mathrm{x} \tilde{r})] dm + 2\int_m \tilde{r} \mathrm{x} (\Omega^b_{bI} \mathrm{x} \frac{\delta \tilde{r}}{\delta t}) dm + \int_m \tilde{r} \mathrm{x} \frac{\delta^2 \tilde{r}}{\delta t^2} dm \tag{5.8}$$

5.3. INTEGRATION

Using the Equations of motion presented in Section 5.2 the velocity and position can be integrated. The integration will be done with the Runge Kutta-4 method (RK4). RK4 is a single step, explicit method. RK4 method uses four different approximations to describe the change of the parameters during one time-step. These different approximations are then weighted, averaged and used to propagate. Advantages of the RK4 method are the simplicity and stability of the method. Next to, it has a good round-off error accumulation. A disadvantage of this method is that step-size should be obtained by a trial-and-error process, besides; the CPU time of this method can be quite large. The Runge Kutta-4 method can be described using Equation 5.9 and 5.10, where the different constants (k_1-k_4) are obtained using Equations 5.11 to 5.14. And the h is the step size of the integration [22].

$$x(t_0 + h) \approx x_0 + h\Phi = \eta(t_0 + h) \tag{5.9}$$

$$\phi_{RK4} = \frac{1}{6}(k_1 + 2k_2 + 2k_3 + k_4) \tag{5.10}$$

$$k_1 = f(t_0, x_0) \tag{5.11}$$

$$k_2 = f(t_0 + \frac{h}{2}, x_0 + h\frac{k_1}{2}) \tag{5.12}$$

$$k_3 = f(t_0 + \frac{h}{2}, x_0 + h\frac{k_2}{2}) \tag{5.13}$$

$$k_4 = f(t_0 + h, x_0 + hk_3) \tag{5.14}$$

6

ENVIRONMENT

The environment of the launcher and recovery mechanism influences the trajectory very much. In this chapter three different aspects of the environment will be treated. The first subject is the atmospheric model, considered in Section 6.1. The second section, Section 6.2, discusses the gravitational models used in the optimisation and simulation. For the 6DOF simulation a wind model is used to take into account the zonal and meridional winds, which will be explained in Section 6.3.

6.1. ATMOSPHERIC MODEL

The first model explained in this chapter is the atmospheric models. The atmospheric model should provide the density, pressure, speed of sound and the temperature. Temperature and density will be calculated by making use of the NRLMSISE-00 model. The NRLMSISE-00 is an empirical model of thermospheric composition and temperature. This model is based on data on total mass densities from satellite accelerometers, satellite orbits, temperature determined by incoherent scatter, and molecular oxygen densities from the SMM solar occultation experiment [23]. A verified Matlab script of the NRLMSISE-00 model in the aerospace toolbox has been used. In comparison with other models, produces this model predictions for the higher altitude atmospheric parameters.
The speed of sound can be calculated with Equation 2.10. The pressure of the environment can be calculated by assuming an ideal gas using Equation 6.1. The $R_{specific}$ is the specific gas constant, being 287.058 J/(kg K).

$$P = \rho * (T * R_{specific}) \tag{6.1}$$

6.2. GRAVITATIONAL MODEL

As for the atmosphere, multiple models are available for the gravity field of the Earth. In this section three different models will be treated. The first one is a simple central gravity model. In this model the gravity is constant value at the same altitude for the whole trajectory.

Although the gravity will not change for different locations on the Earth , the gravitational attraction,F_{g_0} will not change with altitude. In Equation 6.2 the formula is given for a simple model. In Equation 6.3 the variation with height,h is taken into account. In these equations the G, gravitational constant, M, mass and R, radius are used.

$$F_{g_0} = \frac{GMm}{R^2}\hat{h} \tag{6.2}$$

$$F_g = F_{g_0}\frac{R_e^2}{(R_e+h)^2} = F_{g_0}\frac{1}{(1+\frac{h}{R_e})^2} \tag{6.3}$$

In reality the shape of the Earth is not a perfect sphere with a uniform mass distribution. To take into account the difference with respect to a perfect sphere a Spherical Harmonics model can be used. Using Spherical harmonics the gravity field is approximated by the normal gravitational potential (which can be explained as an infinite series of spherical harmonics) and generates the gravity vector in ECEF frame [24]. Another method to describe the gravitational field is by zonal harmonic representation. In this model the

variation of gravity with longitude is not taken into account. The variation with latitude is much bigger than with longitude due to the oblation of the Earth.

In Figure 6.1 the total gravitational acceleration found for the spherical and for the zonal model is found at a longitude of 69°. In this plot it can be seen that spherical harmonics will fluctuate around the zonal harmonics model. The spherical harmonics model is more accurate; however the difference with the zonal harmonics model is very small.

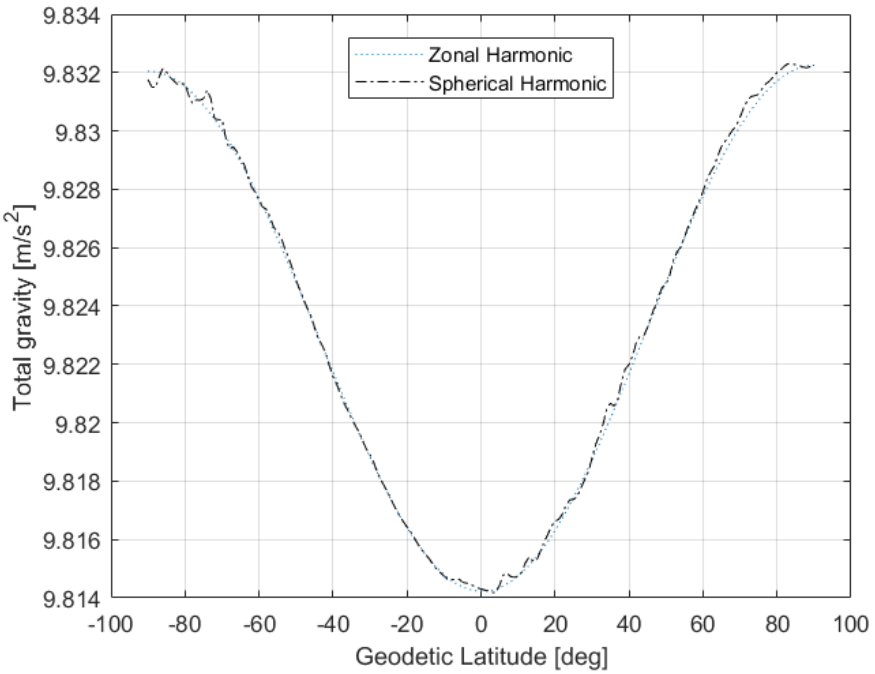

Figure 6.1: Comparison of spherical and zonal harmonics gravity model

The use of a spherical harmonics will take a lot of CPU time. During the construction of the tool it was found that the use of a spherical harmonics will take around 50 times as long as using a simple model as discussed above. During the optimisation of the system CPU time is of great importance. Therefore it has been decided to use a simple gravitation model for the optimiser. For the 6DOF simulator a zonal harmonic representation of planetary gravity has been used. The model used is a verified Matlab function. This model makes use of the default values of the model for the zonal harmonic coefficients (J_2,J_3,J_4) found in Table 6.1[25].

Table 6.1: Zonal gravitational values used

	Equatorial Radius [m]	Gravitational Parameter [m^3/s^2]	Zonal Harmonic Coefficients (J_2, J_3,J_4)
Value	6378.1363e3	3.986004415e14	[0.0010826269, -0.0000025323, -0.0000016204]

6.3. WIND MODEL

For the 6DOF simulation a wind model will be used to include the zonal and meridional winds. This has been done by making use of a validate Matlab routine of the U.S. Naval Research Laboratory Horizontal Wind Model.

The empirical model describes the atmosphere's vector wind fields from the surface to the exobase (450 km) as a function of latitude, longitude, altitude, day of year, and time of day. It is able to represent the variations of middle- and upper-atmosphere winds because they are predominantly driven by in situ solar heating under the periodic cyclical influence of the earth's rotation, tilt, and orbit around the sun [26].

7

GEOMETRY & MASS

This chapter will discuss the geometry and mass properties used. The overall geometry will be discussed and the different mass components. These elements will then be used to calculate the centre of gravity and the mass moment of inertia. The information found in this chapter is needed as input for the Equations of Motion and will also be used to calculate the aerodynamic properties of the vehicle explained in Chapter 8.

In the first section of this chapter the different elements concerning geometry and mass will be handled. The equations used to calculate the centre of gravity and the mass moment of inertia will be explained. Section 7.2 will follow with an in depth discussion about the layout of the whole launcher. The same will be discussed for the first stage in Section 7.3. The second part of this chapter will discuss the geometry and mass of the recovery mechanisms in Section 7.4.

7.1. GENERAL EQUATIONS

The equations needed to calculate the centre of gravity and the mass moment of inertia will be explained in this section. The equations explained in this section will be used to define the overall layout of the launcher and first stage in the next sections.
It will be assumed that the liquid propellant in the tanks are steady and will not move in the tank during one time step. In reality the propellant is sloshing around in the tank.

CENTRE OF GRAVITY

The centre of gravity is the point of an object where if a force is applied the object will translate in the direction of the force and no rotation will occur. The distribution of mass is balanced around the centre of gravity. The centre of gravity will be approached by a system of particles. This results in the following Equation for the calculation of the centre of gravity shown in Equation 7.1. The total amount of particles is denoted with n, the M is the total system mass, m_i and r_i are respectively the mass and the coordinate of the particle.

$$c.o.g. = \frac{1}{M}\sum_{i=1}^{n} m_i r_i \tag{7.1}$$

MASS MOMENT OF INERTIA

The second characteristic of the body considered is the mass moment of inertia. The mass moment of inertia is a tensor that determines the torque needed for a desired angular acceleration about a rotational axis. The higher the mass moment of inertia the more torque required to change the rotation of the body. The mass moment of inertia depends on the mass distribution of the body and can be calculated with Equation 7.2. The second moment of mass with respect to distance from an axis r integrating over the entire mass [27].

$$I = \int_Q r^2 dm \tag{7.2}$$

The mass moment of inertia is an extensive property, which means that the different moments can be added to calculate the total mass moment of inertia. The mass moment of inertia is always calculated around

a certain axis. By using the parallel axis theorem (Steiner's theorem) the mass moment of inertia can be calculated around any arbitrary axis parallel to the original axis[27]. The parallel axis theorem is shown in Equation 7.3. The mass moment of inertia calculated around its centre of gravity I_{cg} is used with the mass of the particle M and the distance between the two axes r.

$$I = I_{cg} + Mr^2 \tag{7.3}$$

For the some simple objects with geometric symmetry, one can determine the moment of inertia in an exact closed-form expression. In Appendix A a list of the closed-form expression used is shown.

7.2. LAUNCHER

The first part considered is the geometry of the whole launcher. The launcher has three different stages. The first stage will be re-used and is discussed in detail in Section 7.3. In this part of the chapter the recovery mechanisms will not be taken into account in the centre of gravity and mass moment of inertia calculations as it will only affect the properties slightly.

7.2.1. GEOMETRY

First the overall geometry will be considered. As stated the launcher consist of three stages. The cross-section of the launcher is over the whole length constant and has a diameter of 1.4 meters. An overview of the launcher can be found in Figure 7.1. The blue round and cylindrical elements are the different fuel and oxidiser tanks. The smallest light blue objects are the helium tanks. The green triangle shaped elements represent the engines.

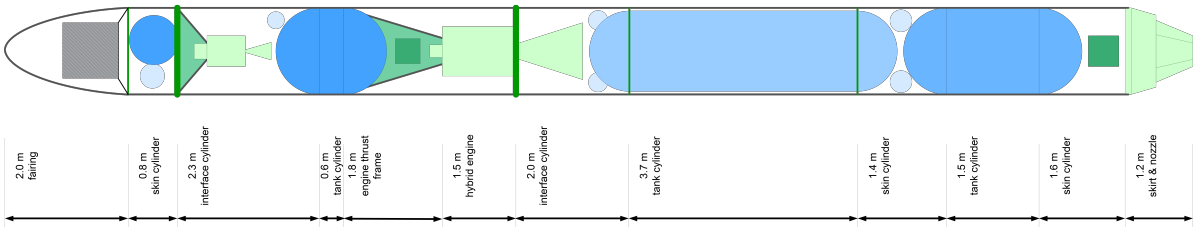

Figure 7.1: Lay-out geometry launcher

.

7.2.2. MASS

The total take-off weight of the launcher, without recovery mechanisms is 15076 kg. During the ascent of the launcher 10550 kg will be spend on fuel and oxidiser.

7.2.3. CENTRE OF GRAVITY AND MASS MOMENT OF INERTIA

Figure 7.1 has been used to calculate the centre of gravity and the mass moment of inertia. It will be assumed that the vehicle is perfectly symmetrical in the x-body axis. This means that the centre of gravity will be on the x-body axis, and so only the position on the x-axis needs to be calculated. The position of the centre of gravity has been calculated with respect to the bottom of the launcher, being the right side part of Figure 7.1. In the code written the centre of gravity will be updated at every time step. Five different points of centre of gravity have been formulated shown in Table 7.1. The first situation is at take-off; at this point all fuel will be present. The second situation is at one quart of the burn time. The next point is at half way of the ascent trajectory including the first stage. The fourth point is at three quarters of the burn time of the first stage. The last position is the point just before separation.

Table 7.1: Centre of gravity position launcher

	take-off	1/4	mid-way	3/4	burn-out
x-position centre of gravity [m]	7.6915	7.9720	8.4044	9.1571	10.7972

In Table 7.1 it can be seen that the centre of gravity will start to move upwards when burning the fuel. The change in centre of gravity will start very slow, but will increase the closer to burn-out.

The mass moment of inertia around its centre of gravity using the centre of gravity found above. As stated before the launcher will be considered perfect symmetrical this means that the following relation, Equation 7.4 will hold for the mass moment of inertia.

$$\begin{vmatrix} I_{xx} & I_{xy} & I_{xz} \\ I_{yx} & I_{yy} & I_{yz} \\ I_{zx} & I_{zy} & I_{zz} \end{vmatrix} = \begin{vmatrix} I_{xx} & 0 & 0 \\ 0 & I_{yy} & 0 \\ 0 & 0 & I_{zz} \end{vmatrix} \tag{7.4}$$

This means only the values for I_{xx}, I_{yy} and I_{zz} needs to be calculated. Because the launcher is symmetrical around the x-body axis I_{yy} and I_{zz} are equal to each other. The script written will calculate the mass moment of inertia at every time step. In Table 7.2 an overview of the mass moment of inertia, for the same point as discussed in Table 7.1, can be found.

Table 7.2: Mass moment of inertia launcher around centre of gravity

	take-off	1/4	mid-way	3/4	burn-out
I_{xx}[kg m^2]	3696.5557	3050.2457	2404.1807	1758.1157	1111.8057
I_{yy}[kg m^2]	219410.78	200228.07	178029.14	149403.79	102710.20
I_{zz}[kg m^2]	219410.78	200228.07	178029.14	149403.79	102710.20

The mass moments of inertia found in Table 7.2 show the more propellant is burned, the smaller the mass moment of inertia will become. The smaller the mass moment of inertia the faster the object will react on a torque. The launcher will be more sensitive to moments at burn-out than at launch.

7.3. FIRST STAGE

After separation of the first stage, the first stage will be brought back to the Earth to be recovered. In this section the geometry of the first stage will discussed.

7.3.1. GEOMETRY

The first stage has a total length of 11.4 meter and a constant diameter of 1.4 meters. An overview of the launcher without recovery mechanisms can be found in Figure 7.2. The blue cylindrical elements are the fuel and oxidiser tanks. The smallest light blue objects are the helium tanks. The green triangle shaped elements represent the engines.

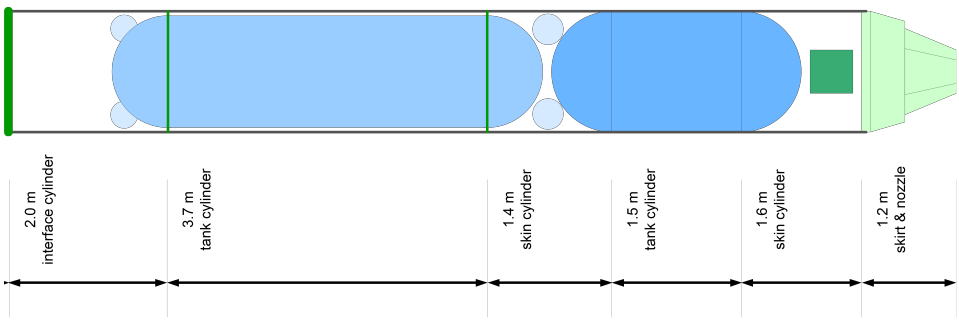

Figure 7.2: Lay-out geometry first stage

.

At separation the engine will be pointed downwards. After separation the first stage will be turned with its engine into the flight velocity. In this way the engine can be used for retro-propulsion and can be used as heat shield.

7.3.2. MASS

The total mass of the first stage after separation, without recovery mechanism, will be 1290 kg. For the first iteration it will be assumed that to recovery the first stage an extra system mass of 150 kg is needed. For the

recovery making use of the parachute the extra system mass will be placed at the left side of Figure 7.2. For the recovery mechanism making use of only propellant the extra weight will be placed in the tanks.

7.3.3. CENTRE OF GRAVITY AND MASS MOMENT OF INERTIA

Figure 7.2 has been used to calculate the geometrical properties. It will again be assumed that the vehicle is perfectly symmetrical in the x-body axis. The position of the centre of gravity has been calculated with respect to the bottom of the launcher, being the right side part of Figure 7.2. In the software the centre of gravity will be updated at every time step. For both the centre of gravity and the mass moment of inertia four different situations are calculated. The first configuration is the first stage, empty without the parachutes placed on the left side of Figure 7.2. The second configuration is the first stage including extra fuel weight for retro propulsion in the ascending phase with the engine pointed towards the Earth. The third configuration represents the first stage just after the turn. The engine will now be pointed in direction of the flight velocity. Extra propellant will be present in tanks for recovery. The last configuration considered here is the just before landing. The first stage will be now be almost empty and the engine will be pointed towards the Earth.
The results on the centre of gravity and mass moment of inertia can be found in Table 7.3.

Table 7.3: Centre of Gravity and Mass Moment of Inertia first stage

	including parachute	fuel, engine towards Earth	fuel, engine away from Earth	empty, engine towards Earth
x-position centre of gravity [m]	5.1088	4.2265	4.8731	4.0373
I_{xx}[kg m^2]	381.2249999	315.5550	315.5550	278.8050
I_{yy}[kg m^2]	22471.003791666	16879.16	22241.0526	15748.73
I_{zz}[kg m^2]	22471.003791666	16879.16	22241.0526	15748.73

In Table 7.3 it can be seen that the centre of gravity and the mass moment of inertia differ from configuration to configuration. The more weight is placed at the left side of Figure 7.2, the higher the value of I_{yy} and I_{zz} are. This difference will influence how easy the first stage will change its yaw and pitch position. The configuration with fuel and the engine pointed towards the Earth and the empty configuration will need less torque to rotate than the other two configurations.

7.4. RECOVERY MECHANISMS

For the recovery of the first stage three different mechanisms are proposed; retro-propulsion, parachute and IAD. The weight-estimations techniques used for these systems will be explained in this section.

7.4.1. RETRO-PROPULSION

The first recovery mechanism treated is the use of retro-propulsion. This option will increase the total propellant needed and will so increase the tank size. The extra propellant needed will be calculated by the thrust force and thrust duration needed.

The change in mass, the mass flow rate $\dot{m}$, can be written using the specific impulse of the engine, I_{sp}, as:

$$\dot{m} = -\frac{T}{g_0 I_{sp}} \tag{7.5}$$

The actual thrust will be calculated by using Equation 7.6. The actual thrust can be split in the contribution of the engine and the force due to the pressure difference of the exhaust and atmosphere. The first part needs the efficiency of the engine, λ, the mass flow rate, specific impulse, gravitational constant at the surface. The second part is a function of the exhaust pressure, P_e, pressure of the atmosphere P and the exhaust area A_e. The exhaust pressure of the engine is a design variable of the engine and so a fixed number.

$$T = \lambda \cdot \dot{m}(I_{sp} g_0) + (P_e - P) * A_e \tag{7.6}$$

Using the mass flow rate and the thrust duration the total propellant can be calculated. If the total propellant mass is obtained a factor of 1% has been added to include the extra propellant tank mass.

7.4.2. PARACHUTE SYSTEM

The parachute system consists of two parts. The first part is the drogue parachute, which will provide the deceleration during the first part in the atmosphere and will provide stability. The second part is the parafoil which will provide enough drag to safely land. The parafoil is also able to steer the vehicle to a designated point.

DROGUE PARACHUTE

Different drogue parachutes are on the market. The hemisflo ribbon parachute has been chosen for its good performance at high Mach numbers. More on the aerodynamic performances of the drogue parachute can be found in Section 8.2.2.

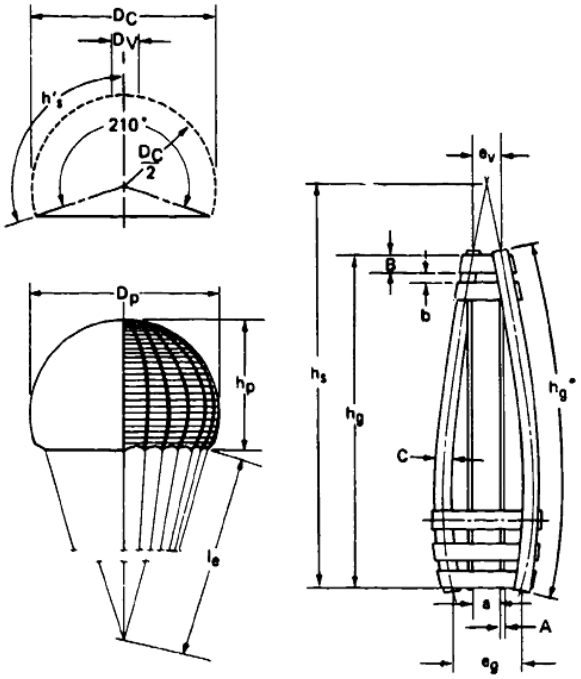

Figure 7.3: Typical Design of a Hemisflo Parachute [2]

.

A typical hemisflo design can be found in Figure 7.3. The canopy of the parachute forms a perfect sphere with the suspension lines connected tangentially. The canopy skirt is the point where the lines connect to the canopy. For flat or conical shaped canopies in and out flutter of the gores is a big problem. The hemispherical shape avoids this movement. Due to the hemispherical shape of the canopy there is no length difference in the leading and trailing edges of the horizontal ribbons. This design will reduce the canopy breathing and high-frequency ribbon flutter. Both phenomena are sources of canopy damage and drag decrease at supersonic velocities [2].

The weight of the hemiflo drogue parachute will be predicted by making use of the TWK Weight Determination Method [28]. This method is practical if no detailed drawings are available, but some primary dimensions are known. The weight of a parachute can then be approximated with Equation 7.7 [2].

$$W_p = S_0 w_c + D_0/s \cdot N_G W_{RT} F_{RT}/1000 + NSLL_S w_{SL} F_{SL}/1000 \tag{7.7}$$

In Equation 7.7 the weight of the drogue parachute will be calculated with the following elements. The first element is the surface of the finished canopy, S_0. The second element used is the specific weight. The specific weight of the canopy, w_c, the radial tapes, w_{rt}, and the suspension lines, w_{SL}, is used. The number of gores in the canopy and the number of suspension lines is denoted with N_G and N_{SL} respectively. The next elements used in Equation 7.7 are the strength of the radial tapes, F_{RT}, and the strength of the suspension lines, F_{SL}. The last element is the length of the suspension lines, L_S.

Using the TWK method some values need to be assumed. It has been assumed that 20 gores are used and 20 slide lines with a length of $2.66 \cdot r_p$. With r_p being the radius of the drogue parachute. The specific weight of the canopy is assumed being 0.00249 kg/m^2 [2].

To deploy the drogue parachute, a mortar will be used. The weight of the mortar can be estimated with Figure 7.4. The total mass of the drogue parachute will be calculated by making use of the TWK and the regression line shown in Figure 7.4. The total mass will then be increased by 50% to include elements not taken into account and to add a safe margin.

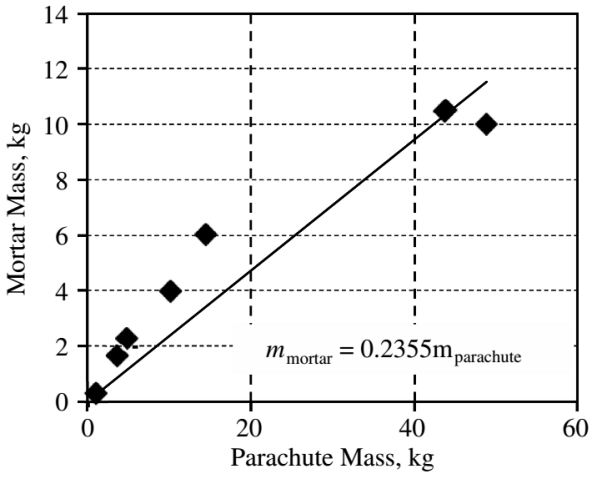

Figure 7.4: Mortar mass regression [3][4]

As been stated before, the surface of the finished canopy is the only variable used in the optimisation. It will be assumed that after deployment the surface of the canopy will increase linearly. The opening of the parachute will be controlled by making use of skirt reefing. The parachute will be opened in 10 seconds.

PARAFOIL

A parafoil is a parachute made from aerodynamic cell structure which inflates by the wind. These ram-air inflation forces push the parafoil in a typical wing cross-section. Most parafoil are made from ripstop nylon. Ripstop fabric is a woven fabric reinforced to resist tearing and ripping. The weight estimation of the parafoil will be performed by making use of the TWK method and making use of SPADES as reference hardware. SPADES is a parafoil delivery system for payloads until 200 kg designed by Netherlands Aerospace Center (NLR), Dutch Space, and parachute supplier Aerazur of France [29]. Although SPADES is designed for much smaller payloads, some in-house knowledge of the NLR will be used.

For the TWK method the following parameters were assumed. The first one is the amount of gores used being 20. In total 30 slider lines were assumed with a length of $4 \cdot r_P$, where r_p is a parameter which determines the size of the parafoil. The total planform area of the parafoil can be calculated by $0.75 \cdot r_p x 1.50 \cdot r_p$.

To steer the parafoil an Airborne Guidance Unit (AGU) is needed. It was found that a typical AGU will weigh 40 kg [30]. The total mass of the parafoil system will be calculated using the TWK method. Then an extra 50% will be added to include neglected masses and to add a safety margin. To conclude the mass of the AGU will be added to the found mass.

The parafoil will be deployed by the drogue parachute at a velocity below the M=0.2 and below the 3 km. The area growth of the parafoil will be controlled as for the drogue parachute. The area will grow linearly, and will be fully deployed within 20 seconds.

7.4.3. INFLATABLE AERODYNAMIC DECELERATOR

The last recovery mechanism considered is the inflatable aerodynamic decelerator. There are different types of IAD's. A trailing isotensoid was chosen.

The mass of the trailing isotensoid inflatable aerodynamic decelerator was calculated using a relationship accounting for the structural and aerodynamic parameters that govern the decelerator efficiency [31]. ac-counts for the mass of meridian tapes, rise and suspension lines, and the canopy mass in the first and second terms shown in Equation 7.8. The C_D-value in Equation 7.8 is the aerodynamic drag of the trailing isotensoid

only. The constants b and c, are shown by Anderson et al. to be 6.9 10^{-5} kgNm and 7.41, respectively [31]. The last term in this equation represents the areal density of the fabric[4].

$$m_{ISO} = bq_{deploy}(C_D A)^{\frac{3}{2}} + cd_f(C_D A) \tag{7.8}$$

An extra 50% mass margin will be added to final masses to account for miscellaneous mass and uncertainty not accounted for in this analysis. To deploy the trailing isotensoid a mortar is required. The mass of this mortar will be calculated by making use of the linear regression line shown in Figure 7.4.

8

AERODYNAMICS AND THERMODYNAMICS

This chapter focuses on the Aerodynamic and Thermodynamics of the system. First some basic aerodynamics will be treated in Section 8.1. In this section the lift and drag coefficient will be explained and the way of estimating these coefficients will be shown. After the basics aerodynamics, the aerodynamics for the three degrees of freedom optimisation will be treated. In Section 8.3 the coefficients for the six degree of freedom simulator will be explained. The thermodynamics is the last part of this chapter and is focused on the heat dissipation during the descent. If the energy received by the system would become too high, the system will burn op in the atmosphere.

8.1. GENERAL AERODYNAMICS FORCES

Aerodynamic forces develop when there is relative motion between the fluid and the body immerse. The aerodynamic force on a body depends on its shape and size, attitude with respect to the flow, the density and velocity of the flow. Three different components can be considered; the lift, L, drag, D, and the side force, Y. Lift is the force perpendicular to the motion of the vehicle pointing away from the top of the vehicle. The drag is in opposite direction of the velocity. The side force is perpendicular to these two forces. In Equation 8.1 the lift formula is shown, in Equation 8.2 the equation for drag is shown, and Equation 8.3 shows the equation for the side force. The C_L, C_D, and C_Y stand for the lift, drag and side force coefficient of the vehicle respectively. The ρ is the density of the flow, the V stands for the velocity of the flow and the S for the surface area.

$$L = C_L \frac{1}{2} \rho \cdot V^2 \cdot S_{ref} \tag{8.1}$$

$$D = C_D \frac{1}{2} \rho \cdot V^2 \cdot S_{ref} \tag{8.2}$$

$$Y = C_Y \frac{1}{2} \rho \cdot V^2 \cdot S_{ref} \tag{8.3}$$

Next to the force components, the moment components are of importance. The moment coefficients are a factor for the rotation around the different axes. It will be assumed that the vehicle is symmetric and only the pitch moment is therefore taken into account. The pitch moment of the vehicle is the moment produced by the aerodynamic force on the vehicle. A moment will be created if the forces are not applied on the centre of pressure, but at the aerodynamic centre of the vehicle. The moment can be calculated in the same fashion as the forces using the moment coefficients. The first moment considered is the roll moment, moment around the x-axis. The moment is found in Equation 8.4, using the roll coefficient C_l and the chord length, c. The pitch moment, Equation 8.5 and the yaw moment, Equation 8.6, can be calculated in a similar fashion using the pith moment, C_m, and yaw moment coefficient, C_n respectively.

$$l = C_l \frac{1}{2} \rho \cdot V^2 \cdot S_{ref} \cdot c \tag{8.4}$$

$$m = C_n \frac{1}{2} \rho \cdot V^2 \cdot S_{ref} \cdot c \tag{8.5}$$

$$n = C_n \frac{1}{2} \rho \cdot V^2 \cdot S_{ref} \cdot c \tag{8.6}$$

8.2. THREE DEGREES OF FREEDOM

A distinction has been made between the three degrees of freedom and six degrees of freedom coefficients. For the three degrees of freedom simple formulas have been used.

8.2.1. LIFT COEFFICIENT

The first element considered is the lift coefficient. For the launcher itself and the recovery mechanism it will be assumed that in the three degrees of freedom configuration the system will fly with a zero angle of attack. As both the launcher and first stage are symmetrical, a zero angle of attack will result in zero lift.
The parafoil is the only element for which aerodynamic lift will be considered. The parafoil is invented by D. Jalbert, it consists of an all-flexible inflatable wing with an opening at the leading edge of the airfoil for ram-air inflation. The stability is provided by an anhydral deflection, obtained by the lines of equal length spanwise but various length cordwise [2]. The manoeuvrability of the parafoil is obtained by individual or simultaneous downward deflection of the outer trailing edges for turn or glide control [32]. The shape of the parafoil, and so the force coefficients, can be adjusted by deflecting the parafoil. For the first analysis a constant lift coefficient of 0.1 will be assumed.

8.2.2. DRAG COEFFICIENT

In this subsection the drag coefficient of the different components will be explained. The first drag coefficient treated will be the one of the rocket/first stage itself. The second drag coefficient calculated is the drag coefficient of the inflatable aerodynamic decelerator. To conclude relations are shown which will be used to determine the drag coefficient of the parachutes and parafoil used.

The drag coefficient in Function 8.2 needs to be approximated. This will be done by splitting the drag in the zero-lift drag and the induced drag as shown in Equation 8.7[33]. All external aerodynamic components of the vehicle contribute to the overall zero-lift coefficient of the vehicle. The total zero-drag coefficient can be build up out by adding the different drag components. It will be assumed that the external aerodynamic components consist out of the 'fuselage' of the rocket and the four stabilisation fins.

$$C_D = C_{D_0} + K \cdot C_l^2 \tag{8.7}$$

LAUNCHER

The drag coefficient of the launcher will be mainly determined by the shape of the fairing. A standard fairing geometry does not exist; multiple configurations have been used in the past and are still used. The launcher configuration, mission and the flight profile will influence the optimal geometry of the fairing. It has been decided, by the SMILE consortium, based on C_D-values, mass, volume, and heat load estimations that the LV Haack series would be the best design for this mission.

The drag of this shape is dependent on the length to diameter ratio of the fairing. Two different ratio will be consider, being L/D=1.5 and L/D=1.25. The result of the drag curve for L/D=1.5 is shown in Figure 8.1. The information on the drag curve was provided by the NLR.

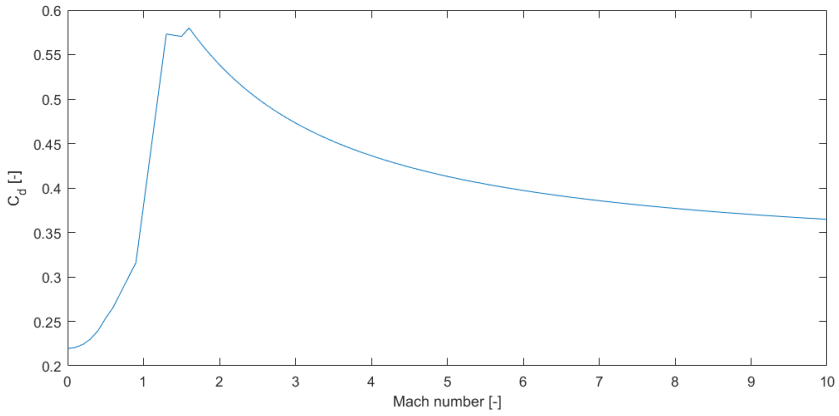

Figure 8.1: Drag coefficient as function of Mach number of the launcher

FIRST STAGE

For the recovery of the first stage the drag coefficient will be kept the same as for the whole launcher. It is expected that the drag coefficient for the aerospike would in reality be a bit higher than for the fairing. The main reason for this is that the fairing is designed to have the lowest drag possible. For the trajectory calculations this would imply that the system would be decelerated a bit less in the simulation than expected in real life. An over prediction of the recovery mechanism will be the result. More on varying drag coefficient and the influence of this will be explained in Section 15.3.

INFLATABLE AERODYNAMIC DECELERATOR

The first deceleration mechanisms based of aerodynamic drag treated is the inflatable aerodynamic decelerator. A trailing isotensoid is chosen for its packing volume and good aerodynamics properties at high mach number[5]. In literature the behaviour of the drag coefficient was found[5]. The results can be found in Figure 8.2. In the analysis the black solid line will be used to determine the drag coefficient.

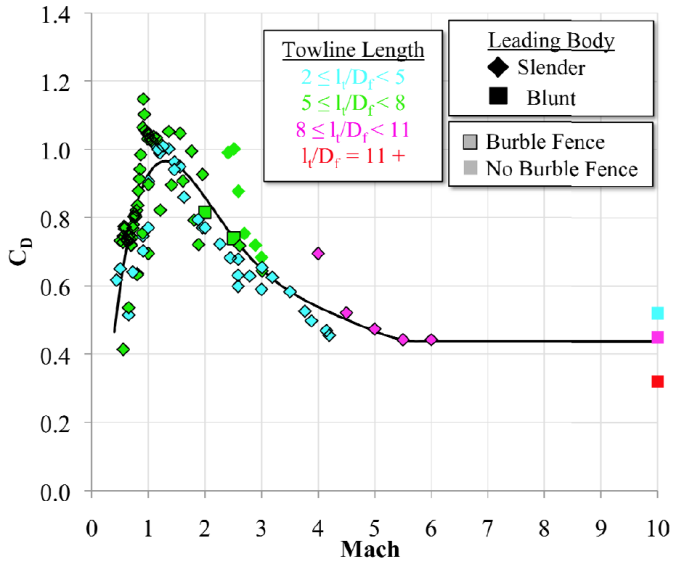

Figure 8.2: Trailing isotensoid drag performance data as function of Mach number[5]

DROGUE PARACHUTE

The drogue parachute will induce drag at an high altitude to decelerate the vehicle and will provide stability to the system [12]. The drogue parachute used in this research is a hemisflo ribbon parachute. This parachute has been chosen as it is proven to be the most practical design for velocities up to Mach 3 and also works sufficient in the wake of a large forebody [2].

The drogue coefficient of the drogue parachute has been predicted by making use of Figure 8.3. In this figure it can be seen that the drag coefficient can be assumed to be around 0.41 from Mach 0 to Mach 1.8. At higher Mach number the drag coefficient will decrease linearly.

PARAFOIL

The parachute system will deploy a parafoil after the drogue parachute. This will be done at a velocity of below Mach 0.2 and an altitude less than 3000 m. The parafoil surface area will be increase linearly, and will be deployed within 20 seconds. The drag coefficient of the parafoil will be assumed to be 0.31.

8.3. SIX DEGREES OF FREEDOM

The force and moment coefficients of the six degree of freedom system have been calculated by making use of Missile DATCOM[34]. Missile DATCOM is a semi-empirical aerodynamics prediction code of the U.S. Air Force for the preliminary design and analysis of missile aerodynamics and performance. It can calculate aerodynamic forces, moments, and stability derivatives as a function of the Mach number, position and for

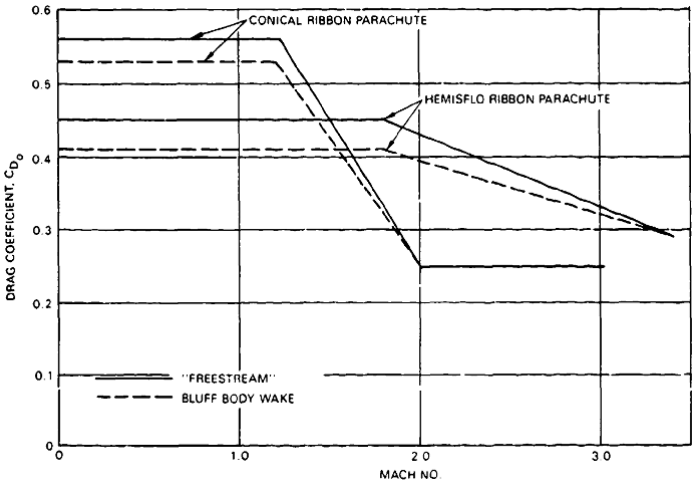

Figure 8.3: Drag coefficient for a hemisflo and conical parachute as function of Mach number [2]

a variety of configurations. The user can add fin configurations that resemble wings [34]. The original version of DATCOM is not available for persons outside of the U.S. as it is restricted to the International Traffic in Arms Regulations (ITAR) . However a limited 1997 version of the software has been distributed as a supplement to the book 'Design Methodologies for Space Transportation Systems' [35]. A major drawback of the software is that it cannot handle asymmetric vehicles. As the vehicle considered will be assumed to be perfect symmetrical this is not an issue here. But more severe for this project is that the limited version only gives valid predictions till an angle attack of 30° after this it switches to an empirically derived model [34][36].

In Figure 8.4 the axis system used in Missile DATCOM has been shown. In this figure the definition of the different angles can be found.

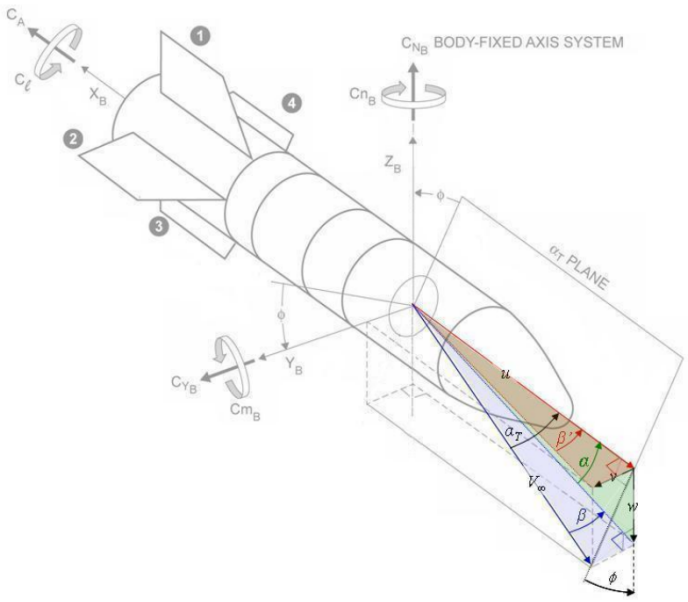

Figure 8.4: Coefficient axis system Missile DATCOM [6]

In this section some results found using Missile DATCOM will be shown and explained. As a lot of results found with Missile DATCOM will look similar not all graphs are shown. First the aerodynamics coefficients found for the launcher are explained. In the second section the aerodynamics of the first stage are treated in different configurations.

8.3.1. LAUNCHER

Based on the geometry treated in Section 7.2, Figure 8.5 gives the aerodynamic coefficients for the launcher. As the launcher will rapidly change its mass and its centre of gravity, the take-off configuration will be considered here.

For the launcher it was found that the launcher is highly unstable at take-off. The graph of the pitch moment coefficient with angle of attack can be found in Figure 8.5. This behaviour of C_m indicates that if the launcher will fly with an angle of attack, this angle of attack will increase further due to the moments induced by the shape and centre of gravity of the launcher. If the launcher will burn up all propellant the centre of gravity will shift a bit towards the nose of the launcher. This movement of centre of gravity will increase the stability a bit; however the launcher will still be unstable.

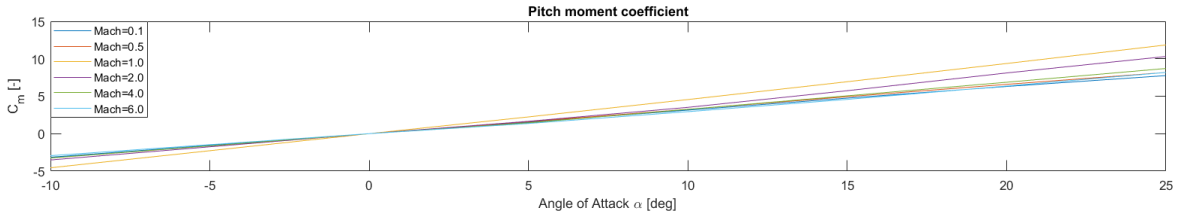

Figure 8.5: Pitch moment coefficient with angle of attack of the launcher at take-off

Because this launcher is highly unstable the launcher should be stabilised with thrust vector control (TVC). Thrust vector control is controlling the angle of the thrust to keep the launcher stable. Because TVC will be used to control the stability of the launcher, the launcher cannot be simulated properly without a control system in the software. As this is outside of the scope of the project, the simulation with 6DOF will start at separation.

8.3.2. FIRST STAGE

After the separation, the first stage will return to the Earth. In Section 7.3 it was shown that the geometry parameters of the first stage are dependent on the configuration and the orientation of the first stage. All different configuration and orientation will therefore have different aerodynamic properties. These different aerodynamic properties have been included in the software tool. The differences between the configurations are very small, therefore only one configuration will be explained in detail. Using the graphs produced the similarities with the other configurations and orientations will be explained.

The configuration considered is the first stage including the parachute system with the engine pointed towards the velocity vector. For this configuration different graphs have been produced. The first graph shows the force coefficient as function of angle of attack for different Mach Numbers. The results are shown in Figure 8.6. In this figure it can be seen that the drag coefficient will have its lowest value at an angle of attack of 0°. This can be explained with Equation 8.7. The total drag coefficient is a function of the base drag and the lift coefficient. The lift coefficient is due to its symmetrical shape zero at an angle of attack of 0°. Increasing the angle of attack will increase the lift and so the total drag. The third force coefficient shown in Figure 8.6 is the side force coefficient. Due to the symmetry of the vehicle this coefficient is constant 0. However if an angle of side slip is introduced a side slip coefficient will be introduced. The same behaviour for C_Y can be seen with angle of side slip as for C_L with angle of attack. This can be explained by the fact that the vehicle is symmetric in the x-body axis.

The second graph considered is the moment coefficient as function of angle of attack for different Mach Numbers, shown in Figure 8.7. This figure shows a linear increase of the pitch moment coefficient with angle of attack, the higher the angle of attack the higher the moment coefficient. This means that the first stage is unstable. Although the first stage is less unstable than the launcher, a control system should be designed.

For all configuration and orientations considered the same kind of behaviour is found. This means that a control system is needed to run the simulation. The control system will keep the angle of attack as small as possible.

8.4. HEAT DISSIPATION

A vehicle that enters the atmosphere has a lot of energy. When it encounters the atmosphere at high speed, a shock wave will form ahead of the vehicle. The atmosphere around the vehicle will induce drag on the vehicle.

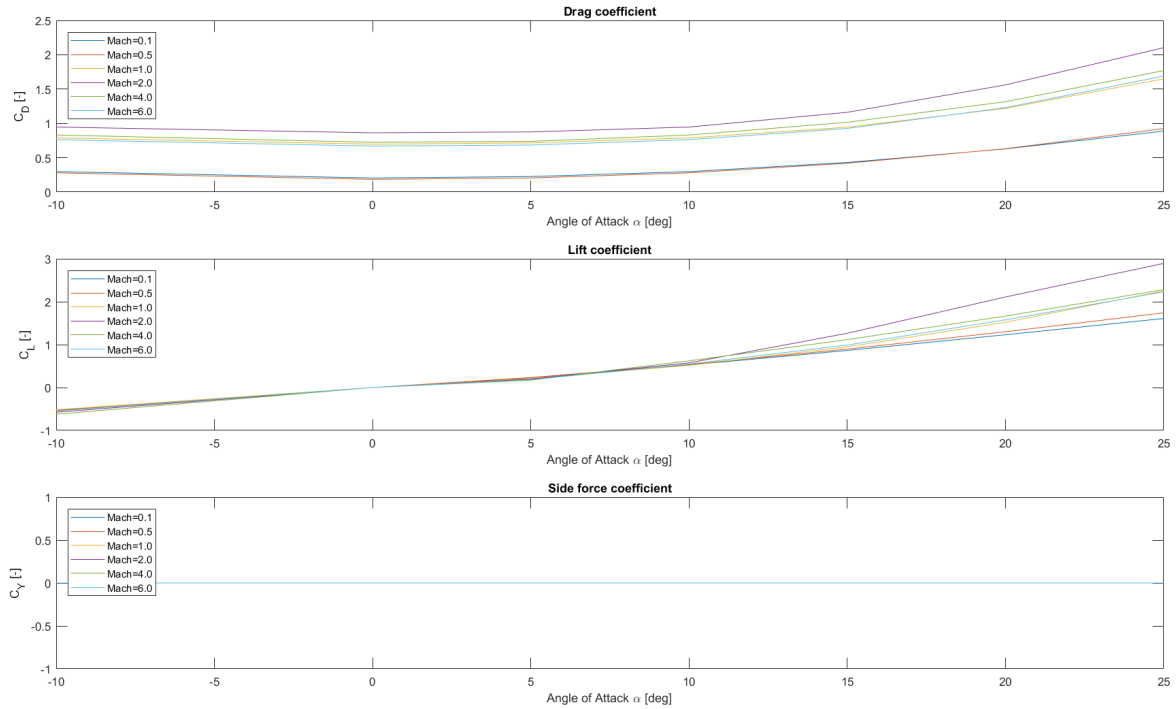

Figure 8.6: Force coefficient as function of angle of attack for different Mach Numbers for first stage carrying parachute system

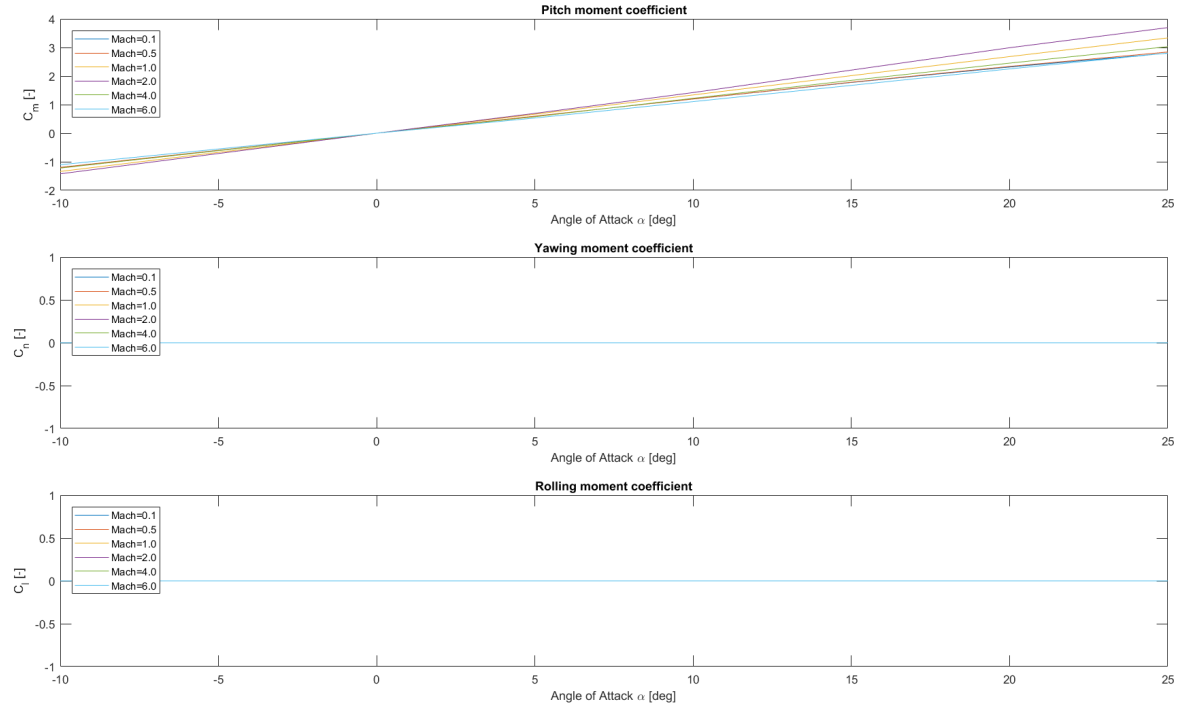

Figure 8.7: Moment coefficient as function of angle of attack for different Mach Numbers for first stage carrying parachute system

This drag will reduce the kinetic energy; this kinetic energy will be transformed in heat.

Two methods were considered to determine the temperature the system will reach. The first method used has been introduced in Chapter 2. Equations 2.11 to Equation 2.18 have been used to calculate the temperature of the vehicle's skin. In this method it has been assumed that the system itself will not heat-up. This assumption will result in a higher wall temperature calculated then will occur in reality, as no conduction is assumed to the rest of the body.

The second method considered is the use of the Sutton and Graves Equation[37]. The Sutton and Graves equation is a very simple formulation shown in Equation 8.8 to calculate the temperature of the vehicle's nose. In this equation the temperature and density of the local environment, T and ρ will be used. The free stream velocity, V will be used and the emissivity, ϵ, and Stefan Boltzman constant, σ, and the nose radius, R_n, are used to calculate the nose temperature. To conclude the constant, k, will change with the Equation used. For the Sutton and Graves equation this constant equals 1.731010^{-4}. Equation 8.8 consist out of three parts, the first is the temperature of the local environment. The second part of the numerator of the formula represents the convective heat. The denominator represents the radiation.

$$T_{nose} = [\frac{T^4 + (k(\frac{\rho}{Rn})^{\frac{1}{2}} V^3}{\epsilon\sigma}]^{\frac{1}{4}}; \tag{8.8}$$

9

COST ESTIMATION

Now that the masses are known, the costs can be estimated. This chapter focuses on the cost of the different designs. Cost is an important trade-off criteria. To compete with other investors the cost per kg payload should be below the €50 000 with a total maximum cost for a launch of 3.5 M€. This means that cost is a major driver. By re-using the first stage the cost of the launcher might be reduced.

There are two different forms of cost needed to be taken into account; the non-recurring costs and the recurring costs. The non-recurring costs contain all the cost which will only be spend once. An example of non-recurring costs are the development costs of the launcher. Once the launcher is developed one does not have to spend more money on development. The recurring costs contain all the facets which will remain once in service, for example the operational costs.

COST RISK AND UNCERTAINTY

Cost engineering is an essential component in any space program. In the early phase of a program the cost estimation determines a factor for the program realisation. If the cost of the program is too high, the project will not be as feasible. On the other hand if the project is under-estimated in cost the risk of financial loss and program failure is high. A good estimation, from the beginning of the design, is essential for a successful project.

The cost estimate is not a fixed value, but a dynamic value. The cost estimation should be reassessed once new information is available. In the beginning of the design there is only limited information is available, but during the design more information will be available. The accuracy of a cost estimation depends on three factors [7]. The first factor is the availability of reliable data. The second factor is the availability of appropriate mix of effective tools, methods and models to perform the estimate which is consistent with the program phase and system definition at the time of the estimate [38]. The last factor is the skilled cost estimator, the cost estimator should have sufficient knowledge and estimating experience is required to bring all the elements successfully together [7].

Risk and uncertainty is something which has to be dealt with during the project. Risk is the probability of the occurrence of a certain event and its impact on the project. Risk is something which can be taken into account during the design. Uncertainty relates to the unforeseen event, and therefore hard to address during the early phases. Besides the risk and uncertainty of events, there is also an uncertainty in the cost estimation. In the early phase of the program there are only a few details known about the project on which an estimation must be build. This makes the uncertainty in the beginning of the project very high.

9.1. COST ESTIMATION METHODS

To assess the cost estimation different methods can be used. There are three main Cost Estimation Methods (CEMs); Parametric cost estimation, Engineering build-up estimation, and Analogy estimation. Other methods have been proposed by ESA and NASA: Expert judgement estimation and Rough order of magnitude estimation, respectively. These five methods will be briefly explained in this section.

PARAMETRIC COST ESTIMATION

The parametric cost estimation is often used during the planning of a project and during the budgeting process for acquisition of a project [39]. It is also the foundation of software used for early phase cost estimation of space programs. In parametric cost estimation a number of mathematical relations- cost estimation relationships (CER)- are derived from historical data. CERs are built by using physical, technical and performance parameters that strongly correlate with program costs. The user can add factors to the CER in order to tune the relationship for a mission[7]. The cost model is as accurate as the underlying data used to construct this CER. The amount of data used and the similarities of the missions determine the reliability of the method [39].

ENGINEERING BUILD-UP ESTIMATION

Engineering build-up estimation is used when all system and sub-system levels are known and defined. Cost estimation can be performed at the lowest level of detail. The project must be broken down in a Cost Breakdown Structure (CBS) and/or Work Breakdown Structure (WBS). These breakdown structures must be done carefully to make sure no elements are duplicated or missing. A mistake in the WBS would reflect directly on the total cost found [40]. A disadvantage of this method is that it is not easy to change the design or requirements, this method is therefore less useful in the early phases of the project [7].

ANALOGY ESTIMATION

The analogy estimation relies on the analogy of different projects. This means that an intensive analyst judgements is needed to determine the similarities of two projects. It can be very hard to find a similar project, and once found the cost estimation is only based on a single data point. On the other hand the method can be used quickly and effectively throughout the different phases of the project [7].

EXPERT JUDGEMENT ESTIMATION

According to ESA, the expert judgement estimation is deemed to be the fourth CEM[41]. Expert judgement is often criticised as it subjective in nature and based on the experience and knowledge of the estimator [7].

ROUGH ORDER OF MAGNITUDE ESTIMATION

Rough order of magnitude estimation is according to NASA deemed to be the fourth CEM [39]. This method is mainly used in the first phase when the project has not been really started and the requirement are not explicit [7].

9.2. COST ESTIMATION METHOD USED

In the previous section five different methods were proposed. Figure 9.1 visualises the different methods and their applicability during the different phases. Following Figure 9.1 a top-down cost estimation would fit the beginning phase of the project better and a bottom-up estimation would fit the last phases of a project. This would mean that a top-down approach would be the best option. However a standard cost model is not suitable for this type of research. In a standard cost model the overall cost can be estimated, but small differences in recovery options are not reflected in the overall cost.

Here, a bottom-up variant will be used to investigated the cost of recovery. The first stage without recovery will cost 800k€. The first stage will be used as baseline for the cost estimation. Four different aspects will be added to this baseline, the stage adaption costs, the deceleration mechanisms costs, the transportation costs, and the refurbishment costs. The cost of control systems and the first stage including adaptions will go down if the first stage is used multiple times. If a stage is re-used in the same year the transportation cost will go down as the costs can be split over multiple launches. Using the different cost elements an Excel model is build. The results of the model will then be compared with a new first stage every flight.

For the decelerate mechanisms, the costs are found in literature. The transportation and refurbishment costs are assessed by making use of expert judgement estimate. The results for the cost of the system will be considered in Section 14.6.

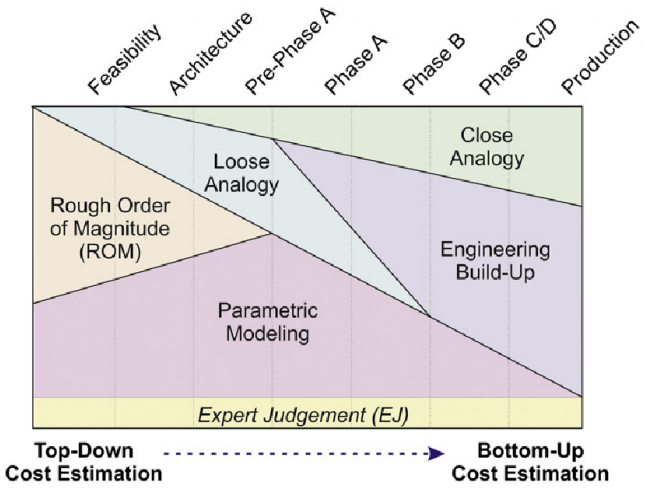

Figure 9.1: Cost estimation models according to project phase [7][8]

.

10

VERIFICATION & VALIDATION

During the construction of the tool, all elements need to be tested. All different building blocks are therefore verified. Besides being verified, the answers produced need to be validated. The answers were compared with real data or validated software. In this chapter the most important elements of the verification and validation are shown. In the first section the validation of the three degrees of freedom trajectory can be found. The second section shows the verification of the genetic algorithm. In Section 10.3 the validation of the weight estimation can be found. The last section shows the validation of the six degree of freedom trajectory.

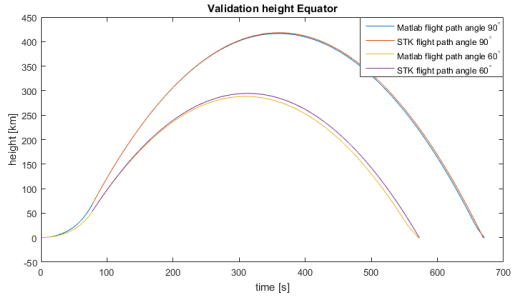

Figure 10.1: Validation 3DOF trajectory, height, launch from Equator

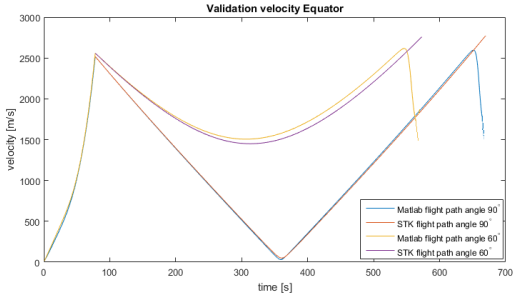

Figure 10.2: Validation 3DOF trajectory, velocity, launch from Equator

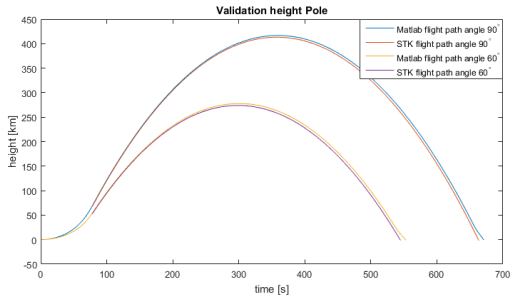

Figure 10.3: Validation 3DOF trajectory, height, launch from Pole

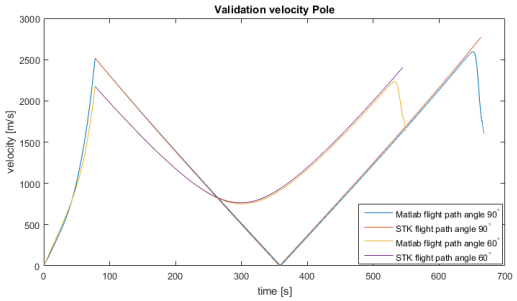

Figure 10.4: Validation 3DOF trajectory, velocity, launch from Pole

10.1. VALIDATION TRAJECTORY

This section contains the validation of the trajectory produced by the optimiser. The first part of this validation is performed using STK. In this first part, the trajectory after separation will be tested. Four different cases were performed, two on the equator and two on the pole. For both locations an initial pitch angle at launch of 60° and 90° were investigated. The result can be found in the Figures 10.1-10.4. In these figures it can be seen that for all situation the height found by the Matlab code is slightly lower than STK found. The difference are a bit bigger for the launch pitch angle of 60°. This can be explained by the fact that the simulator includes higher drag. By launching with a shallower angle the system will stay for a longer period in the

Table 10.1: Comparison Validation data (STK) and 3DOF simulation

	t=92 s			t=143s		
	script value	STK value	relative error	script value	STK value	relative error
Velocity [m/s]	863.059	868.417	-0.62%	2355.707	2441.619	-3.64%
Mach [-]	2.900	2.895	+0.12%	8.515	8.803	-3.39%
Altitude [km]	28.207	27.234	+3.573%	88.177	83.708	+7.36%
Drag [N]	6267.814	7288.470	-16.28%	5.701	14.732	-258.42%
Temperature [K]	852.993	569.461	+149.79%	606.503	814.706	-134.32%
G-force [-]	2.062	2.053	+0.42%	4.855*	4.903*	-1.00%*

atmosphere and will therefore stay for a longer period in the atmosphere. The same can be seen in the figures of the velocity. In these figures it can also be seen that for the STK models the velocities will increase further than the Matlab models. This can again be explained by the drag. Using these figures and explanation of the differences the trajectory models can be verified.
The second part of the validation is the validation of the ascent trajectory. In this part of the validation it was checked if the tool would produce the same numbers as found by the project. The input for both tools is the same input as discussed for the 3DOF simulator in the previous chapters. In this part six different elements were tested. The first elements are shown in Figure 10.5. In this figure the velocity and the Mach-numbers reached during ascent are shown. The data produced by the code are shown in a solid blue line. The validation data is shown with a red dashed line. In Figure 10.6 the altitude and drag numbers found are shown. And the temperature of the nose wall and the G-force experienced during the ascent are shown in Figure 10.7.

To compare the values shown in Figure 10.5 to Figure 10.7, a table has been constructed shown in Table 10.1. In this table the values found for t=92 s and t=143 s are shown. The error of the script in comparison with the validation has been shown in percentages for the different found values. It can be seen that the velocity and Mach number found are slightly lower than the validation data. The altitude found is a bit higher than the validation data. This difference of both the velocity and altitude can be explained by the fact that the pitch angle was not exactly constant for the script and validation data during the ascent phase. The drag numbers found are much lower than the validation data shows. However in Figure 10.6 it can be seen that the drag curve shows more or less the same behaviour. The differences can be explained by a different drag coefficient used. The next figure shows the temperature obtained by the wall of the nose of the system and the G-force experienced during the ascent of the vehicle. For the temperature it can be seen that the differences are quite large. This is because the temperature given by the validation data is also based on empirical data. This figure shows that temperature predictions are very difficult with simple empirical functions. More about temperature calculations can be found in Section 15.1. The last plot considered is the one showing the G-force. In this plot the same behaviour as for the validation data can be seen. The difference in the dip at the end can be explained by the fact that the validation data is following the launcher and the code is following the first stage.

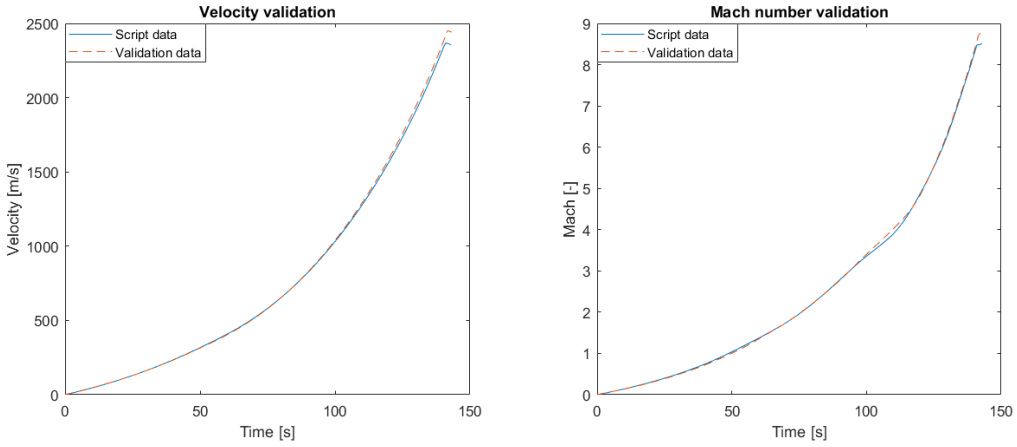

Figure 10.5: 3DOF trajectory validation of velocity and Mach number

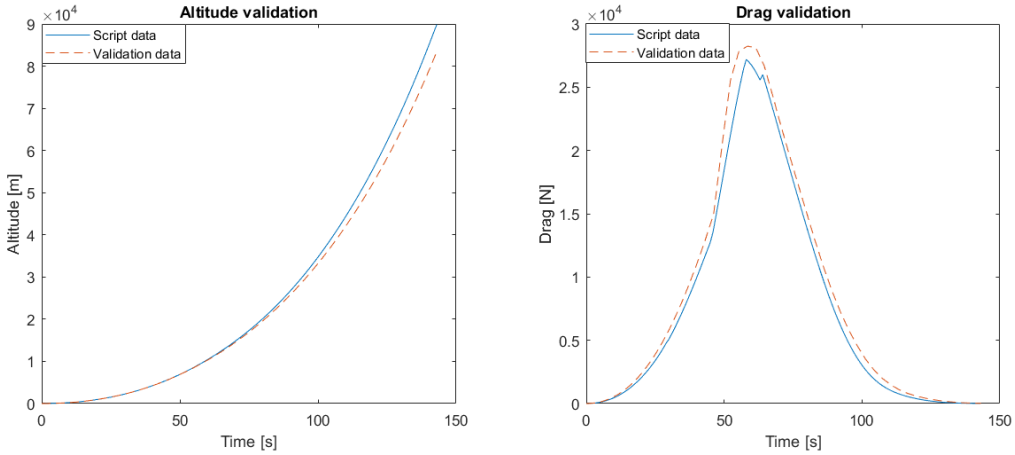

Figure 10.6: 3DOF trajectory validation of altitude and drag force

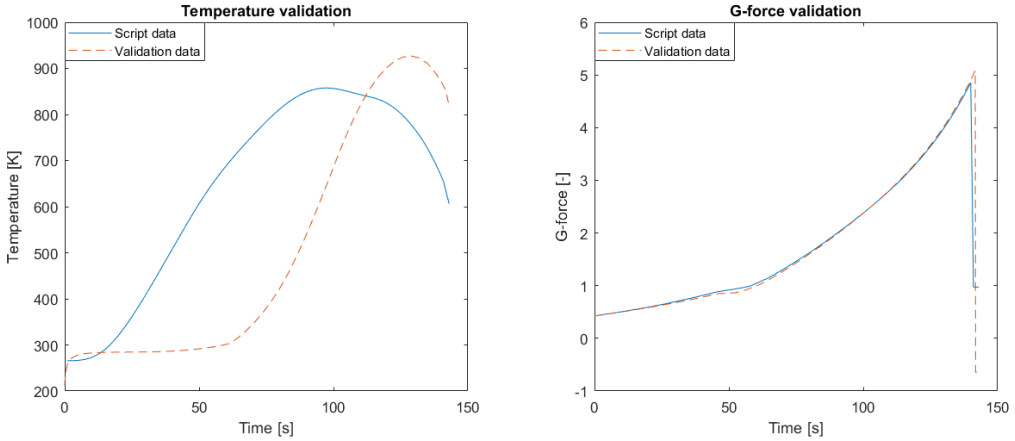

Figure 10.7: 3DOF trajectory validation of temperature and G-force

10.2. VERIFICATION GENETIC ALGORITHM

To find the most optimal configuration the genetic algorithm will be used as described in Section 4.3. To test if the genetic algorithm produces the correct optimum the Himmelblau function has been used, shown in Equation 10.1. This function is highly non-linear, and therefore often used in verification of the genetic algorithm [42]. The Himmelblau function has in total four minima [43]. The different minima are shown in the list below. A surface plot of the Himmelblau function can be found in Figure 10.8.

$$Z = (X^2 + Y - 11)^2 + (X + Y^2 - 7)^2 \tag{10.1}$$

- F(3.0, 2.0) = 0.0
- F(-2.805188,3.131312) =0.0
- F(-3.779310,-3.283186)=0.0
- F(3.584428,-1.848126)=0.0

Using Equation 10.1 the Genetic Algorithm was tested. This was done using 20-bit numbers and a range of -5 to 5. This means that the distance between the points will always be bigger than $9.5367 \cdot 10^{-6}$. Using this selection the Himmelblau function was tested. Depending on the pseudo-random generator used different minima were found. For two of the pseudo-random sets used the results are shown below in Figure 10.9 and 10.10. Figure 10.9 shows that a low function value is found fast. However this solution is discarded in the next generation. The minimum function value is decreased again. The minimum to which the tool converges is $x = 3.5845$ and $y = -1.8481$ with a function value of 0.000. The location of the different minima are shown. In

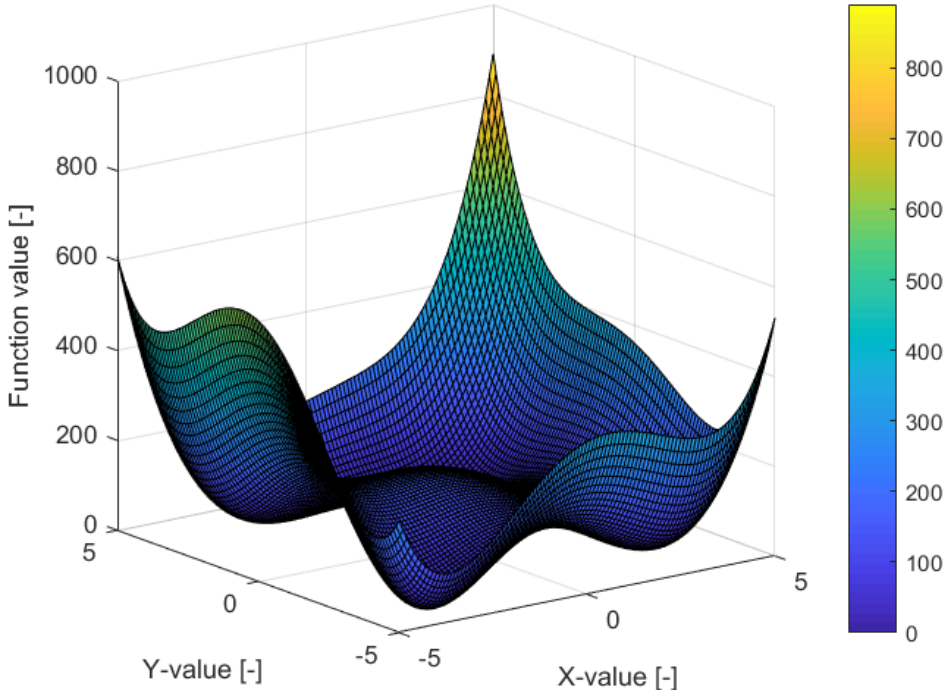

Figure 10.8: Surface plot of the Himmelblau function

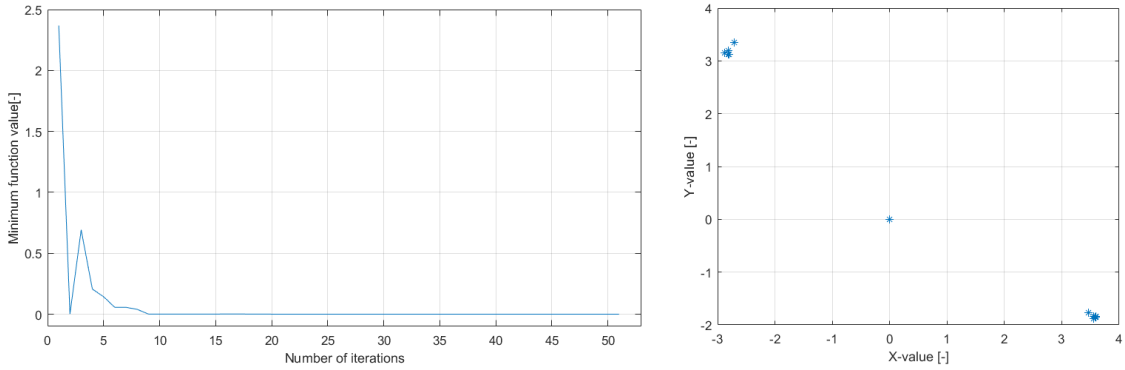

Figure 10.9: Minimum function value and location in population for the Himmelblau function, first set

this figure it can be seen that two different locations were approached by the algorithm. In the end the one in the low-right corner 'wins'. Figure 10.10 shows that the minimum is found faster than for the former set. The location of the minimum differs from the first set and is found at a location of $x = 3$ and $y = 2$.

The more bits, the closer the result matches the real minimum. However the amount of generations needed, and therefore the computation time, will increase. If more bits are used, more combinations are possible and therefore the computation time rises. However the step size becomes much smaller so the closer you can get to the real solution. The amount of grid points depends on the type of problem at hand. Besides this, the speed of convergence and the resulting minimum depends on chance as the computation time depends on the pseudo-random set used. If the best solution is already present in the first generation, the solution is obtained much faster as long as that solution is not thrown away or the minimum number changes due to mutation.

10.3. VALIDATION MASS ESTIMATES

In this section the mass estimates will be validated. In the tool both the drogue parachute and the parafoil weight were estimated using a bottom-up approach. The results found have been validated in two differ-

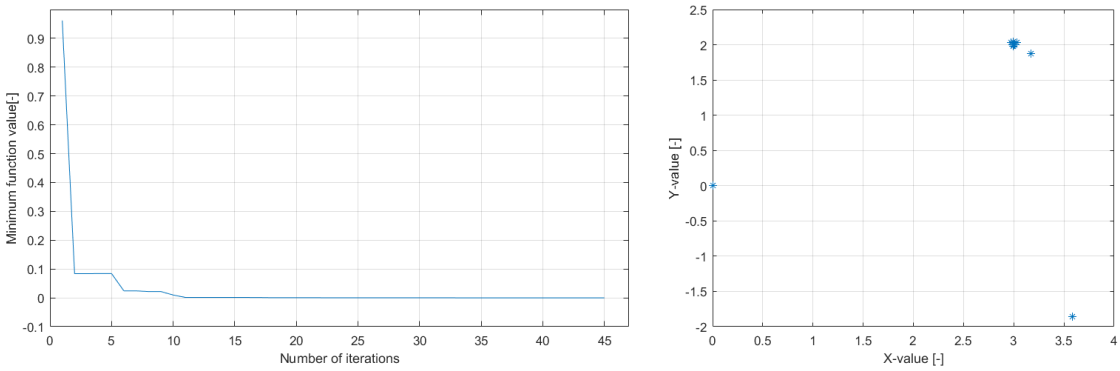

Figure 10.10: Minimum function value and location in population for the Himmelblau function, second set

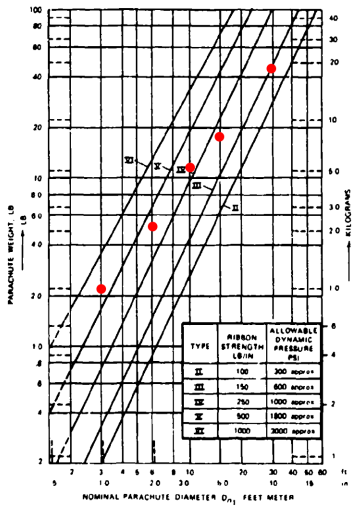

Figure 10.11: Validation drogue parachute weight calculations [2]

ent ways. The drogue parachute weight have been validated using a graph found in the Parachute Design Guide[2]. The red dots shown in Figure 10.11 are the results found using the formulation used in the tool. The results found are within the same range as shown by the figure. If a line would be drawn the slope would be a less steep than the lines shown in the figure. This would result in a bit higher prediction for the lower region of the diameter, and a bit lower prediction for the higher region. In this study only the lower region is of importance, as the drogue parachute is expected to be relatively small. Besides, a margin of 50% is added to the value shown in Figure 10.11.

For the parafoil system the weight is validated in a different way. First lines are drawn for the parafoil weight estimation shown with the dotted black line in Figure 10.12 and the weight estimation including the extra accounted 50% is shown with the blue dashed line. For four different parafoil systems the parafoil size and weight are plotted in the figure. It can be seen that the parafoil weight matches this behaviour quite well. The masses of three of the four parafoils, however, lie above above the predicted value. It is therefore recommended to use the 50% margin.

10.4. VALIDATION TRAJECTORY SIX DEGREES OF FREEDOM

The six degrees of freedom trajectory is validated using the classified WEST simulator from NLR that has been validated with actual flight data. Unfortunately the simulator only provides graphs and no raw data. The validation of the software can therefore only be done by visual inspection.

A hypothetical small sounding rocket is used in both tools. The results found were compared. The details on the hypothetical launcher can be found in Appendix B. The aerodynamic coefficients are obtained from Missile DATCOM. The results of the validation can be found in the following figures. The first figures, Figure

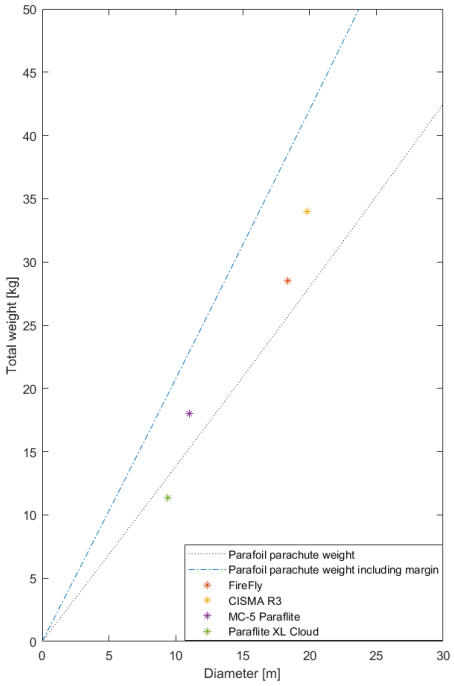

Figure 10.12: Validation parafoil weight calculations

10.13 and 10.14, show the comparison of altitude as function of time. From these figures it can be seen that both tools produce the same shape of trajectory. The NLR simulator produces a maximum altitude that is slightly higher than that produced by the 6DOF thesis software. The NLR simulator uses different environment models, which explains the different culmination altitude.

The second set of figures shows the velocity of the vehicle as function of time. For both tools, Figure 10.15 and 10.16, the velocity will reach almost 160 m/s in 2 seconds. The velocity will decrease until culmination is reached. After culmination the velocity will increase again as potential energy is transformed in kinetic energy. Both tools show the same behaviour with similar values.

For the six degrees of freedom simulation the rotation around the axes is taken into account. As the vehicle is symmetrical and no wind is taken into account in this validation, the angle of side slip does not very much. The roll angle coefficient was set to zero, so the rotation angle around the x-axis of the body is too close to zero to be visible in the graph. The angle of attack and pitch angle are therefore most important and are shown below. The angle of attack as function of time is shown in Figure 10.17 and 10.18. The pitch moment coefficient was shown to be negative with a position angle of attach (see Appendix B). This results in a stable rocket. This stability can be seen in both figures. The angle of attack will stay around zero angle of attack. The behaviour for both figures can be seen. The frequency of the oscillating angle of attack is for both tools the same. For the 6DOF thesis software the angle of attack does not damp out the oscillations as good as shown for the NLR WEST tool. The damping of the motion is caused by the aerodynamic drag.

The pitch angle as function of time is show in Figure 10.19 and 10.20. The initial pitch angle was set to 60°. The pitch angle will slowly decrease until culmination. At culmination the rocket will be pointed horizontally, i.e. the pitch angle is 0°. The rocket will now descent and the pitch angle will decrease further until impact. This is shown in both figures. The oscillation of the decreasing pitch angle is due to the oscillating angle of attack. In the plot of the thesis software a higher fluctuations is seen at the second half of the time interval, this can be explained with the higher oscillations in angle of attack described before.

Figure 10.13 to Figure 10.20 shows that the 6DOF thesis simulator calculates the behaviour well.

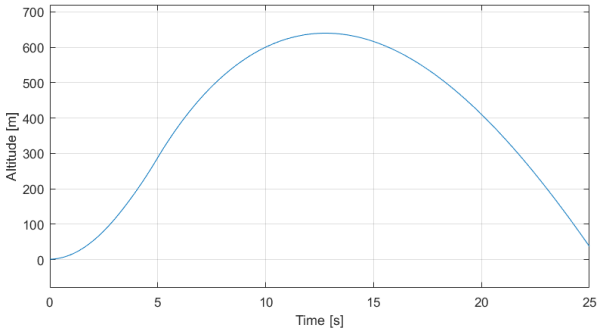

Figure 10.13: Validation Altitude 6DOF Thesis Simulator

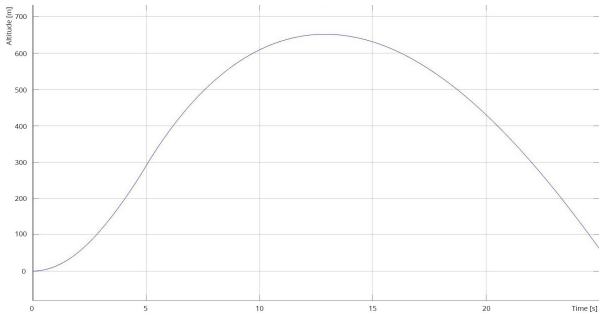

Figure 10.14: Validation Altitude 6DOF WEST NLR

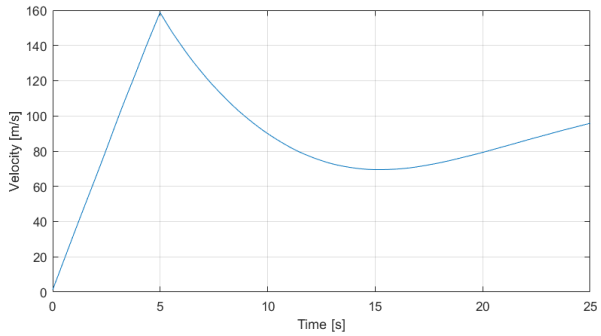

Figure 10.15: Validation Velocity 6DOF Thesis Simulator

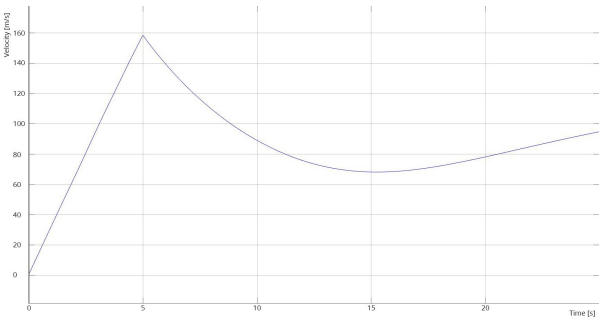

Figure 10.16: Validation Velocity 6DOF WEST NLR

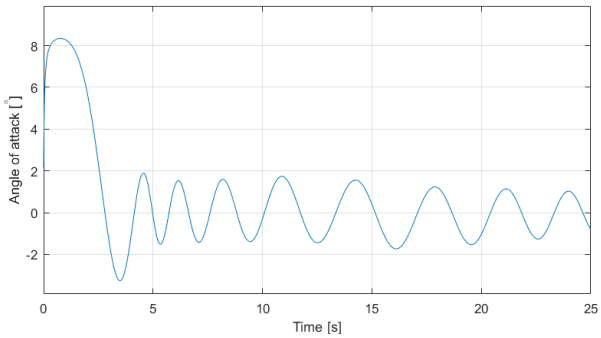

Figure 10.17: Validation Angle of Attack 6DOF Thesis Simulator

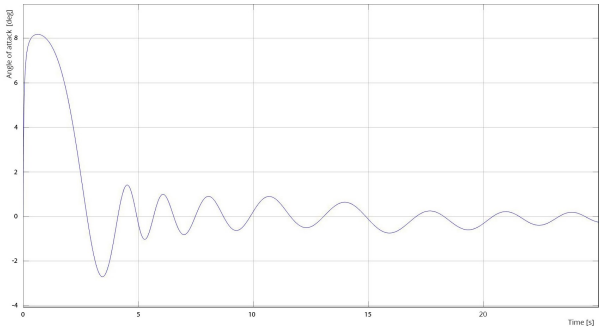

Figure 10.18: Validation Angle of Attack 6DOF WEST NLR

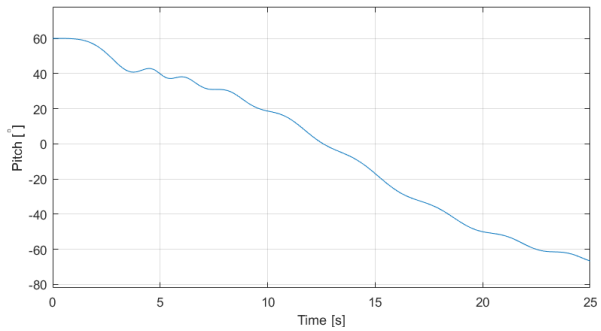

Figure 10.19: Validation Pitch 6DOF Thesis Simulator

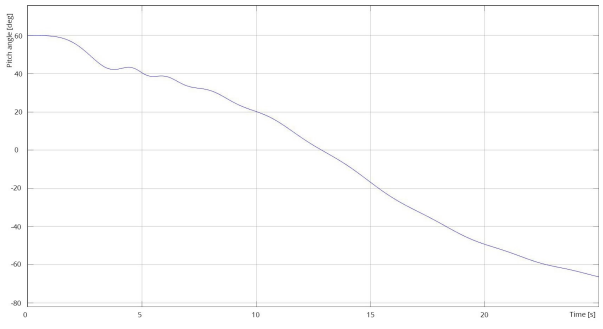

Figure 10.20: Validation Pitch 6DOF WEST NLR

11

RESULTS 3DOF OPTIMISATION SET 1

This chapter shows and discusses the results found for the three degrees of freedom optimisation. As discussed in Chapter 4 some general constraints are needed to run the optimisation. These constraints for the first iteration are found in Table 11.1. The maximum allowable G-force, temperature, and impact velocity is determined by the structure of the first stage. The constraints in Table 11.1 have been used to optimise the

Table 11.1: Constraints first iteration

	First stage	Parachute	IAD
Maximum allowable G-force	15 G	10 G	10 G
Maximum allowable temperature	2000 K	620 K	1900 K
Maximum allowable velocity at 100 m	15 m/s	15 m/s	15 m/s

configuration. First the trajectory will be shown without recovery mechanisms to compare it with the different configurations. Sections 11.2 to 11.8 will be used to explain the optimisation process used for these configurations and to show the results found. The last section of this chapter shows a summary of the results and a comparison of the different options.

11.1. NO RECOVERY MECHANISM

To design the recovery mechanism it is useful to know the trajectory of the first stage without recovery. In this section the trajectory will be shown. First the altitude is plotted against the time, shown in Figure 11.1. The velocity and Mach number are shown in Figure 11.2. Finally, the G-force and temperature plots are shown in Figure 11.3.

In the altitude plot it can be seen that the first stage will reach an altitude of 312 km. On the left side of Figure 11.2 it can be seen that the system will reach 2.3 km/s (Mach=8.5). After burn-out, the first stage will reduce the velocity to 1 km/s at the culmination point (where the vertical velocity is zero). After that, the stage falls back to Earth gaining momentum until a speed of 2.4 km/s (Mach 8). Then, the stage enters the atmosphere, resulting in a drag force that reduces the speed again to an impact velocity of 0.2 km/s. The velocity and Mach-number show a similar behaviour. The difference can be seen around the 570 seconds. The Mach-number shows a sudden drop. This decrease in the temperature is due to the increase of the temperature of the air. A decrease in the temperature results in an increase in the Mach-number. At 575 seconds the Mach-number increases again, as the vehicle is in the warmer layers of the atmosphere.

At entry of the atmosphere the system will reach a G-force of 18.7 at 595 seconds. As the requirement is set at 15 G, a deceleration system is needed to reduce the G-forces. The temperature shown in Figure 11.3 shows an increase in the temperature at ascent. At this stage the launcher is increasing its velocity, this will increase the convective heat. After separation the temperature will go down, as the velocity drops. Above the 120 km, the atmosphere is very thin and no heat convection takes place. At entering the atmosphere the temperature will increase rapidly. The temperature will go down with the decreasing velocity. The temperature reached is above the 2000 K constraint. To control the temperature a deceleration mechanism is needed before entering the atmosphere. The end velocity-requirement is set to be less than 15 m/s. This means that the system should also decelerated to make sure the system will not break at impact.

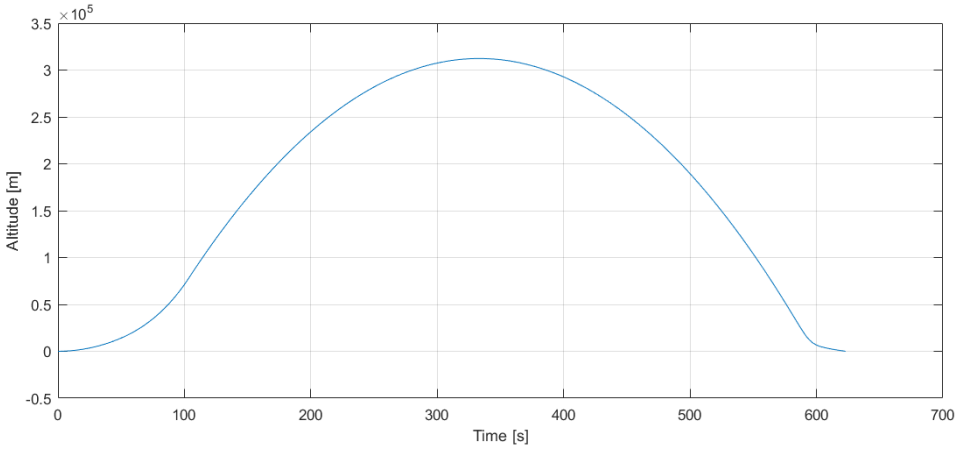

Figure 11.1: Altitude plot no recovery mechanism, set 1

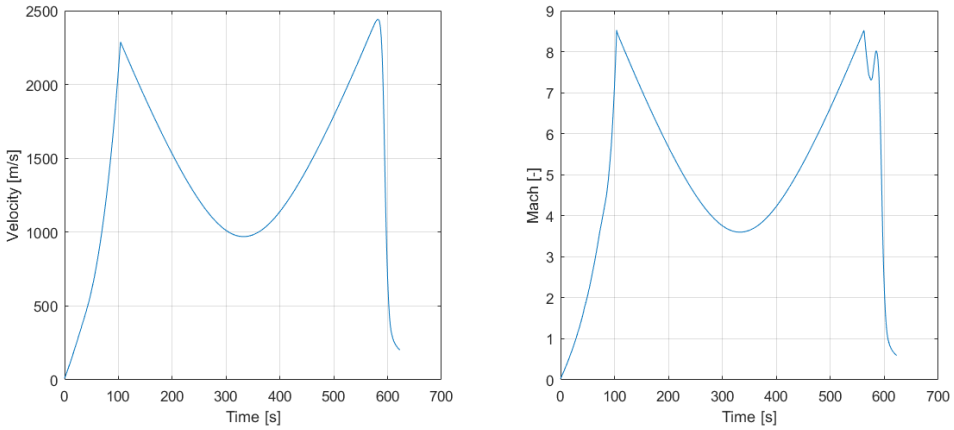

Figure 11.2: Velocity and Mach plot no recovery mechanism, set 1

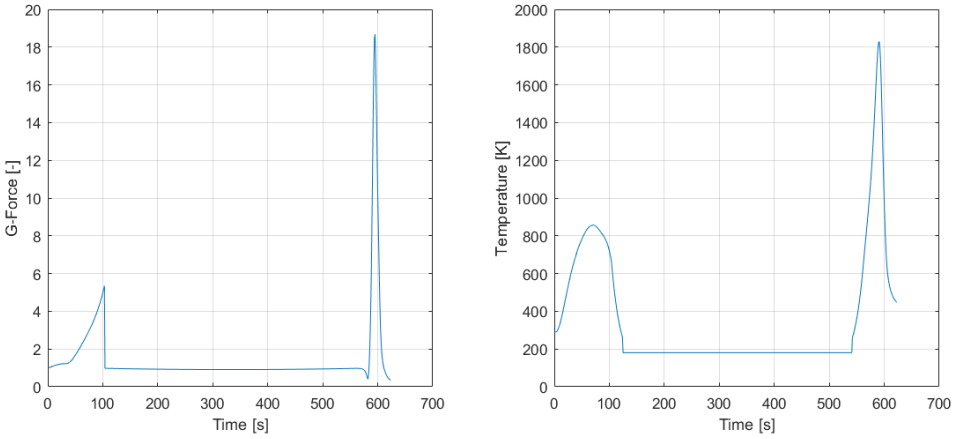

Figure 11.3: G-force and temperature plot no recovery mechanism, set 1

11.2. CONFIGURATION 1

The first results considered are the results found for Configuration 1. This configuration is explained in detail in Section 3.2.1. Configuration 1 uses only one thrust burn. In the optimisation program the thrust is kept constant as the optimisation programme can only handle this.
First a Monte Carlo simulation is used to find the search space for the genetic algorithm. After the Monte Carlo simulation this configuration is investigated using analytical calculations.

11.2.1. MONTE CARLO RESULTS

The Monte Carlo analysis is used to verify if there is a a solution with an end velocity of less than 15 m/s. To make sure the programme does not stop due to G-force constraints, the G-force constraints is played down to 20 G. For this simulation 100 000 combinations are used within the limits shown in Table 11.2. The thrust vector is pointed in perpendicular direction away from the Earth.

Table 11.2: Limits for Monte Carlo simulation Configuration 1

	Start time [s]	Duration [s]	Thrust force [N]
Lower limit	360	50	0
Upper limit	600	300	298800

Using this approach the Monte Carlo simulation only found results with too high end-velocities of more than 50 m/s. From this test, it appears that there is no solution and a genetic algorithm will therefore not function on. A genetic algorithm approach will therefore also not work on this interval.

11.2.2. ANALYTICAL APPROACH

In the last section it is shown that the Monte Carlo simulation did not find any solution, hence the genetic algorithm cannot be used. It has therefore be chosen to use an analytical approach.

As been stated, only a constant thrust level is considered. To make sure the maximum G-force is not met, the thrust burn should start before entering the atmosphere. The engine will burn till touchdown. To comply with the 15 G constraint, deceleration is needed before entering the atmosphere. This results in a constant 10 kN thrust applied till impact, resulting in 400 kg propellant. At impact the vehicle has a velocity of 240 m/s. This means that a higher constant thrust level should be applied which will result in an even higher recovery mass. Besides, if the engine was not used, the aerodynamic drag would decrease the velocity. In this configuration the engine is used, which is very in-efficient as at this point the thrust is not needed.

Configuration 1 is therefore not a suitable option in the current configuration with the current constraints.

11.3. CONFIGURATION 2

The second set of results was found for Configuration 2. This configuration applies two consecutive burns. The first burn ensures that the system stays below the 15 G constraint. The second burn slows the system down below the 15 m/s at 100 meter.

11.3.1. MONTE CARLO RESULTS

Configuration 2 applies the same approach as Configuration 1. The Monte Carlo simulation first verifies if a solution with an end velocity of less than 15 m/s can be found. To do so, the G-force limit is increased to 20G to make sure that the tool will not break because of this limit. In this case 200 000 variable combinations have been tested. The range of the different parameters are found in Table 11.3. The thrust vector has again been applied in perpendicular direction away from the Earth.

The start time of the second burn found in the table is the elapsed time after the first burn. Hence, a start time of zero (0) seconds means that the second burn takes place immediately after the first burn.

Using 200 000 simulations, again only results were found with an end velocity of more than 50 m/s. As no results were found with the Monte Carlo simulation, an analytical investigation is needed.

Table 11.3: Limits for Monte Carlo simulation Configuration 1

	Start time first burn [s]	Duration first burn [s]	Thrust force first burn [N]	Start time second burn [s]	Duration second burn [s]	Thrust force second burn [N]
Lower limit	360	50	0	0	2	0
Upper limit	600	300	298800	200	150	298800

11.3.2. ANALYTICAL APPROACH

A solution was found using the constraints discussed in Table 11.1 using an analytical approach, a solution is found. Using the Tjolkovsky formula, discussed in Equation 2.21, the amount of propellant needed to decelerate the system was calculated. An estimate of the amount of propellant was found and used as input in the script. In this approach assumptions as constant mass and no atmospheric drag were made. Due to this deviation, the found results needed to be modified when using the script. This has been done by making use of a trial-and-error method. In comparison with the Monte Carlo simulation, the angle of the thrust has now been adjusted. The found results are shown below in Table 11.4.

Table 11.4: Values found for Configuration 2, set 1

	First thrust burn	Second thrust burn
Start time	150 s	505 s
Duration	32 s	14 s
Thrust force	18 000 N	30 500 N
Angle[1]	-119°	99°

Using the results found in Table 11.4, the trajectory has been plotted. The first figure, Figure 11.4, shows the altitude as function of the time. It can be seen that due to the first burn, a lower apogee is reached. Furthermore, the total flight duration has been shortened, as the system will reach lower altitudes and therefore need less time to come back to the Earth. The velocity and Mach number as function of time can be found in

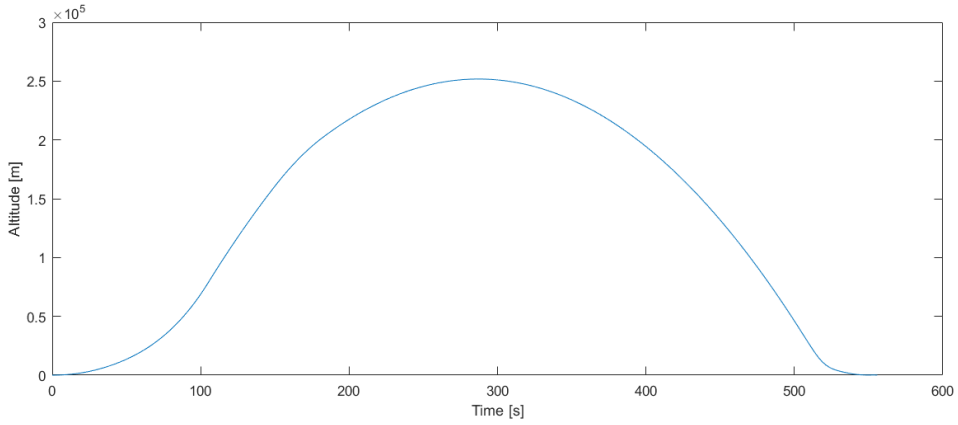

Figure 11.4: Altitude plot Configuration 2, set 1

Figure 11.5. In these plots it can be seen that the second velocity peak is reduced, which is needed to control the G-load. In this figure it can also be seen that the end-velocity of the system is below the 15 m/s. The last figure of this section, Figure 11.6, shows the G-load the temperature reached. It can be seen that both stay below the constraints set.

11.4. CONFIGURATION 3

Configuration 3 makes use of one thrust burn followed by a parachute and parafoil. The thrust burn is used to decelerate before entering the atmosphere to control the temperature reached and the G-forces encountered during entry. The parachute and parafoil are used to decelerate in the last part of the trajectory, to make sure

[1] The angle with the local level horizontal, counterclockwise is defined as positive.

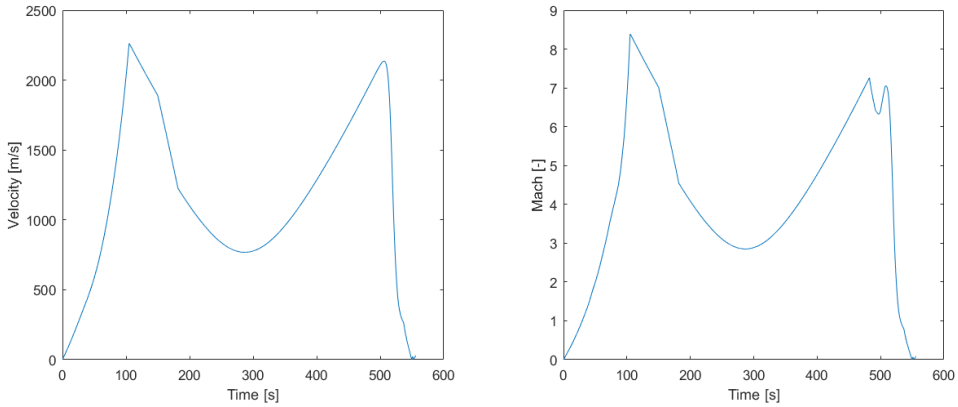

Figure 11.5: Velocity and Mach plot Configuration 2, set 1

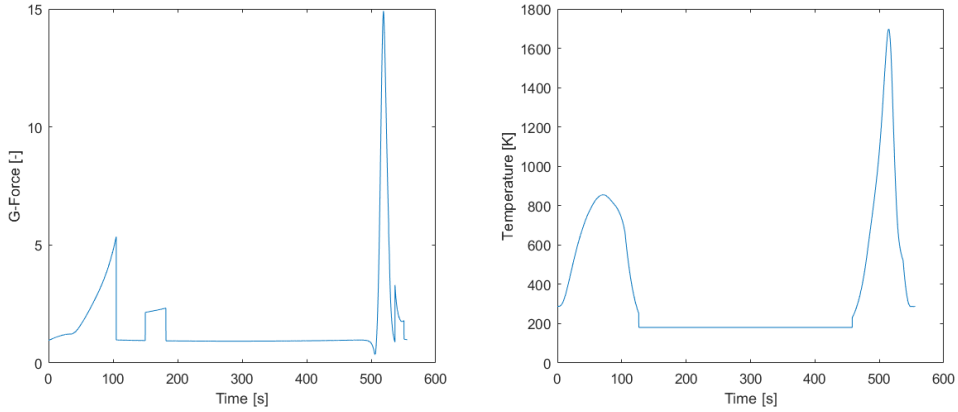

Figure 11.6: G-force and temperature plot Configuration 2, set 1

the system would land with a low speed. First a Monte Carlo method was used to find the search area for the Genetic Algorithm.

11.4.1. MONTE CARLO

As stated, first a Monte Carlo simulation was used to find the search space for the Genetic Algorithm. This has been done by making use of 100 000 variable combinations. The region of the different variables are shown in Table 11.5. The constraints used for the Monte Carlo simulation were the same constraints as set for the overall exercise shown in Table 11.1.

Table 11.5: Limits for Monte Carlo Configuration 3

	Start time	Duration	Thrust burn	Radius parachute	Radius parafoil
Lower bound	300	0	0	0.5	0.5
Upper bound	600	50	298800	10	200

Using the Monte Carlo simulation a region was found which complies with all constraints. This region was used as baseline for the Genetic Algorithm.

11.4.2. GENETIC ALGORITHM

Using the results found in the last second the search area for the Genetic Algorithm was defined, shown in Table 11.6. The population size was set to 200, and a maximum of 50 generations was used as safeguard if convergence would not be reached.

Using these variables the genetic algorithm found a minimum system mass. To find this minimum a total of 27 generations were needed. The minimum system mass in each generation is shown in Figure 11.7. In this figure it can be seen that the minimum total system weight decreases till a minimum is reached.

Table 11.6: Limits for Genetic Algorithm Configuration 3

	Start time	Duration	Thrust burn	Radius parachute	Radius parafoil
Lower bound	400	10	8000	1.5	15
Upper bound	550	50	298800	7	60

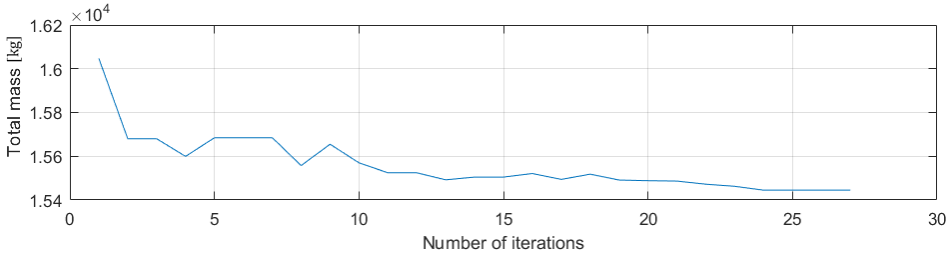

Figure 11.7: Minimum total mass launcher configuration 3 in generation for Genetic Algorithm, set 1

The variables used for the total minimum system mass in the last generation is shown in Table 11.7.

Table 11.7: Result Configuration 3, set 1

	Start time [s]	Duration [s]	Thrust burn [N]	Radius parachute [m]	Radius parafoil [m]
Result for minimum weight	544	36	10415	1.9	20 [1]

Using the values shown in Table 11.7 the following trajectory plots can be found; Figure 11.8-11.10. In Figure 11.8 the altitude as function of the time is shown. In this figure it can be seen that the maximum altitude reached is much higher than for Configuration 2. This can be explained by the fact that the retro-propulsion will be applied after the maximum altitude is reached. Because the total altitude reached is higher and the parafoil will provide some lift the total flight will take longer than for configuration 2.

In Figure 11.9 it can be seen that the retro-propulsion is applied just before the maximum velocity is reached. The velocity curve is flattened before the maximum is reached and so just before the atmosphere is entered. This deceleration of the system will result in a maximum G-load of 15 G, shown in Figure 11.10. The maximum G-load experienced for the drogue parachute is also at the constraint of 10 G. A third peak can be seen around the 650 seconds. At this point the parafoil will open, which results in an increase in the G-load. The right hand side of Figure 11.10 shows the temperature reached of the nose of the vehicle. The maximum temperature is below the set constraint. The temperature of the system at opening of the parachute is below the 600 K, which is also within the limits. In Figure 11.9 and 11.10 it can be seen that by optimising the total mass of the system the optimum will be found just below the constraints set.

11.5. CONFIGURATION 4

The next configuration makes use of retro-propulsion and an inflatable aerodynamic decelerator. The thrust is used to make sure the IAD does not burn-up in the atmosphere or would break due to the accelerations. The IAD have to make sure the system will decelerate enough to provide a safe landing. First a Monte Carlo simulation has been used to find if a solution could be found by the genetic algorithm.

11.5.1. MONTE CARLO

The Monte Carlo simulation has been used to find if a solution was present within the constraints shown in Table 11.1. In Table 11.8 the variable interval used can be found. The maximum IAD size used is based on the currently testes maximum size of the IAD [44]. In total 100 000 combinations of variables have been used to find a solution. Using these values, no results were found. It was found that no solution could be found that reduces the vehicle velocity below the 15 m/s at impact.

[1] The found radius of the parafoil will result in a parafoil of 15x30 meters.

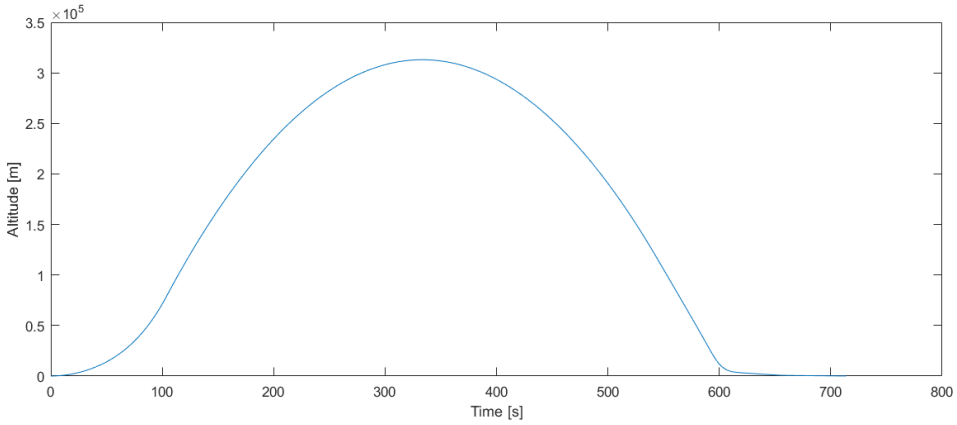

Figure 11.8: Altitude plot Configuration 3, set 1

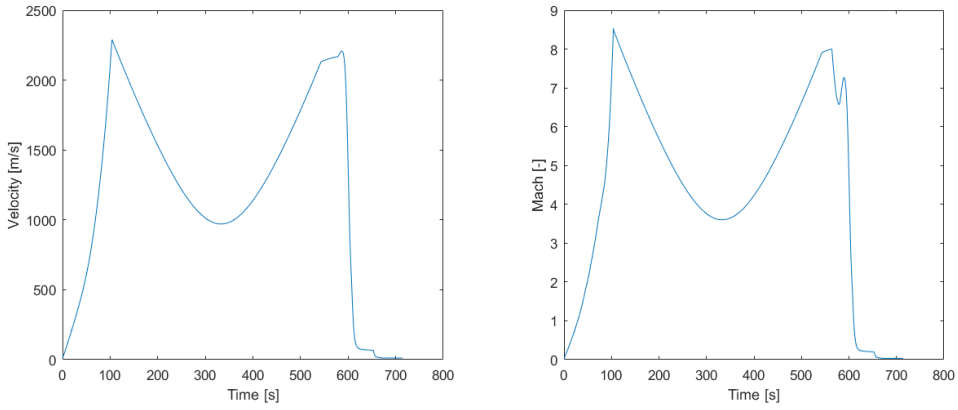

Figure 11.9: Velocity and Mach plot Configuration 3, set 1

11.5.2. ANALYTICAL APPROACH

In Figure 11.2 it was shown that the system would decelerate to an end velocity of 0.2 km/s. To make sure that the system would decelerate to an end velocity of less than 15 m/s. It was calculate that a minimum size of 230 m^2 is needed. This means that an IAD of 17.1 meter in diameter is needed. Currently the biggest IAD tested is 6 meter in diameter. This means that the IAD needed to comply with the end constraint is much bigger than currently or in the near future available.

11.6. CONFIGURATION 5

Configuration 5 will make use of only the inflatable aerodynamic decelerator. First a Monte Carlo simulation was used to verify if a solution could be found. After the Monte Carlo simulation this configuration was investigated analytical.

11.6.1. MONTE CARLO

The Monte Carlo simulation done for the configuration 5 used in total 100 000 simulations. The limits of the parameters used are shown in Table 11.9. It can be seen that maximum area of the HIAD is slightly increased in comparison with configuration 4. This has been done to increase the searching space slightly and to see if a solution could be found.

Using the limits shown in Table 11.9 no vehicle could be found which would comply with all constraints shown in Table 11.1.

11.6.2. ANALYTICAL APPROACH

Because no configuration could be used by the Monte Carlo simulation a more in depth analysis is needed. First of all the system should make sure the maximum G-force and temperature would not be exceeded. The

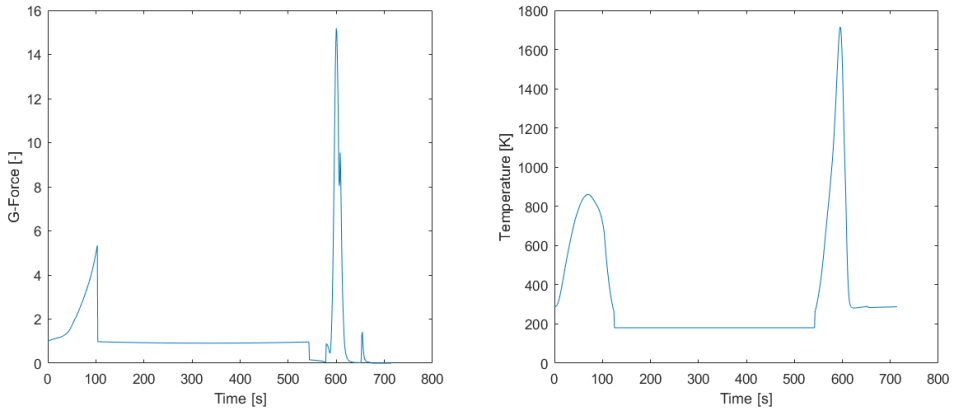

Figure 11.10: G-force and temperature plot Configuration 3, set 1

Table 11.8: Limits for Monte Carlo Configuration 4

	Start time [s]	Duration [s]	Thrust burn [N]	Time opening IAD [s]	Area IAD [m^2]
Lower limit	360	2	0	2	1
Upper limit	600	50	298800	200	120

make sure this would not happen the IAD needs to be deployed as early as possible in the flight. In this way the IAD can benefit as much as possible from the atmospheric drag in the higher atmospheric layers. To not exceed the end-velocity the area of the IAD should be at least 230 m^2 is needed. If the IAD is opened just after separation the maximum G-force will be more than 14 G. This means that the area of the IAD should be even bigger to not exceed the G-load constraint. An area of 560 m^2, meaning a radius of at least 13.4 meter or a 26.7 meter diameter is needed to comply with the maximum G-load constraint.

11.7. CONFIGURATION 6

In configuration 6 the IAD and a parachute system will be used. To find the minimum system mass for this configuration, first a Monte Carlo simulation has been used. After the Monte Carlo simulation the design has been investigated in more detail using an analytical approach.

11.7.1. MONTE CARLO

For the Monte Carlo simulation in total 100 000 simulations were performed. The limits of the different parameters can be found in Table 11.10.

Using the limits found in Table 11.10 no results were found which could comply with the G-load requirement. All simulations showed a too high G-load experienced.

11.7.2. ANALYTICAL APPROACH

With the Monte Carlo simulation no results could be found in the limits shown in Table 11.10. As the system would not be decelerated by any other device before entering the atmosphere the same problem as found for configuration 5 arises. The IAD should have an area of at least 560 m^2 to comply with the maximum G-load requirement. A diameter of 26.7 meter will be needed for the IAD.

As been discussed before the maximum diameter currently available is 6 m. A diameter of 27 meter is therefore considered unrealistic at this moment.

11.8. CONFIGURATION 7

The last configuration considered is configuration 7. This configuration makes use of the IAD and retro-propulsion. First a Monte Carlo simulation is used, followed by an analytic investigation.

Table 11.9: Limits for Monte Carlo Configuration 5

	Time opening IAD [s]	Area IAD [m^2]
Lower limit	120	1
Upper limit	590	150

Table 11.10: Limits for Monte Carlo Configuration 6

	Time opening IAD [s]	Area IAD [m^2]	Duration IAD [s]	Radius parachute [m]	Radius parafoil [m]
Lower limit	120	1	50	0.5	0.5
Upper limit	500	100	500	10	200

11.8.1. MONTE CARLO

For the Monte Carlo simulation 100 000 simulations were performed. The limits used for the different parameters can be found in Table 11.11.

Table 11.11: Limits for Monte Carlo Configuration 7

	Time opening IAD [s]	Area IAD [m^2]	Duration IAD [s]	Start thrust [s]	Duration thrust [s]	Thrust force [N]
Lower limit	120	1	50	10	2	0
Upper limit	500	100	500	400	100	298800

Using the constraints found in in Table 11.11, no results were found. In all simulations, the G-loads encountered when entering the atmosphere are violating the constraints.

11.8.2. ANALYTICAL APPROACH

For the last configuration again the same issue has been found as for configuration 5 and 6. The needed diameter for the IAD to stay below the G-load requirement is 26.7 meter.

11.9. TRADE-OFF

In the former sections all configurations were discussed. It was found that for all configurations using an inflatable aerodynamic decelerator were not suitable. The size of the IAD needed to decelerator was too large.

Two different configurations remain, configuration 2 and configuration 3. The mass needed for the deceleration can be found in Table 11.12. In this table it can be seen that the extra mass needed for deceleration for configuration 3 is 100 kg lower than for configuration 2. Considering only the mass needed for recovery configuration 3 would be the most favourable option. However propellant is much cheaper than a parachute system. So taking into account cost it might be that the configuration 3 is not beneficial. Next to the extra system mass and the cost, the landing system should also be considered. The landing mechanism will depend on the recovery mechanism used.

Table 11.12: Comparison configuration 2 and configuration 3 based on first iteration

	Configuration #2
Fuel mass (1) [kg]	192
Fuel mass (2) [kg]	143
Extra tank mass [kg]	3
Total mass [kg]	**369**

	Configuration #3
Fuel weight [kg]	111
Extra tank weight [kg]	1
Parachute system [kg]	147
Total mass [kg]	**269**

12

RESULTS 3DOF OPTIMISATION SET 2

In the previous chapter results were found for the optimisation of the three degrees of freedom system. After evaluation of these results it was found that a new optimisation was needed as new information became available. First of all the launcher was slightly changed. The second reason was that after evaluation of the structures group of the project it was found that the structure can handle higher G-loads than anticipated before. The new constraints can be found in Table 12.1. In this table can be found that the temperature requirement is not present anymore. After evaluation of the temperature requirement it was found that the temperatures found in iteration 1 were not realistic for this situation. It has therefore be chosen to discard this requirement and make the temperature evaluation part of the follow-up research. Besides, the maximum allowable end-velocity is decreased to 10 m/s. A lower impact velocity will be beneficial for the recovery of the first stage.

Table 12.1: Constraints second iteration

	First stage	Parachute	IAD
Maximum allowable G-force	20 G	10 G	20 G
Maximum allowable end-velocity at 100 m	10 m/s	10 m/s	10 m/s

12.1. NO RECOVERY MECHANISM

Just as for set 1 it is useful to know the trajectory of the first stage without recovery mechanisms. In this way the range of the parameters could be determined. First the altitude is plotted against the time, shown in Figure 12.1. The velocity and Mach number are shown in Figure 12.2. In Figure 12.3 the temperature and the total G-load can be found. In the altitude plot it can be seen that the first stage will reach an altitude of 232 km. This is almost 80 km less than found for set 1. This is due to a difference in pitch angle at separation of the two sets. In Figure 11.2 a rest velocity of around 1 km/s was seen at culmination. For this set the velocity is found to be 2 km/s. This means that the velocity is pointed in a more horizontal direction than for set 1. On the left side of Figure 12.2 it can be seen that the system will reach 2.5 km/s (Mach=9). The system will then reduce the speed to a velocity of 1.9 km/s (Mach=3) and increase its speed to 2.6 km/s (Mach=9). The impact velocity will be 0.2 km/s (Mach=0.6). The total G-load experienced is less then 16 G. This is also less than was found for set 1. This difference in G-load can be explained by the lower culmination point.

At entry of the atmosphere the system will reach a G-force of 16. As the new requirement is set at 20 G, this means that no deceleration mechanism is needed before entering the atmosphere. The end-requirement is kept to be less than 15 m/s. This means that the system should only decelerate during the last part of the trajectory.

In Chapter 11 it was found that the IAD was not able to decelerate the system to the 15 m/s at 100 meter altitude. This means that this system would not be useful, as no deceleration is needed before the last phase and that only two options remains. The first option is Configuration 1, using retro-propulsion to land safely. From here on this configuration will be simply denoted by 'retro-propulsion'. The second option would be using a parachute system. This configuration will be mentioned as 'parachute system'. This configuration is

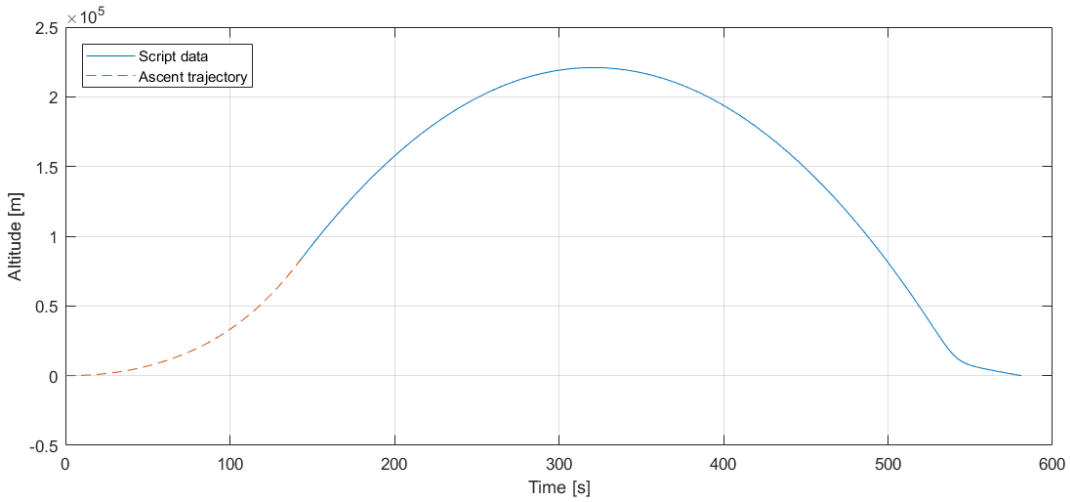

Figure 12.1: Altitude plot no recovery mechanism, set 2

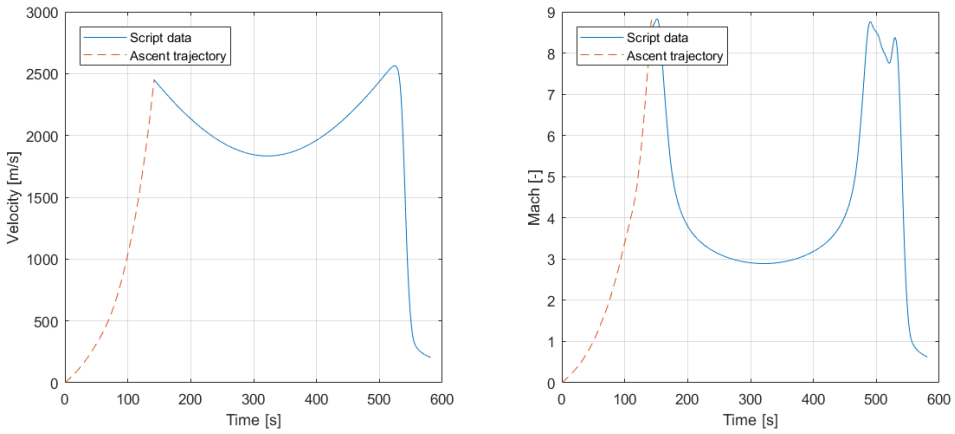

Figure 12.2: Velocity and Mach plot no recovery mechanism, set 2

similar to Configuration 3 discussed in Section 3.2.3 and 11.4. In this case the first thrust burn will not be needed. The results for these two configurations are shown below.

12.2. RETRO-PROPULSION

The first results considered are the results found for Configuration 1. This configuration has been explained in detail in Section 3.2.1. Configuration 1 makes use of a single burn. As been explained in the former chapter, the optimisation program is not able to find a solution for the retro-propulsion alternatives. This configuration has therefore been analysed by an analytical approach explained in Section 11.9.

The results found for this configuration are shown in Table 12.2. It has been chosen to vary the thrust, which result in two different thrust levels, each with a duration of one second. The first second all engines will be used with a throttle setting of 95 %. The second second half of the engine will be used with full power.

Table 12.2: Results for Retro-propulsion, 3DOF

	First second thrust	Second second thrust
Start time	576.9 s	577.9 s
Duration	1 s	1 s
Thrust force	200 000 N (94.6% throttle)	105700 N (half engines)

Using the results found in Table 12.2, Figure 12.4 to 12.6 have been plotted. The altitude of the vehicle can

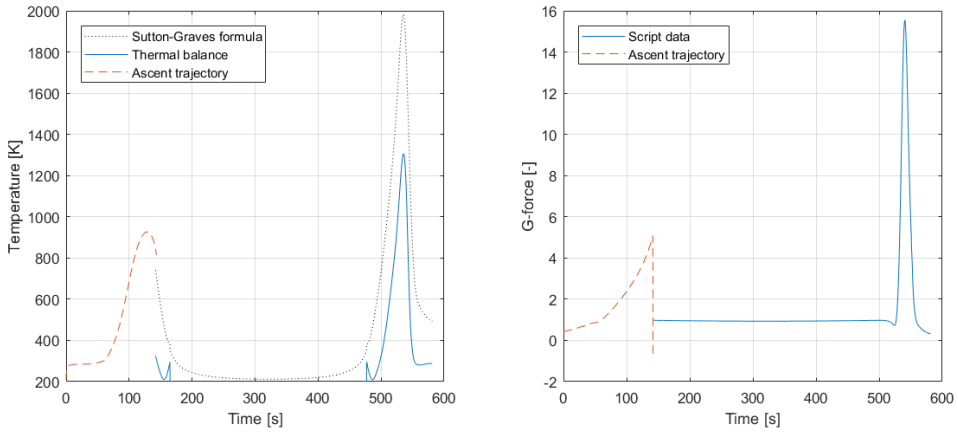

Figure 12.3: Temperature and G-load plot no recovery mechanism, set 2

be found in Figure 12.4. At 576.9 seconds the retro-propulsion will start. At this moment the vehicle will be at an altitude of 145 meters.

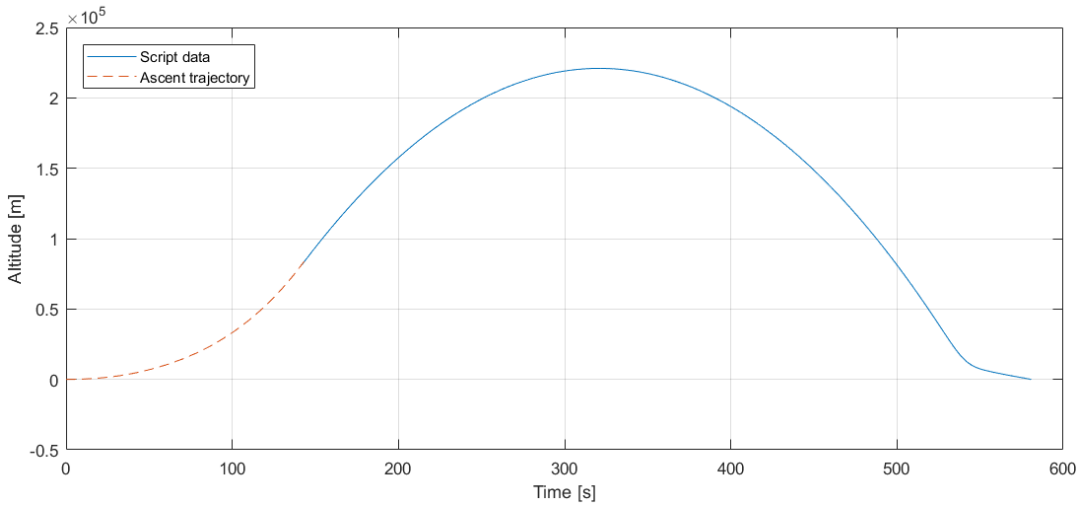

Figure 12.4: Altitude plot retro-propulsion 3DOF, set 2

In Figure 12.5, the velocity and Mach as function of the time can be found. In this figure it can be seen that at 576.9 seconds the engine will be ignited. At the moment of ignition, the velocity of the vehicle is 219 m/s. The retro-propulsion will reduce this velocity below the 10 m/s. Some propellant is still left to reduce the velocity to 0 m/s.

The temperature and G-force obtain during the flight is shown in Figure 12.6. On the left side of this figure the temperature as function of the time can be found. Two different approaches are shown. The black dotted line shows the results found using the Sutton and Graves formulation. The blue solid line shows the temperature calculated using the thermal balance approach. It can be seen that the Sutton and Graves formulation gives a higher temperature than the requirement; however the thermal balance shows a lower temperature. The G-load experienced by the system is below the required 20 G. During the two seconds of thrust, the G-load experienced is around the 17 G.

12.3. PARACHUTE SYSTEM

The parachute system configuration makes use of a drogue parachute and parafoil. The parachute and parafoil decelerate the system in the last part of the trajectory to ensure that it will land with a low speed. The genetic algorithm was used to find the optimal design. To run the genetical algorithm the constraints

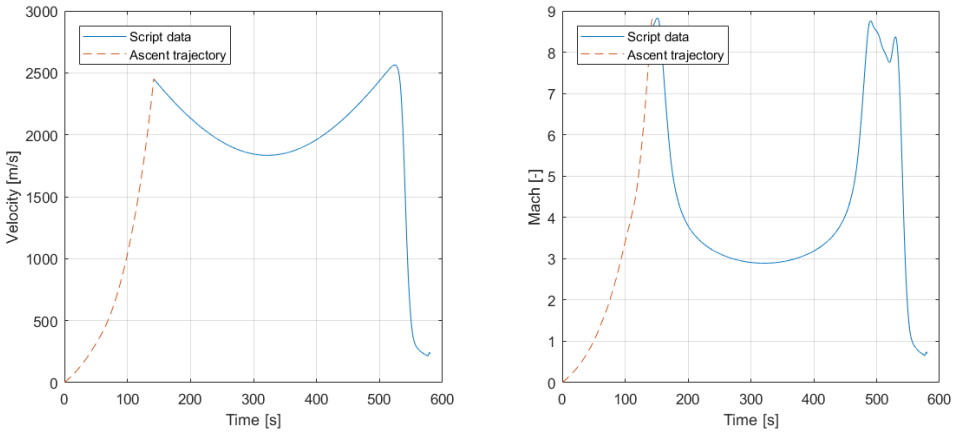

Figure 12.5: Velocity and Mach plot retro-propulsion 3DOF, set 2

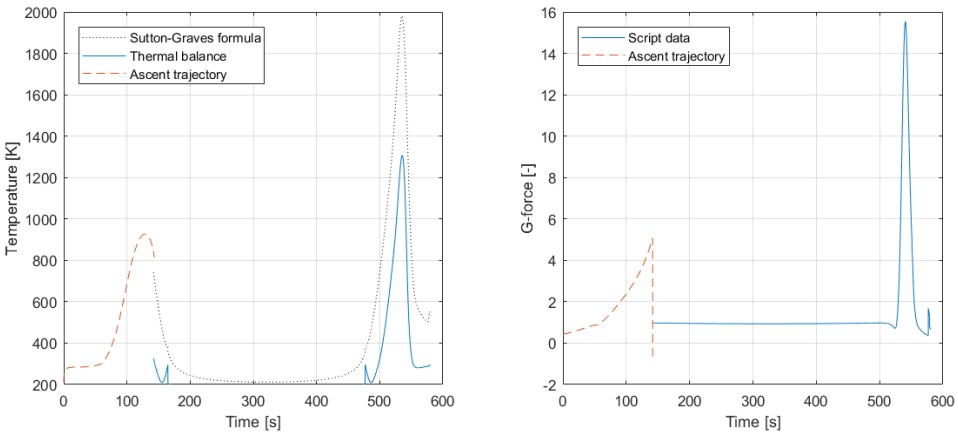

Figure 12.6: G-force and temperature plot retro-propulsion 3DOF, set 2

shown in Table 12.1 have been used. The limits of the size of the parachute and parafoil were based on the results found for set 1 and are shown in Table 12.3.

Table 12.3: Limits for Genetic Algorithm parachute design

	Radius parachute	Radius parafoil
Lower bound	1.7	18
Upper bound	1.9	22

The genetic algorithm found a solution using a population size of 200, and a maximum of 50 generations, as safeguard if convergence would not be reached. In total 22 generations were needed to ensure convergence. The minimum system mass in each generation is shown in Figure 12.7. The variations in this figure are much smaller than for Configuration 3 set 1. This can be explained by two reasons. The first reason is that a smaller search region has been chosen. Due to this smaller region less outliers are found. The second reason is that fewer systems are optimised in this assignment. The variables of the lightest design is shown in Table 12.4.

Using the values shown in Table 12.4 the following figures (Figure 12.8 - 12.10) are produced. The altitude as function of time is shown in Figure 12.8. This figure shows that around 550 seconds the descent of the vehicle is slowed. At 550 seconds the drogue parachute is opened. In total it will take 640 seconds to land the vehicle safely.

[1] The found radius of the parafoil will result in a parafoil of 15.75x31.5 meters.

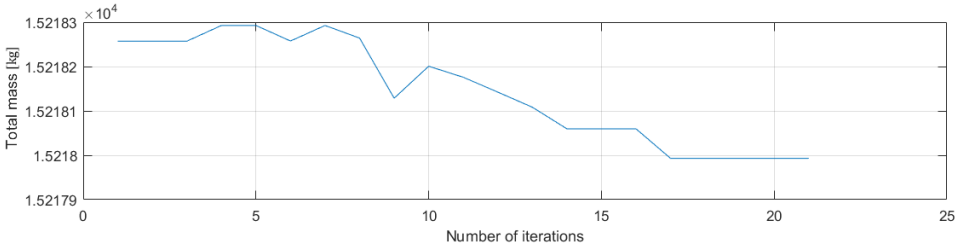

Figure 12.7: Minimum total mass launcher in generation for Genetic Algorithm, parachute design

Table 12.4: Results Parachute system design

	Radius parachute [m]	Radius parafoil [m]
Result for minimum weight	1.80	21[1]

The velocity and Mach curve can be found in Figure 12.9. Comparing this figure with Figure 12.2 shows that the drogue parachute will decelerate the system further till equilibrium is reached. This equilibrium is shown by the almost constant velocity between 570 seconds and 610 seconds. Then the parafoil will open and again a reduction of the velocity can be seen. The system will now be decelerated to a velocity below the 10 m/s. The G-load and temperature experienced by the vehicle can be found in Figure 12.10. The temperature plot, shown on the left hand side of the figure, shows two different approaches. The black dotted line shows the results obtained from the Sutton and Graves formula. The blue solid line shows the temperature calculated by using the thermal balance. The Sutton and Graves formulation shows a temperature of 450 K at opening of the drogue parachute. The thermal balance shows a temperature of 900 K. The two methods lead to very different results. The thermodynamics should therefore be investigated in more detail. Section 15.1 provides more information regarding thermodynamics.

The right hand side of Figure 12.10 shows the G-load experienced by the system. The figure shows that the G-load will stay all time below the 20 G. At opening of the drogue parachute a peak of 8 G can be seen, which is less than the 10 G limit. At 610 seconds the parafoil has been deployed. This deployment can be seen in the third peak of the blue solid line. The deployment induces a G-load of 2.5 G. This value is also far below the constraint.

12.4. COMPARISON

Two different recovery mechanisms were investigated in this chapter. Both configurations stayed within the set constraints. This means that both options should be considered in more detail. The results on the mass estimation can be found in Table 12.5. In comparison with the first estimates the needed mass for recovery shrunk with more than 50%. In the first iteration retro-propulsion was needed to stay below the 15 G. This thrust burn has been discarded as the maximum allowable G-load was increased. Another difference is that the retro-propulsion variant has a lower recovery weight than the parachute system. In the first iteration, the opposite result was found. The difference in recovery mechanism mass between the options was found to be less than seen for the first iteration. The results found are quite close and so the different landing mechanisms are very important to pick the best option.

Table 12.5: Comparison recovery mechanism mass of retro-propulsion and parachute system based on second iteration

	Retro-propulsion
Fuel mass [kg]	98
Extra tank mass [kg]	1
Total mass [kg]	**99**

	Parachute system
Parachute system [kg]	95
AGU [kg]	40
Total mass [kg]	**135**

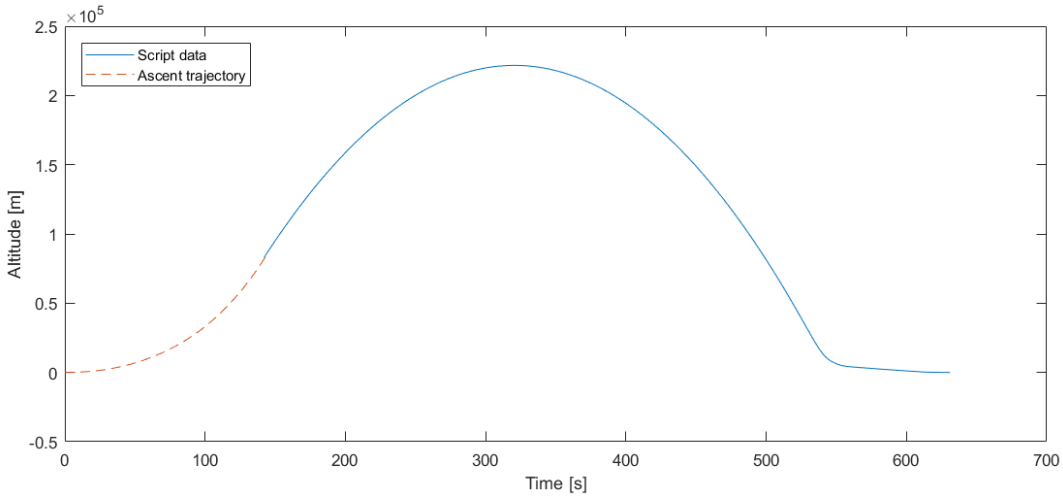

Figure 12.8: Altitude plot Parachute system design, set 2

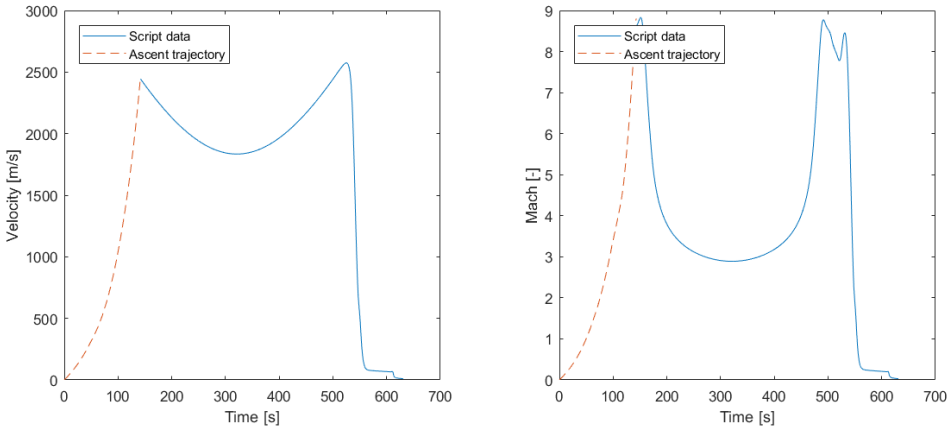

Figure 12.9: Velocity and Mach plot Parachute system design, set 2

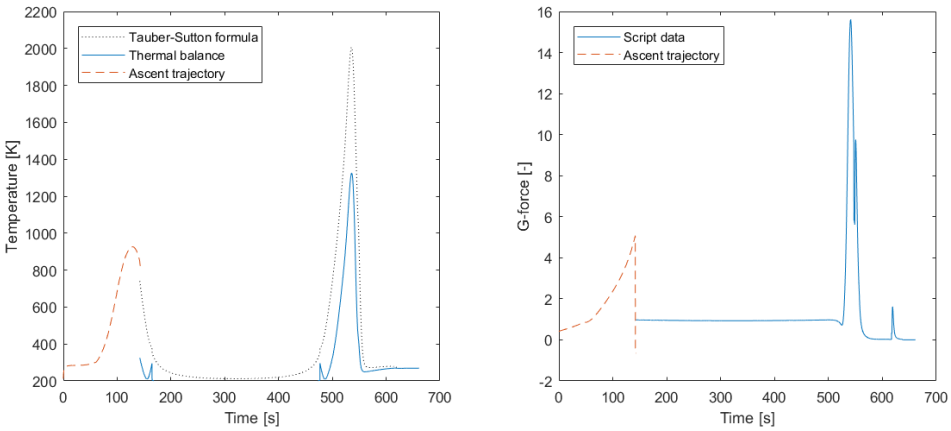

Figure 12.10: G-force and temperature plot Parachute system design, set 2

13

Six Degrees of Freedom Simulation

In Chapter 12 the recovery systems were optimised to the minimum take-off mass. Two different options were considered, retro-propulsion system and the parachute system option. In this chapter these two options are investigated using a six degrees of freedom simulation. The same separation conditions, velocity, pitch and altitude, have been used. In this chapter it will be investigated how strong the control system should be and what the impact point of the first stage will be. The results found will be used in the next chapter. First the results for the retro-propulsion option will be given and explained. The second part will be dedicated to the parachute system configuration.

13.1. Retro-propulsion

In Section 12.4 it was calculated that the propellant and extra tank mass would weigh 99 kg. In this section an extra 50 kg will be added to the system to include the landing system mass.

In this simulation a time step of 0.01 seconds is used. The control system is used till the system is descended to a height of 60 km. At this point a better control system will be needed as the atmosphere gets denser and so will the moments produced become larger.

The different trajectory profiles are shown below. The altitude of the first stage can be seen in Figure 13.1. The velocity profile is shown in Figure 13.2. The results found are similar to the results shown for the 3DOF simulation. The maximum altitude obtained and the velocity are slightly higher. This difference can be explained by the slightly higher system mass, due to the landing system. A higher system mass will increase the velocity as the system will decrease less due the deceleration forces, using Newton's second law.

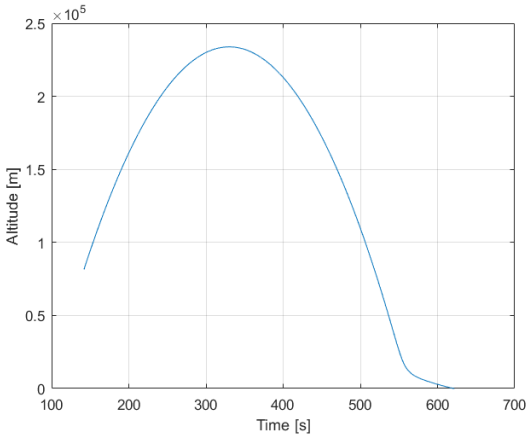

Figure 13.1: Altitude profile Retro-propulsion 6DOF

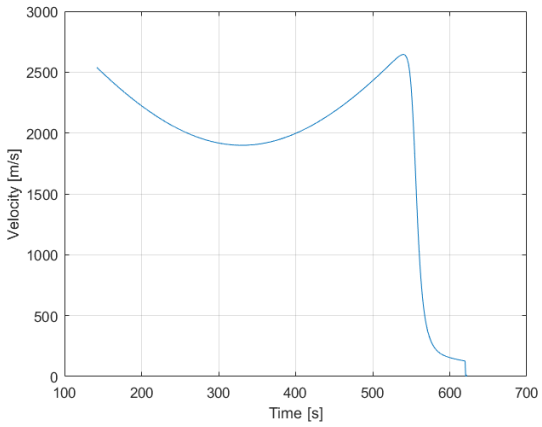

Figure 13.2: Velocity profile Retro-propulsion 6DOF

The temperature and G-load are shown in Figure 13.3 and Figure 13.4 respectively. Comparing these results with the obtained 3DOF results it can be seen that the second peak for the G-load is slightly higher than for the 3DOF results. Furthermore the temperature peak calculated using the Sutton and Graves formulation

is slightly higher. This increase of G-load and temperature can be explained by the increase of the system mass.

In Figure 13.5 and in Figure 13.6 the angle of attack, and angle of side slip, and the pitch angle as function of time are shown. Figure 13.5 shows that the control system is able to keep the angle of attack and the angle of side slip to small angles. This means that the engine will be pointed towards to the velocity vector. The pitch angle will change from a pitch angle of 40°, to an angle of 0° at apogee. The pitch angle after culmination will decrease even further to impact.

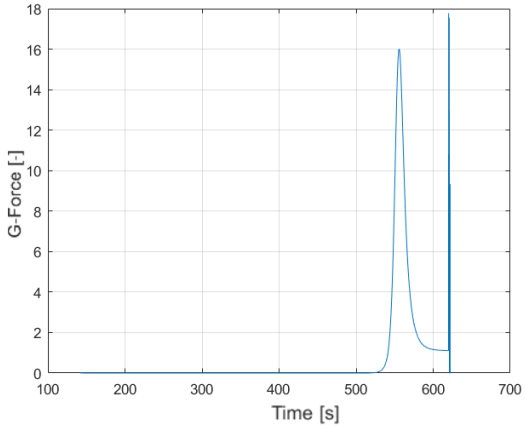

Figure 13.3: G-load profile Retro-propulsion 6DOF

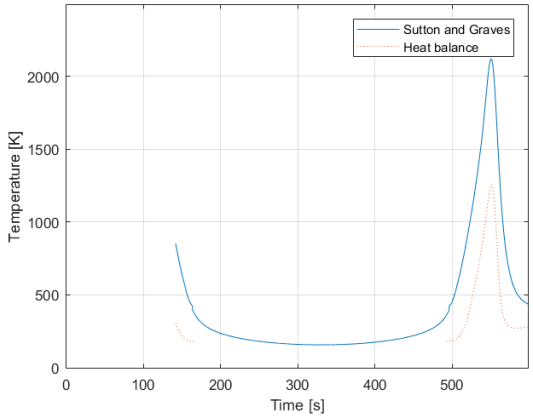

Figure 13.4: Temperature profile Retro-propulsion 6DOF

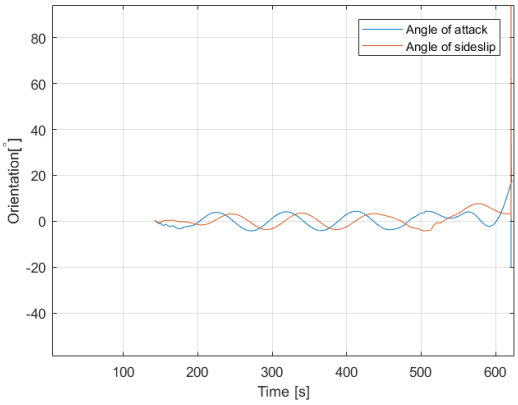

Figure 13.5: Angel of Attack and Side slip profile Retro-propulsion 6DOF

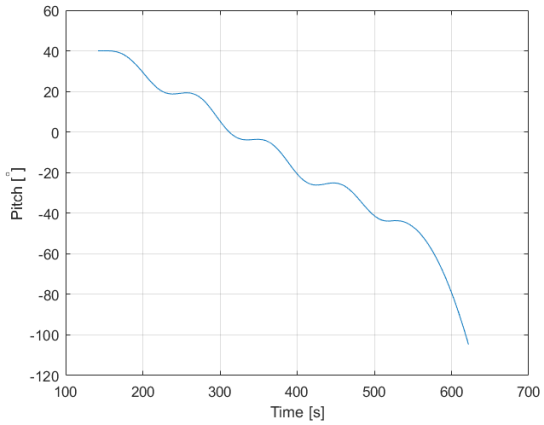

Figure 13.6: Pitch angle profile Retro-propulsion 6DOF

To conclude the projected trajectory of the first stage can be seen in Figure 13.7. The distance covered by the first stage will be approximated 825 km. For the control system a small control algorithm was used. This resulted in a total of 5829 N force needed to stabilise the first stage. A cold gas thruster will have a maximum specific impulse of 73 s in vacuum [45]. Using this in combination with Equations 2.7 and 2.8. It can be concluded that 8.1 kg of propellant is needed to stabilise the first stage before entering the atmosphere.

13.2. PARACHUTE SYSTEM

In Section 12.3 it was calculated that a drogue parachute with a radius of 1.8 m was needed in combination of a 15.75 x 31.5 meter parafoil. The total weight of the recovery mechanism was estimated to be 135 kg. In this section an extra 50 kg will be added to the system to include the landing system mass. In the following chapter the landing mass will be calculated.

In this simulation a time step of 0.01 seconds is used. The control system is used till an altitude of 60 km is reached. At this point a stronger control system will be needed as the atmosphere gets denser and so will

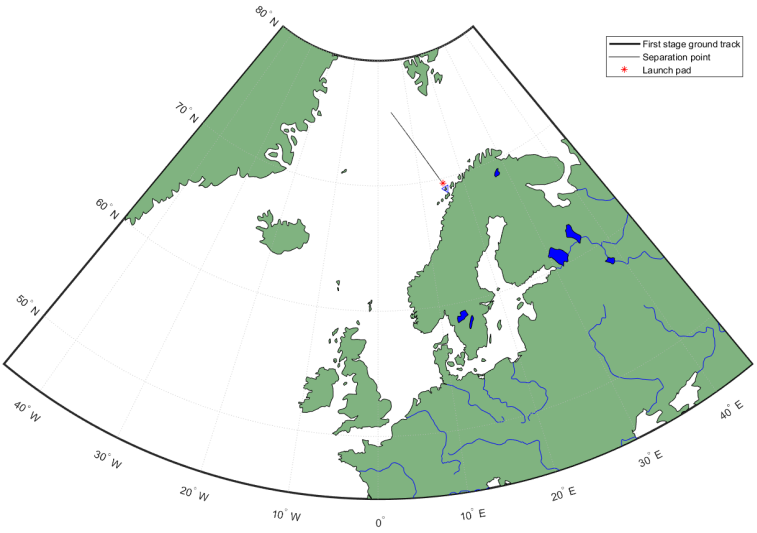

Figure 13.7: Ground Track Retro-propulsion 6DOF

the moments produced become larger. The control algorithm written will not be able to anticipate as fast as needed. At an altitude of 60 km a perfect control algorithm will be assumed.

The different trajectory profiles are shown below. The altitude of the first stage can be seen in Figure 13.8. The velocity profile is shown in Figure 13.9.

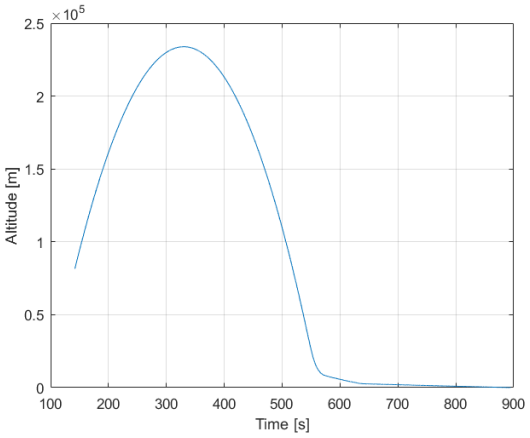

Figure 13.8: Altitude profile Parachute 6DOF

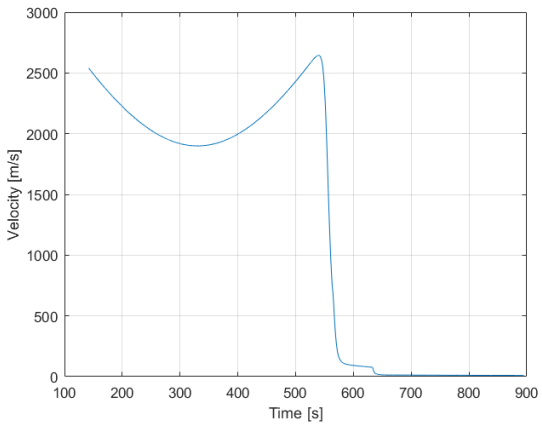

Figure 13.9: Velocity profile Parachute 6DOF

The temperature and G-load are shown in Figure 13.11 and Figure 13.10 respectively. The figures show more or less the same behaviour as for the retro-propulsion option. The aerodynamic properties are similar and the difference in recovery mechanism mass is also marginal. The differences are observed after drogue deployment. The total time required is much longer than for the 3DOF simulation and the retro-propulsion system. In comparison with the 3DOF simulation this difference can be explained by the fact that lift is considered for the system. For the 3DOF option lift was not considered as an angle of attack of zero was assumed. The velocities reached by the 6DOF simulation are slightly higher as the vehicle is heavier (due to the landing mechanisms) and the separation conditions were the same.

To conclude the projected trajectory of the first stage can be seen in Figure 13.14. The distance covered by the first stage is 840 km.

For the control system a total of 5908 N force is needed to stabilise the first stage. A cold gas thruster will have a maximum specific impulse of 73 s in vacuum. Using this information in combination with Equations 2.7 and 2.8. It can be concluded that 8.25 kg of propellant is needed to stabilise the first stage before entering

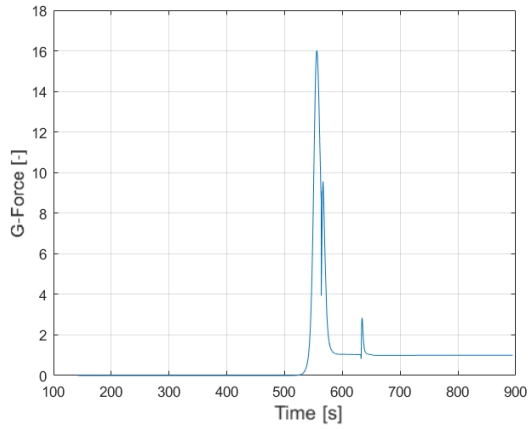

Figure 13.10: G-load profile Parachute 6DOF

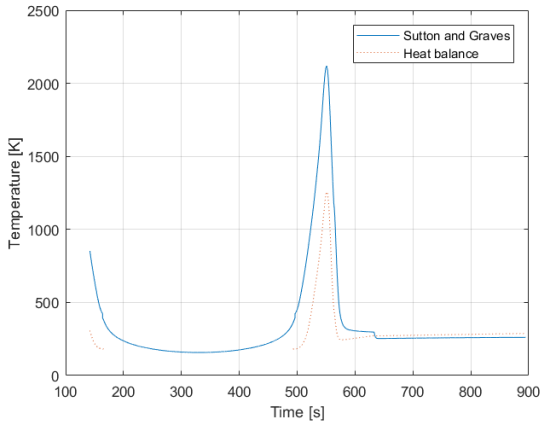

Figure 13.11: Temperature profile Parachute 6DOF

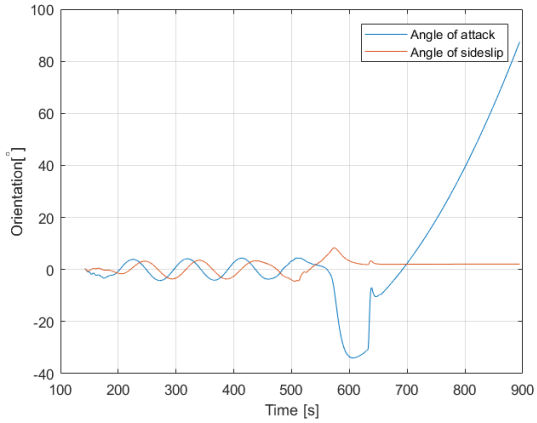

Figure 13.12: Angel of Attack and Side slip profile Parachute 6DOF

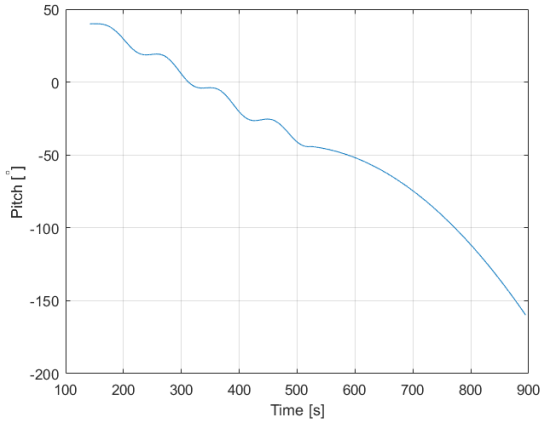

Figure 13.13: Pitch angle profile Parachute 6DOF

the atmosphere.

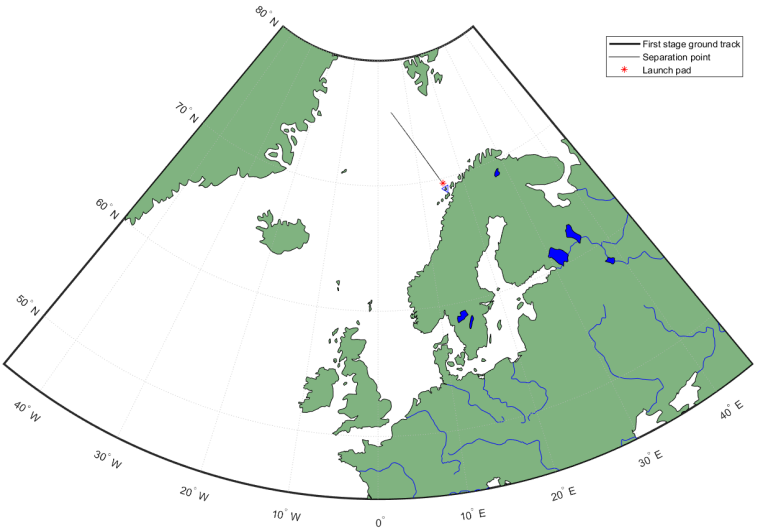

Figure 13.14: Ground Track Parachute 6DOF

14

DESIGN

In Chapter B the results found with the six degrees of freedom simulator were shown. It was explained that by just comparing the weight of the system no proper trade-off could be made. In this chapter both options will be designed in more detail. In this way more knowledge of the systems will be known and a trade-off will make more sense. The information shown in this chapter will be used in the next chapter were the conclusion will be presented. This chapter will include multiple facets of the design. In the first section, Section 14.1, it will be explained which elements, not treated before, are needed for recovery. The first design aspect considered is the mass prediction of the recover mechanism which is shown in Section 14.2. Once the mass has been predicted the volume needed to store the elements are discussed in Section 14.3. The numbers found in Section 14.2 and 14.3 will be used in Section 14.4 the explain how the different elements will be placed in the first stage. Section 14.5 will explain what the impact will be on the launcher. The cost of the recovery will be discussed in Section 14.6. The last section, Section 12.4, of this chapter will make a comparison of the different purposed options.

14.1. EXTRA ELEMENTS

Till this point the focus was on the deceleration of the vehicle. In this section other elements needed will be discussed. The first element is the control mechanism used during descent. After deceleration, the vehicle needs to be landed. This will be discussed in the second part of this section.

14.1.1. CONTROL MECHANISMS

As shown in Section 8.3 the first stage is unstable. This means that the active guidance is needed for the first stage. To control the re-entry flight different elements will be used. Two different elements will be used to define the position and attitude of the system. The first element is a global navigation satellite system (GNSS). Using a GNSS the position of the vehicle will be determined. This will be done by having contact with at least four different satellites. Four different satellites are needed for the four different dimensions; position in three directions and time. The second element will determine the orientation of the vehicle. The system used is an inertial measurement unit (IMU). An IMU will measure the body's angular rate, using a combination of accelerometers and gyroscopes. IMUs have a tendency to have a drift. This drift will be corrected by making use of the information obtained by the GNSS.

The input of the GNSS, and IMU will be processed by an On Board Computer (OBC). The OBC will apply sensor fusion, which combines data from different sources to calculate the position and orientation in a more accurate way than the sensors would produce by them self. By making use of Kalman filtering the measurements from the sensors will be matched to the expected values from the equations of motion, so that the accuracy is improved.

Once the position and orientation is determined the OBC will calculate the force and moment needed to correct any deviations from the intended trajectory. The OBC will send this information to the reactions control system. The reaction control system of the first stage will make use of cold gas thrust. Cold gas thrusters can produce small forces and so moments to stabilise the vehicle. The stabilisation using the cold gas thruster have already treated and calculated in Chapter B.

Besides the Guidance Navigation and Control (GNC) system described briefly above the system will also

include a communication system. The communication system will ensure connection with the vehicle. In this way the position will be known by the recovery team. Once the system is landed the ship knows where to pick up the first stage.

14.1.2. LANDING MECHANISMS

Once the vehicle has reduced its speed the system has to land to be brought back by a ship. Two different landing mechanisms will be considered. The first one is landing by making use of airbags or an air bed. The second mechanism considered is a Mid Air Recovery (MAR).

AIRBAGS AND AIR BED

The airbag option can be used by both the retro-propulsion system and the parachute system. Airbags as a landing mechanism have been used for the first time successfully on July 4 in 1997 by the Pathfinder on Mars. In 1.50 seconds the gas generators inflated the six 1.8 m diameter lobes. A system of internal and external cords served to restrain the loads, stiffen the airbag system, and connection to the lander [46].

The airbags and air bed will make sure that the vehicle does not sink and that the vehicle is shielded from the salty sea water. The vehicle will float on top of the airbags in the sea.

If the parachute system is used the parafoil can be attached to the side of the vehicle. In this way the orientation of the vehicle will be changed to horizontally. The air bed will be inflated before touching the air. At impact the system will still have a horizontal velocity. The parafoil will provide a gliding soft landing on the sea. Once the horizontal velocity is also reduced the vehicle will float on the air bed on the sea. The engine will be sealed to make sure no water will come into the engine and pumps. The ship will sail towards the first stage and will lift the stage out of the water. A schematic drawing can be found in Figure 14.1.

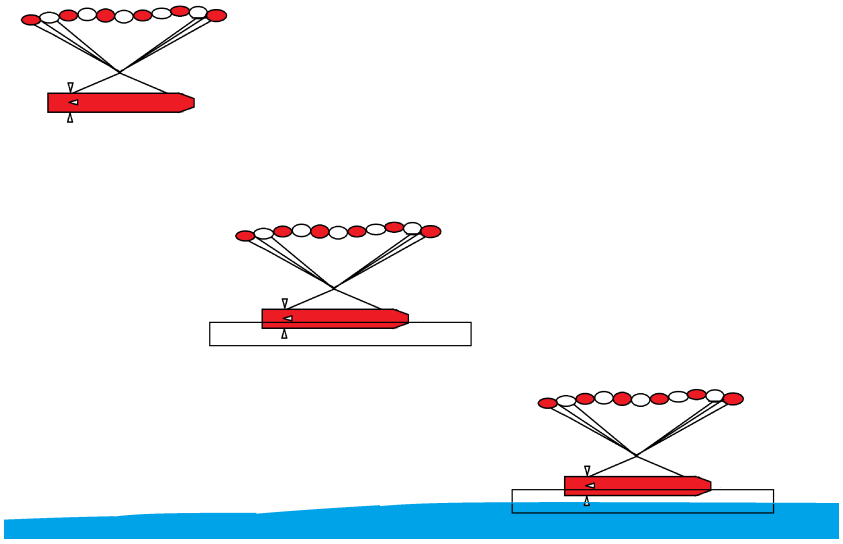

Figure 14.1: Schematic drawing landing with air bed

For the retro-propulsion system airbags will be used. The airbag will be used to let the system float and will be used to absorb the landing shock. The airbags will be inflated during the last descent phase. Just before touch down the vector thrust control in combination with the reaction control system will turn the vehicle from vertical position to horizontal position. The vehicle will touch the water and turn over onto the water. A schematic drawing of this system can be found in Figure 14.2.

MID AIR RECOVERY

The mid air recovery can only be considered for the option using parachutes. The MAR is a concept in which a second vehicle catches the first stage in the air. The vehicle used is often a helicopter as a helicopter has as advantage with respect to an air plane that it can hover above an airfield of cargo stacking [47]. In the past multiple systems have already been retrieved using a MAR manoeuvre, for example the Genesis sample return mission [13]. The investigations on the re-use of the Atlas V booster's RD-180 engine gave more insights in using MAR for the reuse of a stage or booster [48].

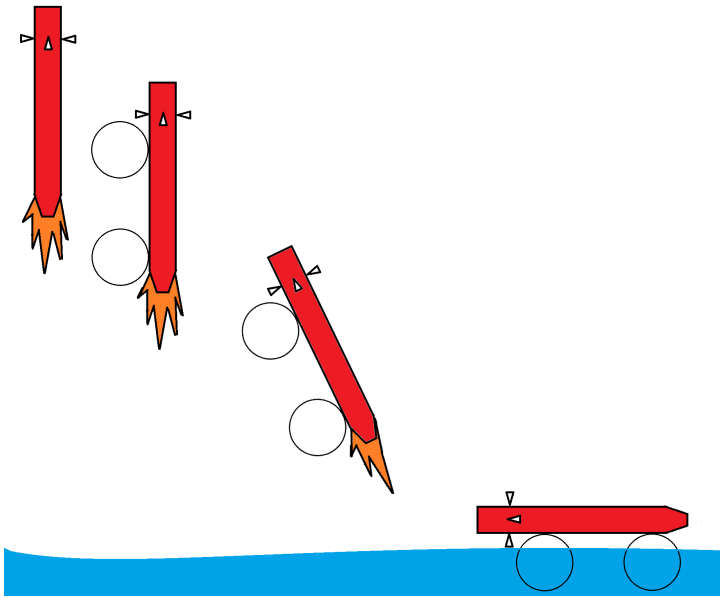

Figure 14.2: Schematic drawing landing airbags

The landing of the MAR will go as follows. The drogue parachute will be used to stabilise and decrease the velocity of the first stage and to deploy the main parafoil. The main parafoil will decelerate the vehicle and bring it to a height a helicopter can reach. The helicopter will loiter at the edge of the safety radius. The helicopter is continuously updated with the position of the system and confirmation on the deployment of the drogue and main parafoil will be send to the helicopter. The helicopter will now fly towards the system till visual contact can be made. The helicopter will then go laterally to the right just past the suspension line stopping the motion once the trailing engagement line is resting against the capture hook suspension line. The helicopter will now climb until the capture hook has the engagement in the mouth of one or more of its latching arms[13]. Once the helicopter has caught the vehicle it will drag the vehicle towards the ship. A schematic drawing of the MAR can be found in Figure 14.3.

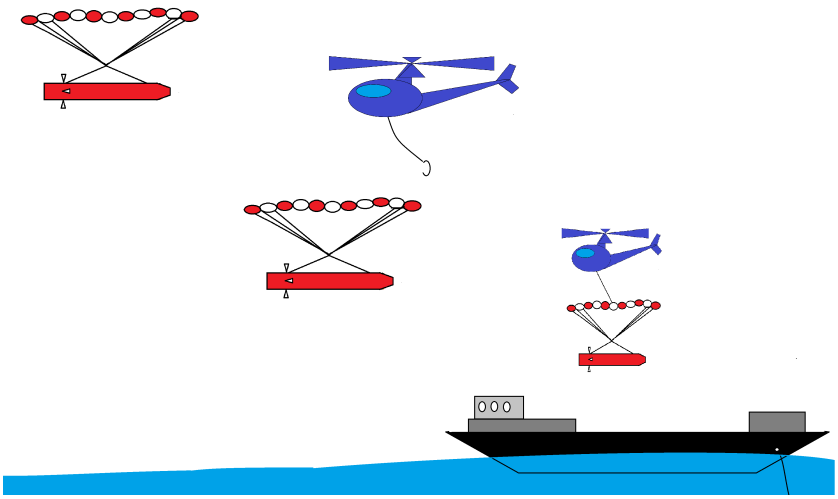

Figure 14.3: Schematic drawing Mid Air Recovery

The capabilities of the MAR have been investigated in the last years. The loads which need to be handled by the helicopter will be up to 1.2 G [49]. There are limitations to the speed at which the MAR can be performed. Research has shown that the engagement speed should be at 1.2 times the helicopter translation speeds to assure a good capture [13].

To recover the vehicle in this way a helicopter, pilot, and a landing platform on a ship is needed. It has

been shown in the past that stunt pilots from the film industry are very suitable of performing these kinds of manoeuvres. After a training of one day they were already capable of performing a MAR [13].

The main advantage of this landing procedure is that the first stage will not come in contact with salty water. Therefore, normal functional testing would be sufficient without engine removal, breakdown and re-building [49]. This would decrease the turnaround time and cost significantly.

14.2. MASS

In this section the different mass elements of the recovery will be considered. The first mass element considered is the mass needed for the deceleration of the first stage. The second element is the mass needed for the control system. The third element is the system needed for the landing. The last element includes the extra system and propulsion mass needed to adjust the first stage to bring the extra mechanisms to the desired separation point.

14.2.1. DECELERATION MECHANISM

The first deceleration mechanism considered is the retro-propulsion configuration. This design uses the main engine of the launcher. The extra mass of the system will therefore include the mass of the propellant and the extra mass of the propellant tank to store the extra propellant. It has been shown in Section 12.4 that the extra propellant needed for the retro-propulsion is 98 kg. The extra mass needed to carry the propulsion will be 1 % of the propellant needed. This means that an extra kilogram is needed for the propellant tank.

For the parachute system decelerate mechanism different elements are needed. The first element is the drogue parachute. In Section 12.4 it has been shown that a total of 6 kg should be reserved for the drogue parachute. Besides the drogue parachute 89 kg is needed for the parafoil. To steer the parafoil an AGU is needed. For the AGU a total of 40 kg has been reserved. This means that a total of 135 kg has been taken into account for the deceleration using a parachute system.

14.2.2. CONTROL MECHANISM

As been stated in Subsection 14.1.1 different control mechanisms are needed to control the system. The GNSS, IMU, and OBC will be mounted in a box with a total weight of less than 1 kg. The Reaction Control System consists of four thrusters and two tanks with pressurised gas (nitrogen). The dry mass of the RCS is about 3 kg. It was calculated that for both retro-propulsion and parachute system around 8 kg nitrogen was needed. In Table 14.1 an overview of the weight of the different control system used is listed.

14.2.3. LANDING MECHANISM

For the landing different systems were introduced in Subsection 14.1.2. Two different solutions were using an airbag and air bed. These different forms have different weight properties. First the mass of the air bed will be considered. Using Archimedes' principle the volume needed for the air bed is calculated with Equation 14.1[50]. Assuming a mass of 1300 kg and a density of the sea water of 1.025 kg/l, the volume needed is 1.26 m^3.

$$\rho g V = mg \tag{14.1}$$

The air bed will be placed around the launcher. With a launcher diameter of 1.4 m, the air bed should be 4.4 m in length to fit around the launcher. Four meter will be used for the air bed. To make sure no water will come into the engines the air bed will be made 14 meters long. The total surface of the air bed will be 56 m^2. This means that 2.3 cm of the air bed will be in the water. To add some margin and to place the air bed above the water level the air bed will be made 10 cm high. This means that the air bed will have a volume of 5.6 m^3 and the surface of the air bed will be 115.6 m^2. The air bed will be made out of polypropylene. If a sewing margin of 20% is assumed, 138 m^2 is needed. The material mass of the skin of the air bed, assuming 1 mm thickness and 0.9 g/cm^3 will become 124.83 kg. The air bed will be filled with nitrogen. Nitrogen has a density of 1.2506 kg/m^3 at 273.15 K and 1 atm. To fill the air bed at least 7 kg of nitrogen will be needed, assuming 1 atm pressure. To store 7 kg of nitrogen a tank will be needed. A tank of 10 kg will be assumed. This will results in a total air bed weight of 141 kg.

The air bag option is more complex. The air bags will not only make sure the system will float but will also absorb the impact. To understand the system needed, first the impact will be calculated. To do so the system will be approached as an inverted pendulum, shown in Equation 14.2. The centre of gravity of the first stage

will be treated as point mass on a weightless pendulum. The r is the distance of the centre of gravity to the outlet of the engine.

$$\dot{\theta} = \int \ddot{\theta} dt \approx \frac{M}{I} \approx \frac{grsin(\theta)}{I} \tag{14.2}$$

Using formula 14.2, Figure 14.4 have been produced to show the angular velocity. If a initial angular velocity of 5∘/s produced by the engine is assumed, it can be seen that the angular velocity will be 30∘/s at impact. The first stage is 11.4 meters long, which results in an impact velocity of 6 m/s. If this impact velocity is absorbed by the airbags and a crush depth of 60 cm is assumed. The system should be stopped in 0.1 second. Using Equation 2.6, this will result in a deceleration of 120 m/s^2. This means that the first stage should handle more than 12G in the z-y body plane. The first stage cannot handle these forces on one point and therefore the launcher should be covered in the full length with airbags. In this way the impact of the launcher will be spread over a longer duration and area.

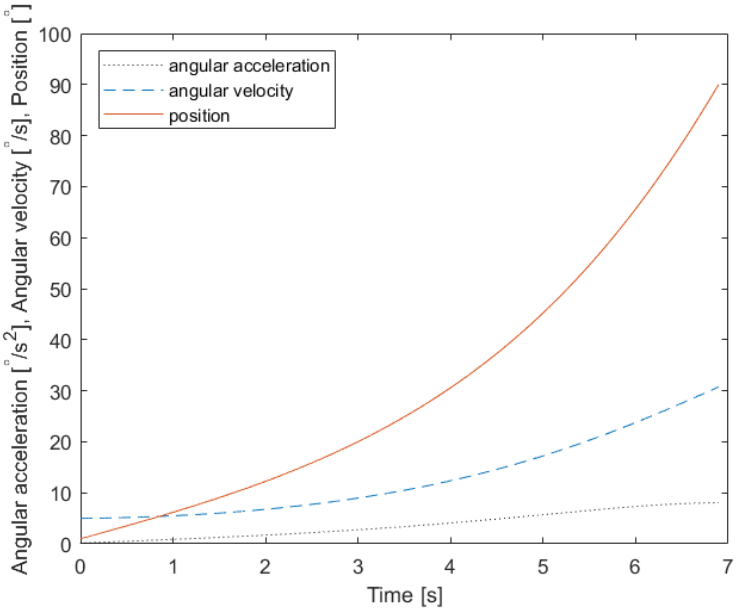

Figure 14.4: Angular acceleration, velocity, and position of the turnover of the first stage

To handle the impact of the launcher and to ensure that the first stage will float on the water, the full length of the first stage will be covered with airbags. Two airbags are needed at each position to keep the first stage stable on the water. If it will be assumed that all airbags have the same size and 50% will underwater, the following Equation can be derived, Equation 14.3. Using that the full length of the first stage should be covered by airbags, Equation 14.4, Equation 14.5 can be derived.

$$V = \frac{3}{4}\pi r^3 \frac{2n}{2} \tag{14.3}$$

$$l = 2rn \tag{14.4}$$

$$V = \frac{2}{3}\pi r^2 l \tag{14.5}$$

Using the total volume needed following Archimedes principle and Equation 14.5, it has been calculated that 21 airbags at each side of 0.243 meter radius are needed. Each airbag will have a volume of 0.06 m^3 and a surface area of 0.7414 m^2. In total 2.52 m^3 of gas will be needed. Airbags are inflated with an inert gas, nitrogen and argon are often used [ref]. Nitrogen is slightly lighter and will therefore be chosen. The density of Nitrogen is 1.2506 kg/m^3 at 273.15 K and 1 atm. In total at least 3.15 kg of nitrogen is needed. The tank needed for the nitrogen will weigh around 2 kg.

The skin of the airbags cover in total 31.14 m^2 using a sewing margin of 20% will bring the total fabric surface needed to 37.4 m^2. Assuming the airbags will be made out of polypropylene with a skin thickness of 1 mm and a density of 0.9 g/cm^3 the skin will weight in total 33.6 kg. In total the airbag system will weigh 39 kg.

For the MAR the landing will be provided by a secondary system. This means that for this configuration no extra landing mechanism weight needs to be considered.

For the airbag system the assumed mass in Chapter B was quite accurate. The MAR option, did not need a landing mechanism, this will result in only a slightly smaller parafoil than calculated in Chapter B. The parachute system with air bed need is heavier than expected, this will result in an increase in he parafoil size. An update of the found numbers should be used in a next iteration.

14.2.4. EXTRA PROPELLANT NEEDED FOR ASCENT

The first stage will become heavier due to the recovery, control, and landing mechanisms used. The same separation point needs to be met by the first stage, extra propellant is therefore needed. The extra propellant needed will be calculated by the 3DOF simulation. The results found for the different configurations can be found in Table 14.1.

14.2.5. EXTRA STRUCTURE MASS

To handle the extra mass used for recovery the structure of the first stage will increase. For this first order approximation it will be assumed that the structure mass will increase linearly. The result can be seen in Table 14.1.

14.2.6. MASS OVERVIEW

Using all elements shown above three different mass breakdowns have been made. The result can be found in Table 14.1.

Table 14.1: Mass overview

	Retro-propulsion with airbags	Parachute system with air bed	Parachute system with MAR
Initial first stage mass [kg]	1061	1061	1061
Deceleration [kg]	99	135	135
Control [kg]	12	12	12
Landing [kg]	39	141	-
Structure [kg]	14	38	14
Extra ascent propellant [kg]	739	1924	696
Separation mass first stage [kg]	1225	1377	1222

14.3. VOLUME

The different elements needed for recovery will also take up space in the launcher. In this section for the different mechanisms the space needed will be explored. Once it is know how much space the different elements will take, it will be explained in Section 14.4 where the different elements will be placed.

14.3.1. DECELERATION MECHANISM

The extra volume needed for the propellant tank has been scaled linearly with the increased propellant mass needed. For the parafoil and parachute system a total volume of 1 m^3 is calculated. The results are shown in Table 14.2.

14.3.2. CONTROL MECHANISM

The control mechanisms used are already installed in control unit. This control unit has the size of cube of 10 cm. The total volume used for the control unit will therefore be 0.001 m^3. Next to the control unit, four different thrusters and two tanks to store the cold gas will be used. The cold gas tank will take the biggest space in the tank. In total 8 kg was needed, it will be assumed that the volume of the two tanks will be 0.1 m^3 in total.

14.3.3. LANDING MECHANISM

The extra volume needed to store the landing mechanism is again dependent on the landing mechanism used. For the parachute design with the air bed landin, the air bed should be stored and the nitrogen tanks. It was calculated that 138 m^2 skin material with a thickness of 1 mm was needed. It will be assumed that 50% volume extra will be needed to pack the skin. This results an a package of 0.21 m^3. The 10 kg nitrogen tank will take around 0.03 m^3.

For the air bags less volume will be needed as the systems needed will be smaller. The skin of all the airbags together is 37.4 m^2, with a thickness of 1 mm. Using a packing efficiency of 67 % will result in a total volume needed of 0.0561 m^3. The 2 kg nitrogen tank will cover 0.01 m^3.

The last landing option considered was the MAR. For the MAR no extra volume is needed in the first stage itself.

14.3.4. EXTRA VOLUME NEEDED FOR ASCENT

In Subsection 14.2.4 it was explained that extra propellant is needed to bring the first stage to separation point. The propellant needed for this exercise needs to be stored in the tank. The extra volume needed has been calculated using the propellant needed. The result can be found in Table 14.2.

14.3.5. VOLUME OVERVIEW

This last subsection on volume needed for recovery shows an overview of all needed space to store the recovery mechanisms. The results can be found in Table 14.2. The results of the numbers found will be used to place the different elements in the first stage. The placement of the elements will be done in Section 14.4.

Table 14.2: Volume overview

	Retro-propulsion	Parachute system with airbags	Parachute system with MAR
Deceleration [m^3]	0.098	0.939	0.939
Control [m^3]	0.101	0.101	0.101
Landing [m^3]	0.24	0.066	-
Ascent propellant [m^3]	0.733	1.365	0.690

14.4. OUTLINE

The information found on the mass and volume on the recovery mechanisms will be used in this section to design the outline of the first stage. For the three different methods three different designs will be presented. In Figure 14.5 the three design are visualised. The first vehicle shows the first stage without recovery mechanisms.

The second vehicle drawn is the first stage with retro-propulsion. In comparison with the first vehicle the propellant tanks are bigger to store the extra propellant needed for the ascent and descent phase. For the landing airbags will be used. These airbags will be placed around the structure. The nitrogen tanks to fill the airbags will be placed between the tanks. This position has been chosen the keep the distance to all airbags minimal, and at the same time to make not too much adjustment to the first stage. To control the movement of the first stage, a control unit and cold thrusters will be placed. The control unit will be placed in the upper interface cylinder in the middle of the firs stage, visualised with a small square. Four small cold thrusters will be placed at the same height around the first stage, with an angular distance of 90°. The tanks used to feed the thrusters will also be placed in the same area.

The third vehicle shown, shows the parachute system with air bed landing. As been shown in Table 14.2 the option needs the most extra ascent propulsion. The tanks needed for this option will therefore be the largest. The kerosene tank cylinder increased from 1.5 meter to 1.81 meter and the oxidiser tank cylinder increased from 3.7 meter to 4.28 meter. The air bed will be placed around the cylinder. To do so the diameter of the vehicle will increase to 1.44 meter. The air bed will be filled by nitrogen tanks, which are placed between the fuel and oxidiser tanks. The control unit and the cold gas thrusters are placed on top of the oxidiser tank. In total four cold gas thrusters will be used, placed around the cylinder with an angular distance of 90 °. At the same height and on top of it, the AGU and parachute system will be placed.

The last vehicle drawn in Figure 14.5, shows the first stage used in the MAR option. The tank size needed

is similar to the size needed for the retro-propulsion. To control the movement of the first stage, the control unit with four cold gas thrusters and tanks will be used.

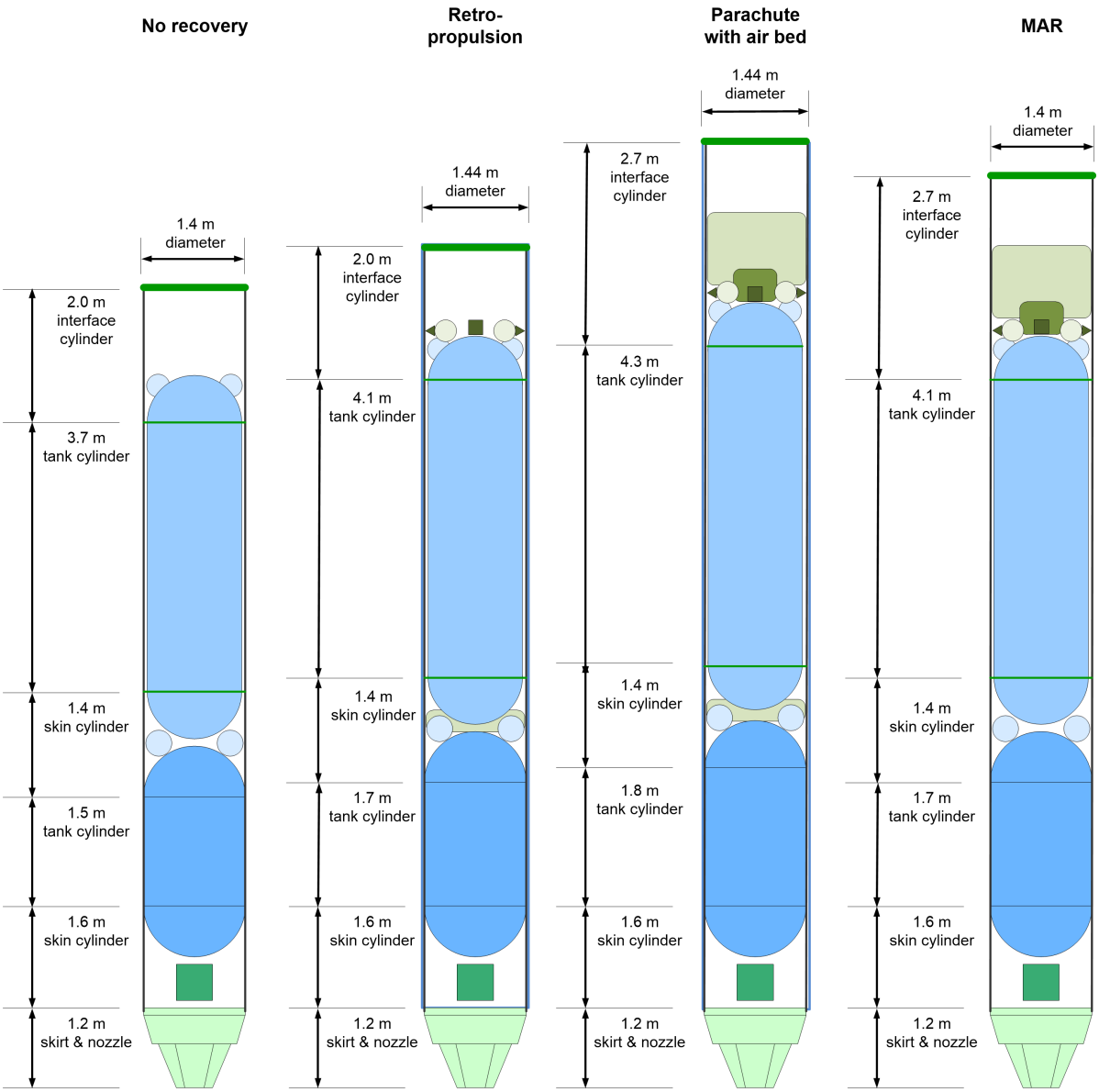

Figure 14.5: Schematic drawing outline first stage for different designs

14.5. IMPACT ON LAUNCHER

The outline of the different options found in the former section will all have a different impact on the launcher. Three general aspects will be treated in this section. The first one is the propulsion of the launcher, the second one is the stability of the launcher, and the third on is the drag coefficient experienced by the launcher.

PROPULSION

In Table 14.1 it was shown that for the different options, different amounts of extra propulsion were needed. As more propellant needs to be expelled, a longer burn time will be needed till separation. This increase in time to separation point will have an influence on the efficiency of the ascent. Two effects can be seen. First of all the launcher will stay for a longer period in the atmosphere, which will increase the aerodynamic drag experienced. The second element is the gravity loss experienced. The launcher will stay for a longer period with a high pitch angle, which will increase the gravity losses.

STABILITY LAUNCHER

Recovering of the first stage will make the first stage heavier and bigger. A heavier first stage will move the centre of gravity further away from the nose of the launcher. This shift in centre of gravity will decrease the stability of the launcher. It was already mentioned in Section 8.3 that the launcher is unstable. Thrust vector control was already needed. Recovering the first stage will influence the amount of control needed, however as TVC was already used, no new elements are needed.

DRAG COEFFICIENT

For the two options using the airbag and air bed it has been shown that the best option to store the inflatable devices around the first stage. This will increase the cross-sectional area of the launcher. This increase will increase the drag experienced during the flight. For the ascent phase this will be a disadvantage. For the descent phase this can be considered as advantages. In Subsection 15.3.1 the influence of the drag coefficient on the first stage will be investigated.

14.6. COST

The size of the recovery mechanisms and the other needed mechanisms used for recovery were discussed before. To investigate if the recovery of the first stage would be cost-beneficial a cost analysis is needed. The cost of the first stage will be based on different aspects. The different elements can be found in Table 14.3. In this table an overview can be found on the cost of the different systems. Some elements used can be re-used if the stage is recovered. All avionics elements, the structure and extra structure adaption, the AGU, and tanks will be re-used. This means that the total cost of these elements will be split over the different launchers.

In Table 14.4 the total cost per year are shown. In this example 10 launches per year are assumed. Furthermore it is assumed that the redemption of the ship and helicopter is 20 years.

The costs found in both tables are based partly on components already bought by the project. The other costs are estimated with help from partners and (former) employees of helicopter (Airbus Helicopters) and ship manufactures (Zwijnenburg Shipbuilding and Damen Shipyards).

Table 14.3: System and refurbishment cost

	Price (k€)	Amount Parachute + air bed	Price Parachute+ air bed (k€)	Amount Parachute MAR	Price Parachute MAR (k€)	Amount Retro-propulsion	Price Retro-propulsion (k€)
Launcher							
Structure adaption	800	0.07	56	0.14	112	0.069	55.2
Extra fuel launcher	0.001	739	0.739	1424	1.424	696	0.696
Avionics							
RCS	20	1	20	1	20	1	20
OBC	5	1	5	1	5	1	5
COM	20	1	20	1	20	1	20
GNSS	7	1	7	1	7	1	7
IMU	8	1	8	1	8	1	8
Recovery							
Drogue Parachute	10	1	10	1	10	-	-
Parafoil	50	1	50	1	50	-	-
AGU	40	1	40	1	40	-	-
Propellants	0,001	-	-	-	-	110	0,11
Tanks/Cylinder	10	-	-	-	-	1	10
Landing							
Airbag system	50	-	-	-	-	1	50
Air bed system	100	1	100	-	-	-	-
Refurbishment							
Sea water cleaning	100	1	100	-	-	2	200
Inspection	60	1	60	1	60	1	60
NDO	60	1	60	1	60	1	60

Table 14.4: Total transportation cost per year

	Cost [k€]	Amount	Total cost per year [k€]
Ship			
Buying+rebuilding	1000	0.05	50
Labour	90	6	540
Diesel	0.001	20000	20
Maintenance	100	1	100
Unforeseen	50	1	50
Total			760
Helicopter			
Buying+rebuilding	2500	0.05	125
Labour	100	2	200
Kerosene	10	10	100
Maintenance	250	1	300
Unforeseen	50	1	50
Total			775

Using the number shown in the two tables the following result was found, shown in Figure 14.6. In this figure it can be seen that if the first stage is used more than 4 times, that for all options the recovery become cost efficient. It is seen that the MAR option has very high starting cost due to the helicopter, but will be the most cost-efficient is the first stage if recovered for more than 5 times.

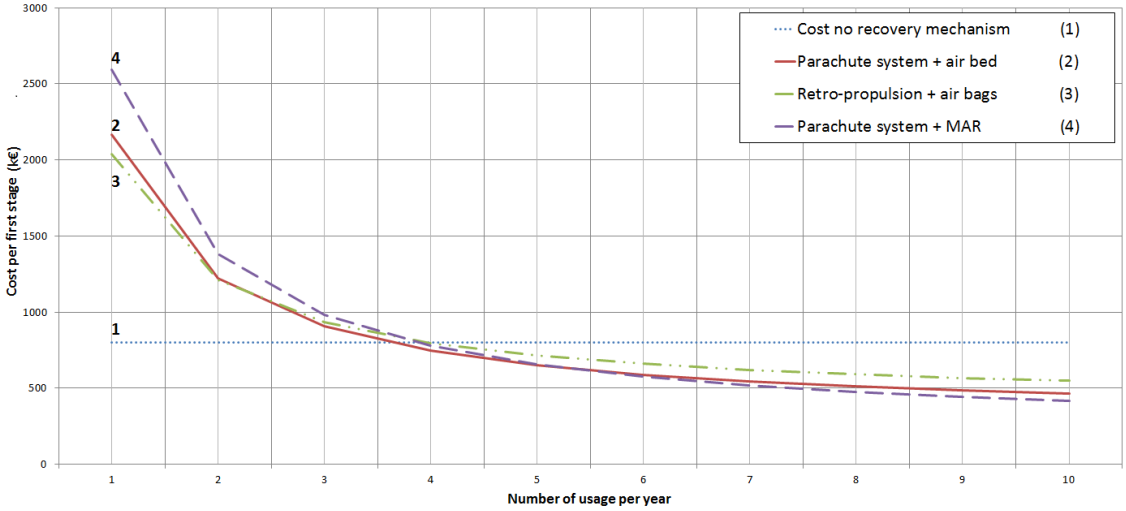

Figure 14.6: Cost analysis

Besides the cost found in Table 14.3 and 14.4 the development cost should also be considered. The more elements used not commercial available the more it will cost and the longer the development will take in general. The air bed as described have not been found in any literature which will increase the development cost.

SMILE is planning to launch ten times per year. It was shown that after four times per year recovering of the first stage becomes cost-beneficial. However it could occur that only 1, 2, or 3 launches will be performed per year, and therefore it is investigated what will happen to the cost model if only 1, 2, or 3 a launch will be performed per year. Figure 14.7 shows the cost for one launch per year. In this figure it can be seen that even if the first stage is used for the 10th time, this is not a cost efficient solution. Performing two launches per year results in Figure 14.8. In this figure it can be seen that only if recovery with the parachute system and an air bed will make recovery cost-beneficial. If this solution is used, the extra cost are repaid after seven times. This means that the first stage will have to fly at least seven times in three and a half years. The last figure shows the cost model if three launches can be performed per year. In this figure it can be seen that if a parachute system with air bed is used, the first stage should be used at least five time. For the retro-propulsion the first

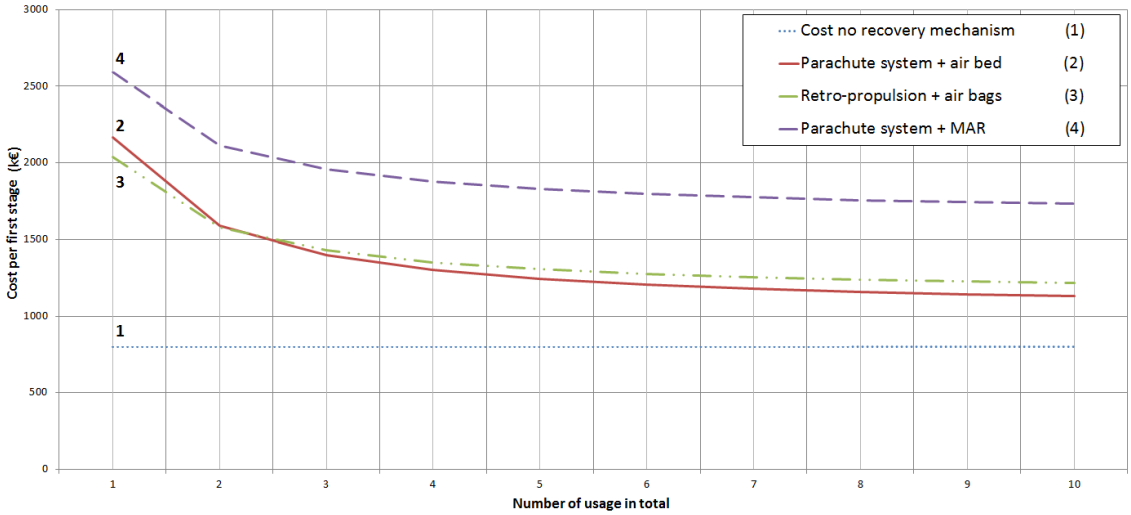

Figure 14.7: Cost figure launching once a year

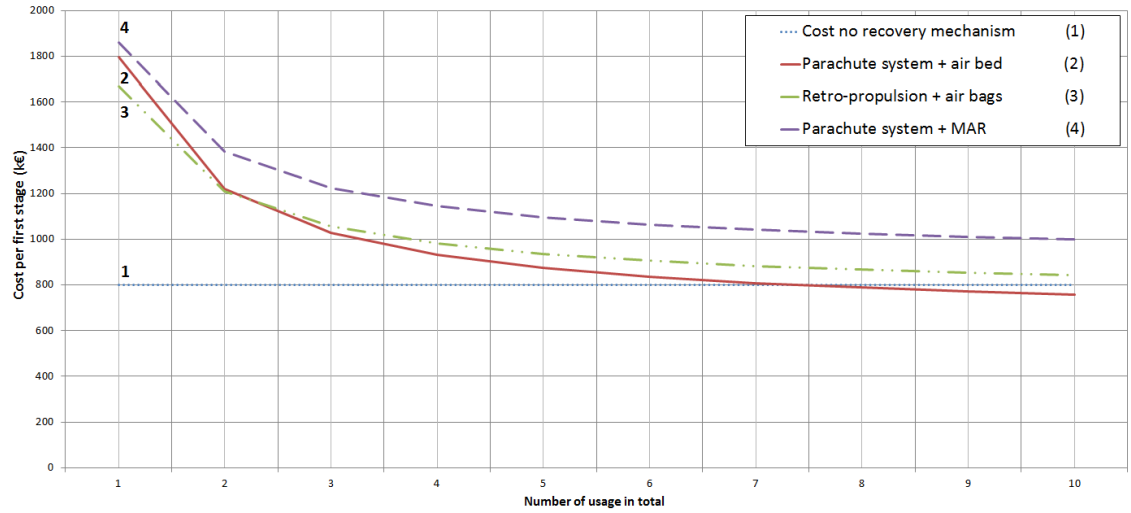

Figure 14.8: Cost figure launching twice a year

stage have to fly at least six times. The parachute system with MAR has to fly at least seven times.

14.7. COMPARISON

In this chapter it was found that the option using the mid-air capture was the lightest option. The starting cost for the MAR capture are however the biggest. The MAR will only become the cheapest when the first stage is re-used more than 5 times. The MAR will require the least amount of adaption to the first stage. The other options will use a wider first stage diameter, what will increase the drag experienced by the launcher.

The parachute system using an air bed, is the heaviest options. However the cost of this option is not higher than for the other options.

Using the retro-propulsion will result in the option with the lowest starting cost, however when re-using the first stage often this option is the least cost-efficient.

For both the air bed and air bag option it should be tested how much the first stage will become in contact with sea water. It should also be tested how well the aerospike engine can survive salty water and if it possible to seal the engine enough.

In the last statement of the former chapter it was shown that the air bed has an extra disadvantage over the others as the development costs will probably be higher.

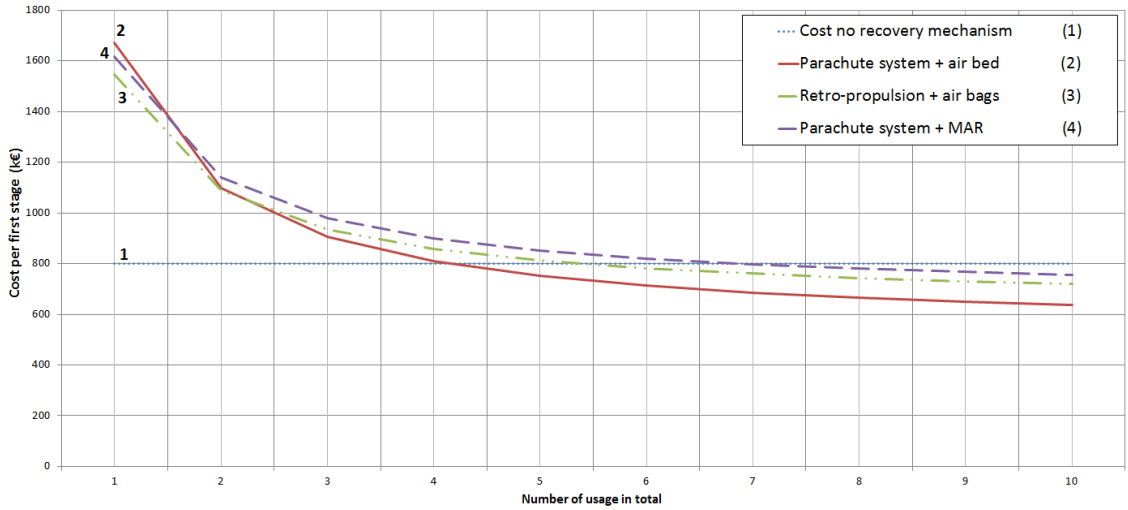

Figure 14.9: Cost figure launching three times per year

15

ANALYSIS

In this thesis results were found for the optimal design in terms of weight. This configuration was used to calculate the cost reduction obtained when re-using the first stage. In this chapter some extra analyses will be performed to find where more research has to done. The first part will go into more detail on the temperature analysis of the system. The second section will find the effect on the aerodynamics of adding fins to the first stage. The sensitivity analysis on the different systems will be shown in Section 15.3.

15.1. TEMPERATURE ANALYSIS

During the optimisation it was found that the temperature calculated was increasing very rapidly in time. In this section more insights will be given about the temperature calculations. In this section mainly the convective heat will be considered as this is the main source of heat for the velocity experienced during descent of the system[51]. The radiative heat will not be significant below the 2.5 km/s. Next to convection the system will conduct the temperature to the rest of the system and will radiate heat to the surrounding.

In the 1950 due to the interest in missile technology research was done to the heating of missiles. On of the first approximations of the convective heat was found by Allen and Eggers[52]. Since then a lot of research have been done to improve this relation. For example the common used Sutton and Graves formulation, Equation 15.1 or the Chapman formula, Equation 15.2[37][53]. Other examples are the Tauber equation, Equation 15.3 and the Detra and Hidalgo Equation, Equation 15.4[54][55]. The first three equation depend on $\sqrt{(\frac{\rho}{R_n})}V^3$. The only difference between the different formulations is the coefficient used. The convective heat flux will therefore be very depended on the formulation, and so the coefficient chosen. The Detra and Hidalgo Equation is slightly adopted with the velocity to the power 3.15.

$$\dot{q_c} = 1.7310^{-4}\sqrt{\frac{\rho}{R}}(V)^3 \tag{15.1}$$

$$\dot{q_c} = 1.6310^{-4}\sqrt{\frac{\rho}{R}}(V)^3 \tag{15.2}$$

$$\dot{q_c} = 1.8310^{-4}\sqrt{\frac{\rho}{R}}(V)^3 \tag{15.3}$$

$$\dot{q_c} = 5.1610^{-5}\sqrt{\frac{\rho}{R}}(V)^{3.15} \tag{15.4}$$

Using the formulations shown in Equation 15.1 to 15.4, the convective heat flux and the total convective heat load have been calculated for the trajectory without recovery mechanisms, shown in Figure 15.1 and 15.2. As already mentioned before, the convective heat calculated depends very strong on the coefficient used. This will result in a difference of 12% for the Tauber en Chapman formulation.

Besides these simple relations more complex formulations have been found. One of them was already shown in Chapter 2. Using this formulation and the formulations shown for the convective heat flow, the temperature of the wall of the nose was calculated. It was assumed that no conduction would take place. This means that the calculated temperature would be higher than the real temperature. The result can be found in Figure 15.3.

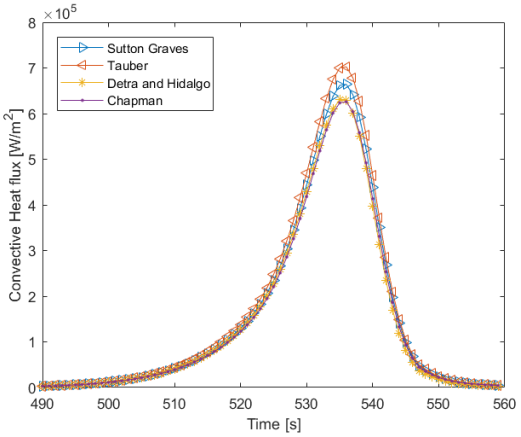

Figure 15.1: Convective heat flux analysis

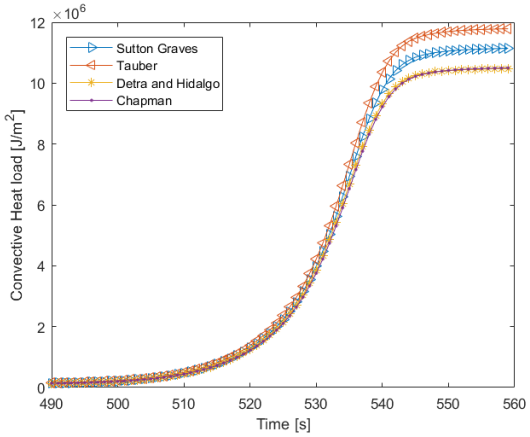

Figure 15.2: Convective heat load analysis

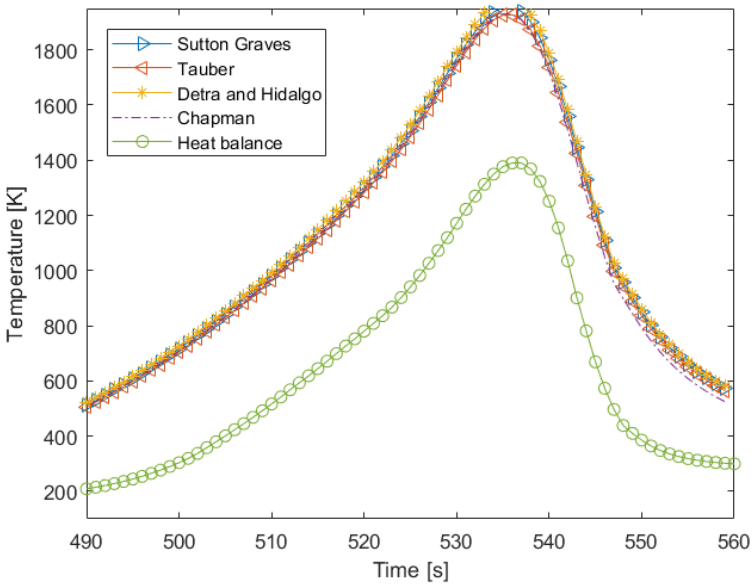

Figure 15.3: Calculated nose temperature analysis

In Figure 15.3 it can be seen that in comparison with the heat balance approach the empirical equation for the convective heat estimate the temperature much higher. The balance approach will take into account more accurately the increased radiation when the temperature of the wall will increase. Furthermore the relations for the heat convection shown in Equation 15.1 to 15.4 are written for re-entry situations and are used often for higher speeds.

Figure 15.3 shows that the temperature calculated of the wall of the nose depends very much on the method used. It is therefore advised to investigate the temperature obtained in more detail. The could be done by making use of CFD (Computational Fluid Dynamic) calculations. CFD calculations will however require a lot of time and calculation power.

15.2. FIN ANALYSIS

In Subsection 14.1.1 it was explained that cold thrusters will be used and are needed as the first stage is not stable. In this way active control will be used. Instead of active control, passive control might be much more beneficial. This can be done by adding fins to the vehicle. First of all by adding fins to the vehicle, the vehicle may become stable. This means that less control will be needed as the vehicle will point the nose towards the stream by itself. If movable fins will be used the fins could also steer the vehicle.

In this section it will be investigated what the benefit of fins would be in terms of stability. To make the vehicle statically stable the centre of gravity should be placed before the centre of pressure. This can be done by moving more weight towards the nose. However this is often not possible. Another option is to add fins to the vehicle.

It was found using Missile DATCOM that adding fins to the first stage can make the first stage stable. Using the found pitch moment coefficient and the 6DOF simulator it was shown that the fins were not able in the higher atmosphere layers to produce a pitch rate high enough to turn the nose of the vehicle into the velocity vector. The result is shown in Figure 15.4. In this figure it can be seen that the fins have almost no effect in higher layers. This means that a control system will still be needed to rotate the vehicle. After 500 seconds a pitch rate is seen, and the vehicle tries to become stable, seen by the oscillations. However the density of the atmosphere increases too rapidly to stay stable.

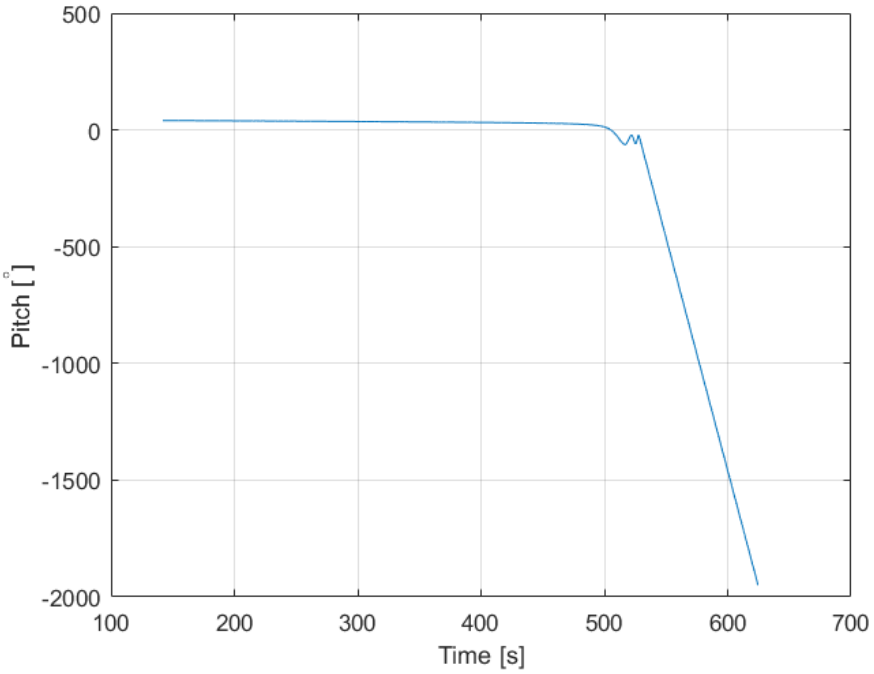

Figure 15.4: Pitch angle as function of time for first stage with fins

Because fins are not useful in the higher atmosphere layers, it does not mean fins should not be considered. The control system designed was only useful in the higher atmosphere layers. If the system is at a lower altitude the density is much higher, which produce a higher moment. This means that in this region fins could be efficient in combination with a control system. Besides, the fins could be used to steer the vehicle. The use of fins should therefore be investigated in more detail in a next study.

15.3. SENSITIVITY ANALYSIS

In the former chapters results were found on the trajectory of the first stage and the cost. In this section it will be found how sensitive these numbers are to input changes.

15.3.1. TRAJECTORY

First the sensitivity of the trajectory of the first stage with separation conditions will be investigated. In this analysis three different inputs will be changed, the separation velocity, height and pitch angle. The impact on the maximum G-load experienced, the maximum temperature obtained, and the end-velocity will be considered. The same aspects will be considered in the second part of this subsection, but now the sensitivity with the drag coefficient of the first stage will be considered.

SEPARATION CONDITIONS

To test the how sensitive the maximum G-load, maximum temperature and end-velocity is to the separation conditions three elements are varied. The first element is the separation altitude. Five different values are used for the altitude. The second element is the separation velocity, seven values are used. To conclude the pitch angle is varied, using five different values. No recovery mechanisms will be considered to compare the different elements and to be applicable for both configurations.

In Figure 15.5 and 15.6 the maximum G-load obtained for the different trajectories is shown. The results found in this thesis did not have any deceleration mechanism before entering the atmosphere. To keep this configuration the maximum allowable G-load is 20G. This limit is shown with a black solid line. All separation conditions above this line need an extra deceleration mechanism. For example separating the first stage with a pitch angle of 40 ° at an altitude above the 50 km, can only be done in this configuration if the velocity is below the 3.25 km/s. The second elements seen in these figures is that the a change in the pitch angles has a bigger effect on the maximum G-load experienced than a change in the altitude. Although a change in pitch angle cannot be compared one-o-one with a change in the altitude. It can be seen that a pitch angle change of 15 ° will push the trajectory towards the 20G limit. While a separation change of 30 km is still far within the margins. However for all three input parameters, separation velocity, altitude and pitch angle, holds that with a slightly change the G-load limit will not be exceeded.

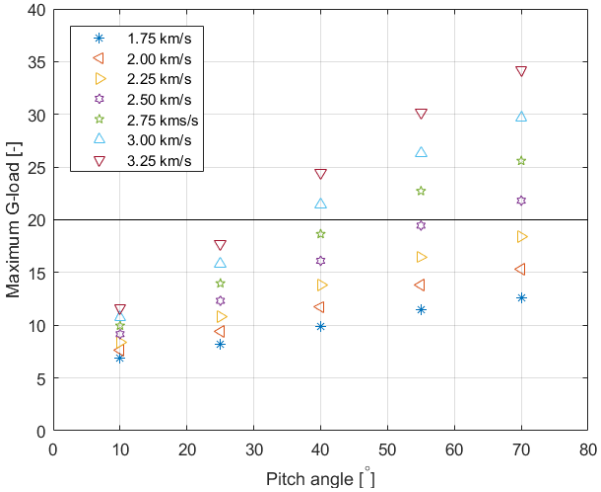

Figure 15.5: G load for constant separation altitude as function of pitch and velocity

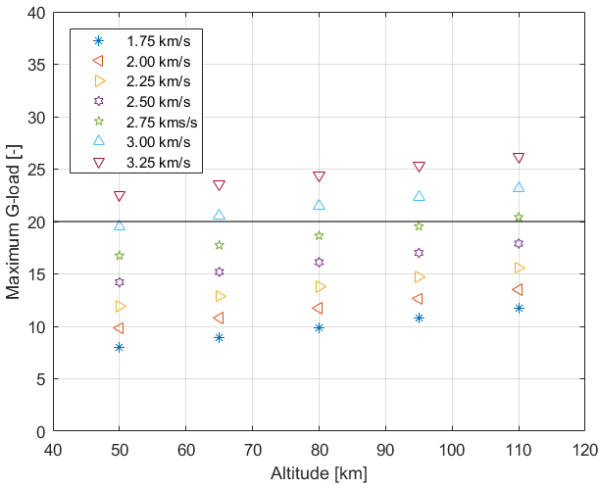

Figure 15.6: G load for constant pitch (40°) as function of altitude and velocity

The second element considered is the maximum temperature obtained during recovery, shown in Figure 15.7 and 15.8. The temperature found has been calculated using the heat balance. Comparing these plots with the figures shown for the maximum G-load, it can be seen that the temperature varies less with pitch angle than the G-load. Using the input for the separation condition no limit has been found using the limit of 2000 K and the temperature calculations. However in Section 15.1 it has already be mentioned that the temperature of the system should be investigated in more detail.

The last element considered is the end-velocity of the system. The end-velocity will determine the size of the recovery mechanism. In Figure 15.9 the end-velocity as function of separation velocity and as function of the separation pitch angle is shown. Figure 15.10 shows the end-velocity as function of the separation altitude and separation velocity. It can be stated in general that a higher pitch angle and higher separation altitude, and a higher separation velocity will result in a bigger recovery mechanism needed. However a change in separation altitude will have only a small effect on the end-velocity. The change in pitch angle will change the ratio between horizontal and vertical velocity. For the low pitch angles, or high horizontal velocity, it can be seen that the higher the separation velocity the lower the end-velocity. For the higher pitch angles, or higher vertical velocity, a higher end velocity is observed. This difference can be explained by ratio of the deceleration of the aerodynamic drag and the acceleration due to the gravitational acceleration.

DRAG COEFFICIENT

The second sensitivity considered is the sensitivity of the maximum G-load, maximum temperature and end-velocity of the system as function of the drag coefficient of the first stage. In this case the separation condi-

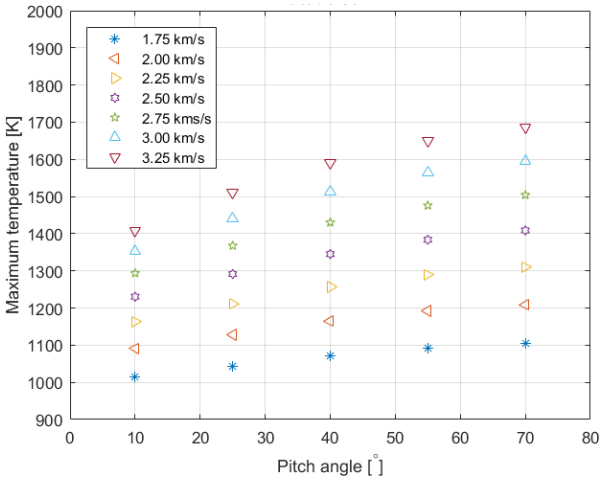

Figure 15.7: G load for constant separation altitude as function of pitch and velocity

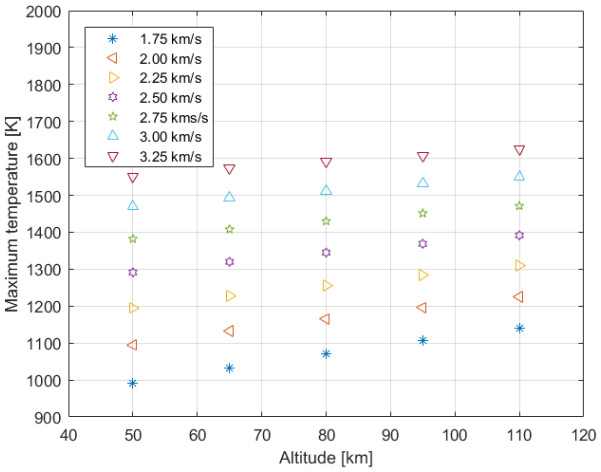

Figure 15.8: G load for constant pitch (40°) as function of altitude and velocity

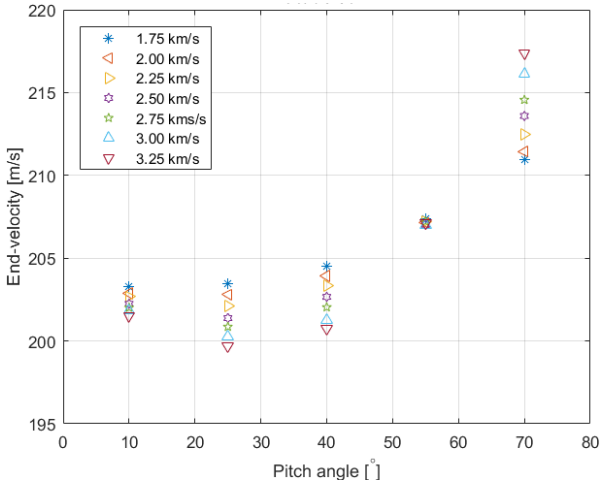

Figure 15.9: G load for constant separation altitude as function of pitch and velocity

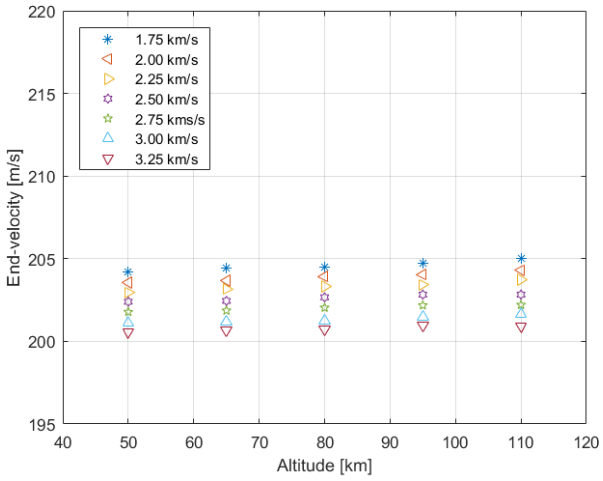

Figure 15.10: G load for constant pitch (40°) as function of altitude and velocity

tions will be kept constant, and the drag coefficient will be changed by a percentage. The first element considered is the maximum G-load shown in Figure 15.11. In this figure it can be seen that the drag coefficient has an influence on the maximum G-load experienced. In this figure it can be seen that if the drag coefficient is very small, 0.25% of the drag coefficient, the maximum G-load is the smallest. The G-load is based on aerodynamic deceleration; if the drag coefficient is very small the vehicle will not be decelerate much in comparison with higher drag coefficients. This can also be seen by Figure 15.13 were the end-velocity is plotted. If the drag coefficient is higher the maximum G-load will be lower with an increase in drag coefficient. In these cases the vehicle will decelerate in the higher layers of the atmosphere before the point of maximum dynamic pressure is reached.

The second figure considered shows the maximum temperature of the wall of the nose as function of the drag coefficient. It can be seen that the higher the drag coefficient the more the system will be decelerated. Which resulted in a lower temperature reached. An increase of 25% in drag coefficient can result in 50 degrees higher temperature. However even for very small drag coefficients the maximum temperature will not exceed the limit.

The last element considered is the end-velocity of the system. It can be seen that the higher the drag coefficient, the lower the end-velocity. If only 25% of the drag coefficient is used the system will not be able to decelerate from supersonic to subsonic. The higher the drag coefficient the shallower the curve and so the differences in end-velocity are smaller.

Using the figures considered it can be concluded that purely looking at the descent phase the drag coef-

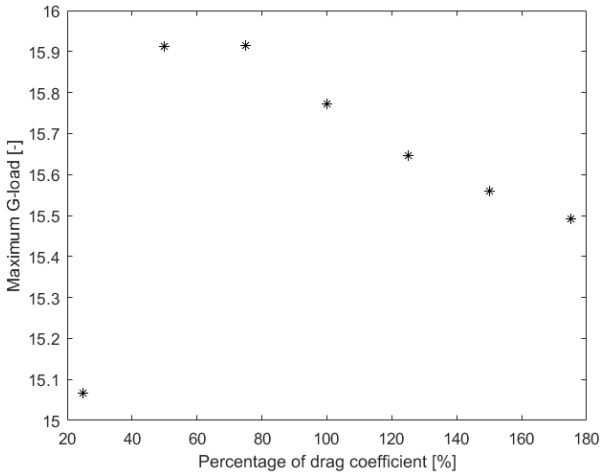

Figure 15.11: G-load as function of drag

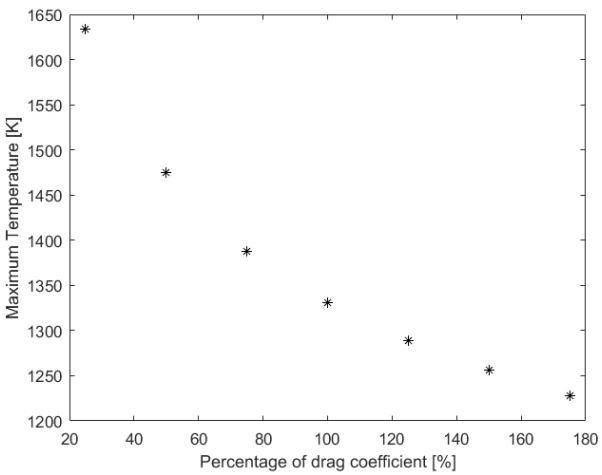

Figure 15.12: Temperature as function of drag

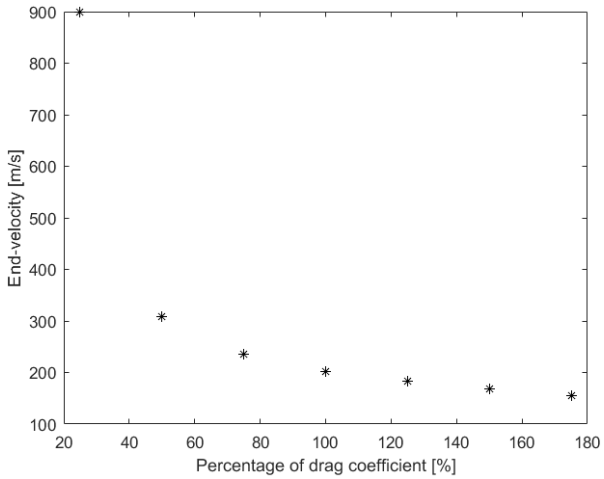

Figure 15.13: End-velocity as function of drag

ficient should be as high as possible. For ascent trajectory the launcher should have a smallest as possible drag coefficient to limit the drag losses. An increase in the drag coefficient will not add much value, as the decrease of end-velocity is small. However the drag coefficient should not be decreased to much. At least 50% of the assumed drag coefficient should be achieved, to prevent that the vehicle will not decelerate to sub-sonic speed.

15.3.2. COST

The third part of the sensitivity analyses is testing the sensitivity of the cost model. The cost-efficiency will mainly be dependent on the recurring cost. In Figure 14.6 it was already seen that even if the starting cost are very high, for example due to the use of a helicopter, the cost will shrink with the number of usages. The recurring cost will be added to the cost found in in Figure 14.6. The three different options will have first stage cost of between the 475 and 550 k€ when re-using the first stage 10 times a year. If an extra 300 k€ is needed for refurbishment each time, there will be no cost-benefits anymore. The extra cost may seem exorbitant, however 300 k€ equals to have a team of 10 people working for 5 weeks on the refurbishment, extra to the cost already taken into account. It is therefore of great importance that it should be tested how much time and money it would take to refurbish the first stage.

A retrospective analysis of the space shows that, *"Today's commercial spacecraft companies must be willing to make substantial up-front investments if they wish to reduce the recurring costs associated with vehicle maintenance and operations. Money and effort spent during the initial phases of design can lead to substantial savings during the latter period of operations"* [56].

16

CONCLUSIONS & RECOMMENDATIONS

To expand the capabilities of small satellites, a dedicated launcher is needed. To cut the cost of such a launcher, recovery of the first stage needed to be investigated. To research this, the question

"What is the performance gain in terms of cost when reusing the first stage of the launcher within the SMILE project?"

have been investigated. In this last chapter, conclusions concerning this research question are drawn and recommendations are shown in the second section of this chapter.

16.1. CONCLUSIONS

To answer the research question, three different sub-questions are treated, shown below. The results found on these questions will first be explained, followed by the answer on the research question.

- *What are the boundaries of recovering the first stage of a small launcher launched from Andøya?*
- *What is the performance gain in terms of gross take-off weight of the different options within the SMILE project?*
- *Which of the different options within the SMILE project is the best option in terms of gross take-off weight, cost, sustainability and operational flexibility for recovering the first stage?*

The first step in this research is to investigate the boundaries of the recovery of the first stage of a small launcher launched from Andøya. In the first chapter it was found that if the launcher is launched from Andøya, the first stage will land on water. Furthermore, it was seen that recovery mechanisms are needed to bring the first stage safely back to the Earth.

Chapter 12 explained that using the constraints shown in Table 12.1, no deceleration mechanisms are needed before entering the atmosphere. The only recovery mechanism needed is to decelerate the vehicle during the last phase just before impact.

In the previous chapter, on sensitivity, the boundaries on recovery were investigated in more detail. First of all, it was found that the temperature of the vehicle should be investigated in more detail, as the temperature predictions are dependent on the method used. The recovery should therefore be investigated on thermodynamics in more detail. The second element found in this chapter, is the dependence on the separation conditions. It was found that an increase in the separation angle will increase strongly the maximum G-force experienced. An increase of 10° in the separation angle will result in an exceedance of the maximum allowable G-force. An increase in the separation angle would therefore result in a different design, as a deceleration mechanism is then needed before entering the atmosphere.

From these different chapters it can be concluded first of all, that the launching from Andøya will mean a water landing. Secondly, that in the current situation and with the current knowledge, no deceleration mechanism is needed before entering the atmosphere. However if the separation conditions changes, resulting in

a higher culmination point, this statement should be reviewed.

The second sub-question was to investigate the performance gain in terms of gross take-off weight of the different options within the SMILE project. In Table 14.1 an overview was shown of the mass of the different elements. It was concluded that the retro-propulsion option was the lightest option concerning the deceleration mechanism, with an extra mass of 99 kg. The parachute option is almost 1.5 times as heavy, with an extra system mass of 135 kg. Besides the deceleration mechanisms, the landing mechanisms contributes to the extra system mass for recovery. It was found that for the recovery using a parachute system with an air bed, a landing mechanism of 141 kg is needed. Taking into account the different landing mechanisms showed that the retro-propulsion and MAR options do end up with almost the same mass for recovery. The parachute system with air bed is the heaviest, with a total extra system weight of 30%. The other two options need an extra system mass of 15%. Besides the extra needed system mass, extra propellant mass is needed to bring the launcher to the separation point.

Using the information found in Chapter 14. The last sub-question on the best option in terms of gross take-off weight, cost, sustainability and operational flexibility for recovering the first stage within the SMILE project, was answered. As shown in the former paragraph, the parachute system with MAR and the retro-propulsion option was shown to be the two lightest options.

The parachute system with air bed was found to be the cheapest when reusing the first stage four time. The parachute system with MAR was shown to be the most cost-efficient when re-using the first stage more than six times a year.

In terms of sustainability, no clear winner can be found. As no environment impact analysis has been performed on the use of the different elements. It has not been researched what the environment impact footprint of the airbags is in comparison with the parachute. However in terms of propellant usage; it can be stated that the parachute system with airbags is the least favourable. The extra propellant needed for the ascent phase is more than 2.5 times than for the other two options.

The last criterion was the flexibility of the configuration. For the retro-propulsion option, the length of the first stage is only increased a bit in comparison with the other options. However the airbags of this option make the first stage wider, and will therefore increase the drag during ascent. The parachute with air bed will make the first stage both longer and wider. The MAR option will only increase the length of the first stage. Using the retro-propulsion or MAR the impact on the launcher will be the smallest. A disadvantage of the MAR is that the recovery can only be done at good weather conditions, which makes this option less flexible. For the other options bad weather is still a problem to retrieve the first stage from the water. However the first stage can float for a while on the water, which makes it a bit more flexible.

Using the different criteria explained, two options are the most suitable within the SMILE project, retro-propulsion with air bags and the mid air recovery. However for the retro-propulsion option it was assumed that aerospike engine can handle sea water. If the engine cannot handle sea water as well as expected, the re-furbishment cost will increase, or in the worst case, the engine cannot be reused. The most preferable option of recovery configurations will therefore be the parachute design with a mid air recovery.

Re-using the first stage four times or more per year will result in a cost reduction. It can be concluded that recovery of the first stage, within the SMILE project, is cost beneficial. The performance gain in terms of cost when reusing the first stage of the launcher within the SMILE project is almost 50% if ten launches are realised per year with the same first stage.

The constructed 3DOF optimisation tool, the 6DOF simulator and the cost model constructed for this thesis work can easily applied to the cost analysis of the recovery of other launchers. The tool can provide a first order estimate on the cost efficiency of the recover of the first stage. The same tools could also be used for the recovery of the second or third stage. Besides, the simulators produced can be used for every 6DOF motion, with a small adaption, from air planes to cars.

16.2. RECOMMENDATIONS

In this thesis it was found that recovery of the first stage is cost-beneficial. It was found that if the first stage is used more than four times a year, re-using becomes cost efficient. This last section will state recommendations for further research of the recovery of the first stage. The recommendations are divided in three sections. The first section will describe the recommendations in a general aspect. The technical recommendations are described in the second part. The last section will describe the recommendations on the cost.

GENERAL RECOMMENDATIONS

First of all it should be mentioned that the performed research is an iterative process. The found numbers for landing should update the assumed 50 kg of landing mass and a new optimisation should be done. Besides, the project is still ongoing and so the design of the launcher is not finalised yet. This means that the design variables used, should be kept updated during the project. New iterations will be needed to design the most optimal recovery design.

During the research performed in this thesis assumptions were made. The assumption made should be checked in more detail. The impact loads, moment loads, vibrations encountered during recovery should be investigated. The results found should be used in a structural analysis. In this way it will be ensured that the first stage can handle the proposed recovery design. Another assumption made was about the capabilities of the GNC system. It was assumed that the GNC can handle the disturbance when entering the atmosphere. The GNC system should be designed to handle the conditions. The GNC algorithm needs to be written. Subsequently, the tool should be updated to incorporate the GNC system. Next ot the GNC algorithm, fins can also provide stability or steer the vehicle. As stated in Section 15.2, it should be investigated if fins would be beneficial in the lower layers of the atmosphere.

Another aspect what will need more research is the recovery conditions. Depending on the recovery method used different preferred launch conditions will hold. It should be investigated what kind of weather conditions the recovery mechanism can still handle. If the winds are very strong the recovery impact point might deviate. The engine performance will change with temperature. For the MAR the visibility is also of importance. Any down fall may also influence the recovery of the first stage. To conclude thunder storms might complicate the recovery as the safety of the employees have to be ensured.

TECHNICAL RECOMMENDATIONS

On a technical point of view more research should be done. First of all, it was already mentioned that the temperature analysis needs more effort. In Section 15.1 it was shown that depending on the formula used the temperature reached will change. More research is therefore needed. It is advised to analyse the temperature with CFD computations. The aerodynamic properties should also be investigated in more detail. In the simulation aerodynamic coefficient found with Missile DATCOM was used. However it was shown that Missile DATCOM is especially at the higher angles of attack and side slip angles not accurate[36].

Another technical point which should be considered is the ignition of the second stage. If a design as shown in Figure 14.5 will be used, the parachute system will be placed on the top of the first stage. Once the first stage is separated the first stage will be open on the top. This means that if the second stage is ignited too early the parachute system will fire-up. It should therefore be investigated what the minimum distance should be to ignite the second stage.

A very important part which should be tested is if retro-propulsion is possible with the aerospike. Igniting and using the engine at high velocities with air coming in the engine is a challenge. Besides the engine, the parachute system should also be investigated and designed in great detail.

Point of interest is the use of the engine during the entry of the atmosphere. In this analysis it was found that using the engine during re-entry would not be needed. However there are some reasons to investigate this part in more detail. The first reason is for the film cooling. After evaluation of the temperature it can be concluded that the engines needs to be cooled during re-entry. For an aerospike engine film cooling is often used. Film cooling is done by using a small amount of propulsion to cool the surface of the engine. Depending on the design of the engine, it might be that film cooling can only be used when firing the engine. This means that if cooling of the engines is needed, the engine needs to be fired. The second part of the reason is that using retro-propulsion will induce a bow shock around the vehicle. This bow shock will protect the vehicle against high air velocities. The first stage will therefore experience a lower velocity, which will decrease the

convective heat. Another advantage of this bow shock, is that the apparent area of the vehicle will increase. This will increase the drag coefficient.

COST RECOMMENDATIONS

A very important assumption of the cost evaluation is that the engines can handle salty water. If an option of recovery will be chosen with the chance of coming into contact with salty water, it should be investigated if the engine can handle salty water. In general it should be investigated in more detail how much the refurbishment of the engine would cost. It was explained in Subsection 15.3.2, that the cost of the refurbishment will influence the profit enormously. The prediction of the cost and time for refurbishment was one of the problems of the Space Shuttle [56]. Looking at the cost diagrams shown in Figure 14.6, it can be seen that if the first stage is only used once or twice the cost are much higher than for a non-recoverable first stage. This means that it should be tested if the first stage can fly the amount of times as predicted. Next to the refurbishment and the testing of the engines, the logistics of the recovery should also be investigated in more detail.

A

CLOSED FORM MASS MOMENT OF INERTIA

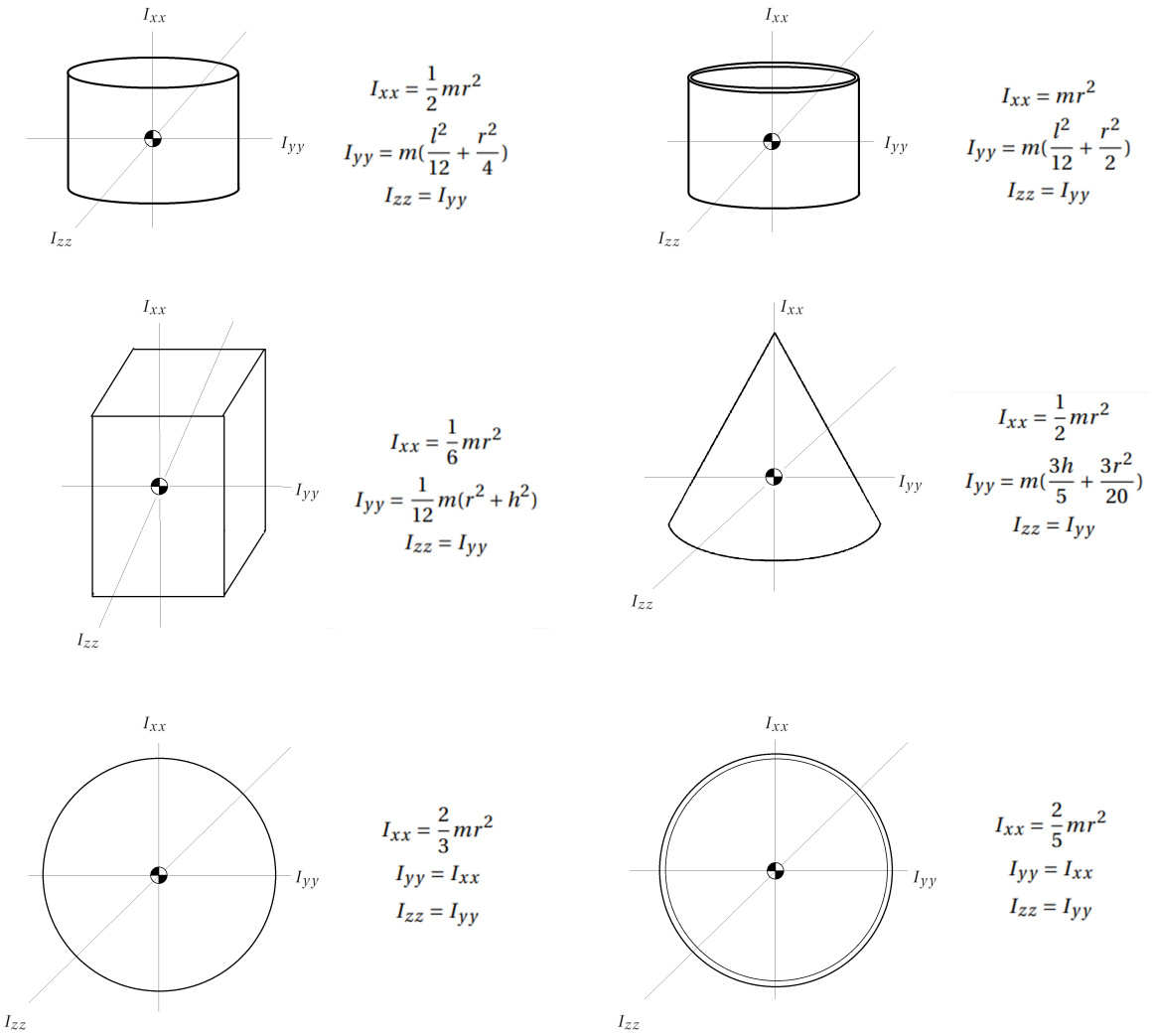

Figure A.1: Used Closed form formulation Mass Moment of Inertia

.

B

INPUT DATA FOR VALIDATION 6DOF

In this appendix the input values used for the six degrees of validation can be found. First the mass, thrust, and outline properties of the rocket have been defined and are shown in Table B.1.

Table B.1: Input values for validation 6DOF

Mass	
Start mass [kg]	75
Empty mass [kg]	60
Mass flow [kg/s]	3
Thrust	
Burn time [s]	5
Thrust [N]	3000
Initial pitch [°]	60
Outline	
Radius [m]	0.2
Chord [m]	0.2
Ixx start [kgm^2]	4
Ixx end [kgm^2]	2
Iyy start [kgm^2]	250
Iyy end [kgm^2]	100
Izz [kgm^2]	Ixx
Izx=Ixz=Iyz=Izy=Ixy=Iyx [kgm^2]	0

Next to the information found in Table B.1, the aerodynamic properties are important to validate the model. First the force coefficient are defined. The formulation for the drag coefficient can be found in Equation B.1. The drag coefficient is a function of the Mach number, M, the angle of attack α, the angle of side slip β. The lift coefficient can be found in Equation B.2. The lift coefficient is a function of angle of attack. For the side force coefficient the same formulation can be found as for the lift coefficient, but now a function of beta. This is due to the symmetry of the rocket. The minus sign is due to the sign convention in the tool.

$$C_D = 0.6515 - 0.5506M + 0.2826M^2 + 0.0105(\alpha^2) + 0.0105(\beta^2) \tag{B.1}$$

$$C_L = (0.0305 - 0.0546M + 0.1889M^2)\alpha \tag{B.2}$$

$$C_Y = -(0.0305 - 0.0546M + 0.1889M^2)\beta \tag{B.3}$$

Beside the force coefficients the aerodynamic moment coefficient should also be considered. No roll moments will be taken into account, Equation B.4. For the pitch and yaw moment the same formulation can be found. For the pitch moment the formulation is a function of the angle of attack, shown in Equation B.5. For the yaw moment coefficient, the coefficient is a function of the side slip angle, Equation B.6. This can again be explained with the symmetry of the validation rocket.

$$c_l = 0 \tag{B.4}$$

$$c_m = (-0.1036 + 0.2250M - 0.4423M^2)\alpha \tag{B.5}$$

$$c_n = (-0.1036 + 0.2250M - 0.4423M^2)\beta \tag{B.6}$$

BIBLIOGRAPHY

[1] NASA History, *Genesis aircrew, chutes... scores,* https://www.nasa.gov/mission_pages/genesis/multimedia/src_test.html (2007), [Online; viewed on 21 July 2017].

[2] T. W. Knacke, *Parachute Recovery Systems Design Manual* (Naval Weapons Center China Lake, CA 93555-6001, March 1991).

[3] I. G. Clark, A. L. Hutchings, C. L. Tanner, and B. R. D., *Supersonic inflatable aerodynamic decelerators for use on future robotic missions to mars,* Journal of Spacecraft and Rockets **46**, 340 (2009).

[4] M. J. Miller, B. A. Steinfeldt, and R. D. Braun, *Investigation of drag-modulated supersonic inflatable aerodynamic decelerators for sounding rocket payloads,* Journal of Spacecraft and Rockets **52**, 383 (2015).

[5] B. P. Smith, C. L. Tanner, M. Mahzari, I. G. Clark, R. D. Braun, and F. M. Cheatwood, *A historical review of inflatable aerodynamic decelerator technology development,* IEEE Aerospace Conference , 1 (2010).

[6] C. Rosema, J. Doyle, and U. M. Auman, L, .

[7] O. Trivailo, M. Sippel, and Y. Sekercioglu, *Review of hardware cost estimation methods, models and tools applied to early phases of space mission planning,* Progress in Aerospace Sciences **53**, 1 (2012).

[8] C. Lillie and B. Thompson, *Parametric cost estimation for space science missions,* Advanced Optical and Mechanical Technologies in Telescopes and Instrumentation **7018-81**, (2008).

[9] B. T. C. Zandbergen, *Thermal Rocket Propulsion (version 2.05)*, Tech. Rep. AE4-S01 (Delft University of Technology, Faculty of Aerospace Engineering, 2016).

[10] J. Wertz, *Mission Geometry; Orbit and Constellation Design and Management* (Microcosm Press, El Segundo, USA, 2001).

[11] S. Olaru, S. Mitu, C. Niculescu, A. Slişteanu, R. Popescu, and C. Mihai, *The birth and evolution of the textile material flying machines,* Industria Textila **58**, 186 (2007).

[12] J. D. Maynard, *Aerodynamic Characteristics of Parachutes at Mach Numbers from 1.6 to 3,* Tech. Rep. NASA-TN-D-752 (National Aeronautics and Space Administration, NASA Langley Research Center; Hampton, VA United States, 1961).

[13] D. S. Jorgensen, R. A. Haggard, and G. J. Brown, *The past, present, and future of mid-air retrieval,* in *18 th AIAA Aerodynamic Decelerator Systems Technology Conference and Seminar* (2005).

[14] J. Stein, C. Madsen, and S. A., *An overview of the guided parafoil system derived from x-38 experience,* in *18th AIAA Aerodynamic Decelerator Systems Technology Conference and Seminar, Aerodynamic Decelerator Systems Technology Conferences,Munich, Germany* (2005).

[15] NASA History, *X-38 team successfully flies largest parafoil parachute in history,* https://spaceflight.nasa.gov/history/station/x38/parafoil.html (2000), [Online; viewed on 21 May 2017].

[16] L. A. Davis, *First stage recovery,* Engineering **2:1**, 152 (2016).

[17] T. Nace, *The billionaire's race to colonize space: Blue Origin versus SpaceX,* http://thenextweb.com/insider/2016/04/13/blue-origin-vs-spacex-2-billionaires-race-colonize-space/#gref (2016), [Online; viewed on 3 August 2016].

[18] A. D. Olds, R. E. Beck, and others, *Irve-3 post-flight reconstruction,* in *AIAA Aerodynamic Decelerator Systems (ADS) Conference Daytona Beach, Florida* (2013).

[19] D. M. Bose, R. Winski, J. Shidner, C. Zumwalt, C. O. Johnston, D. R. Komar, F. M. Cheatwood, and S. J. Hughes, *The Hypersonic Inflatable Aerodynamic decelerator (HIAD) mission applications study,* in *AIAA Aerodynamic Decelerator Systems (ADS) Conference 2013* (2013).

[20] D. E. Goldberg, *Genetic algorithms in search, optimization, and machine learning* (Addison-Wesley Publishing Company, Boston, USA, 1989).

[21] J. Mulder, W. van Staveren, J. van der Vaart, E. de Weerdt, C. de Visser, A. in 't Veld, and E. Mooij, *Flight Dynamics Lecture Notes* (Faculty of Aerospace Engineering, Delft University of Technology, 2013).

[22] J. R. Dormand and P. J. Prince, *A family of embedded runge-kutta formulae,* Journal of computational and applied mathematics **6.1**, 19 (1980).

[23] A. C. Aikin, J. M. Picone, A. E. Hedin, and D. P. Drob, *NRLMSISE-00 Empirical Model of the Atmosphere: Statistical Comparisons and Scientific Issues* (NASA Goddard Space Flight Center; Greenbelt, MD United States, 2001).

[24] D. Hsu, *Comparison of four gravity models,* in *Position Location and Navigation Symposium, IEEE* (1996).

[25] A. Tewari, *Atmospheric and Space Flight Dynamics Modeling and Simulation with MATLAB and Simulink* (Birkhäuser, Boston, USA, 2007).

[26] D. P. Drob, J. T. Emmert, J. W. Meriwether, J. J. Makela, E. Doornbos, M. Conde, G. Hernandez, J. Noto, K. A. Zawdie, S. E. McDonald, J. D. Huba, and J. H. Klenzing, *An update to the horizontal wind model (hwm): The quiet time thermosphere,* Earth and Space Science **2**, 301 (2015).

[27] A. M. Bedford and W. Fowler, *Engineering Mechanics: Dynamics,* fifth edition in si units ed. (Pearson, Singapore, 2007).

[28] K. E. French, *A new correlation of parachute weight data,* Journal of Spacecraft and Rockets **8**, 71 (1971).

[29] J. Wegereef and H. Jentink, *Spades: A parafoil delivery system for payloads until 200kg,* in *17th AIAA Aerodynamic Decelerator Systems Technology Conference and Seminar* (2003).

[30] W. Wegereef and H. Jentink, *Modular approach of precision airdrop system spades,* in *19th AIAA Aerodynamic Decelerator Systems Technology Conference and Seminar Williamsburg, VA* (2007).

[31] M. S. Anderson, H. L. Bohon, and M. M. Mikulas, *Structural Merit Function for Aerodynamic Decelerators* (NASA TN-D-5535, Langley Research Center, Nov 1969).

[32] J. D. Nicolaides, R. J. Speelman, and G. L. Menard, *A review of parafoil programs,* in *1968 Aerodynamic Deceleration Systems Conference, El Centro California* (1986).

[33] T. J. Mueller and J. D. DeLaurier, *Aerodynamics of small vehicles,* Annual Review of Fluid Mechanics **35:1**, 89 (2003).

[34] *MISSILE DATCOM USER'S MANUAL -1997 FORTRAN 90 REVISION,* final report for period april 1993-december 1997 ed. (1998).

[35] W. Hammond, *Design Methodologies for Space Transportation Systems (AIAA Education)* (American Institute of Aeronautics and Astronautics, 2001).

[36] J. M. Simon and W. B. Blake, *Missile datcom: high angle of attack capabilities,* the AIAA Atmospheric Flight Mechanics Conference, Portland, Oregon (1999).

[37] K. Sutton and R. A. Graves, *A General Stagnation-point convective-heating equation for arbitrary gas mixtures,* Technical Report NASA TR R-376 (National Aeronautics and Space Administration, Washington, 1971).

[38] C. Meisl, *Techniques for cost estimating in early program phases,* Engineering Costs and Production Economics **14**, 95 (1988).

[39] NASA Office of Evaluation, *NASA Cost Estimating Handbook Version 4.0* (Electronic resource, 2015).

[40] Shermon D, *Systems cost engineering—program affordability, Management and Cost Control* (USA: Gower Publishing Limited, 2009).

[41] ESA, *Engineering costing techniques in esa,* http://www.esa.int/esapub/bulletin/bullet81/greve81.htm (1995), [Online; viewed on 11 June 2017], Orginally from ESA Bulletin 81.

[42] R. A. Reklaitis, G. V. and K. M. Ragsdell, *Engineering Optimization, Methods and Applications* (Wiley, New York, 1983).

[43] G. P. Rangaiah, *Stochastic Global Optimization*, volume 2 ed. (World Scientific, June 2010).

[44] N. L. Cheatwood, Neil, *Hypersonic inflatable aerodynamic decelerator (hiad) technology,* NASA's Game Changing Technology Industry Day (2016).

[45] A. D. Ketsdever and M. M. Micci, *Micropropulsion for Small Spacecraft* (American Institute of Aeronautics and Astronautics, USA, 2000).

[46] D. Cadogan, C. Sandy, and M. Grahne, *Development and evaluation of the mars pathfinder inflatable airbag landing system,* Acta Astronautica **50**, 633 (2002).

[47] S. Antonenko and S. Belavskiy, *Minimum heating entry trajectories for reusable launch vehicles,* Progress in Propulsion Physics **1**, 481 (2009).

[48] M. Gravlee, F. Zegler, and T. Bulk, *EELV partially reusable booster,* in *AIAA SPACE Conference and Exposition* (2010).

[49] M. Gravlee, B. Kutter, F. Zegler, B. Mosley, and R. A. Haggard, *Partial rocket reuse using mid-air recovery,* in *Space 2008 Conference* (2008).

[50] M. Wilson, *Archimedes's principle gets updated,* Physics Today **65** (2012).

[51] A. M. Brandis and J. C. O., *Characterization of stagnation-point heat flux for earth entry,* in *45th AIAA Plasmadynamics and Lasers Conference, AIAA AVIATION Forum* (2014).

[52] Z. R. Putnam and R. D. Braun, *Extension and enhancement of the allen–eggers analytical ballistic entry trajectory solution,* JOURNAL OF GUIDANCE, CONTROL, AND DYNAMICS **38**, 414 (2015).

[53] R. Chapman, *An approximate analytical method for studying entry*, Technical Note NACA TN 4276 (National Advisory Committee for Aeronautics, Washington, 1958).

[54] M. E. Tauber, *A Review of High-Speed, convective, Heat Transfer Computation Methods*, Technical Paper NASA TP 2914 (National Aeronautics and Space Administration, California, 1989).

[55] R. W. Detra and H. Hildago, *Generalized heat transfer formulas and graphs for nose cone re-entry into the atmosphere,* ARS Journal **31**, (1961).

[56] R. P. Ocampo, *The space shuttles commercial potential: A retrospective analysis,* in *AIAA SPACE 2015 Conference and Exposition, Pasadena, California* (2015).